



Biophysical Investigation of Novel Cryoprotectants

A thesis submitted in fulfilment of the requirements for the degree of Doctor of Philosophy

Rekha Raju

Master of Technology (Technology Management), University of Kerala, India

Bachelor of Technology (Electronics & Communication Engineering), University of Kerala, India

School of Science

College of Science, Engineering and Health

RMIT University

November 2019

Declaration

I certify that except where due acknowledgement has been made, the work is that of the author alone; the work has not been submitted previously, in whole or in part, to qualify for any other academic award; the content of the thesis is the result of work which has been carried out since the official commencement date of the approved research program; any editorial work, paid or unpaid, carried out by a third party is acknowledged; and, ethics procedures and guidelines have been followed. I acknowledge the support I have received for my research through the provision of an Australian Government Research Training Program Scholarship.

Rekha Raju

11 November 2019

Acknowledgements

I take this opportunity to thank each and every one who helped me with the successful completion of this Dissertation.

First and foremost, I would like to express my sincere and heartfelt gratitude to my principal supervisor Prof. Gary Bryant for his exemplary guidance, supervision, motivation, support and the encouragement he gave me throughout this research. Gary's doors were always open for clarifying any doubts from the very first day of this PhD. Gary has managed to strike a balance between challenging and encouraging me and I always felt the freedom to express my ideas. Under Gary's guidance, I was fortunate to improve my skills and get some of the best opportunities so far; one of those I would like to mention is the Erasmus PhD short stay at UPC, Barcelona. His knowledge, expertise, patience and the way he manages multiple tasks very well has been amazing me always. Gary always had different plans for advising me in progressing through my PhD topic. I am greatly obliged to him for the final outcome of this thesis. Many thanks Gary, for making me grow as a research scientist.

Secondly, I would like to deeply thank my three associate supervisors, Dr. Brendan Wilkinson, Prof. Juan Torrent Burgues and Dr. Chris Garvey for their invaluable guidance, discussions and support for doing this research. Brendan's expertise in synthesising carbohydrate-based surfactants opened the way to try their potential for future cryoprotective agents. His advice and support were inevitable to elaborate the scope of this thesis and publishing the experimental results in peer reviewed journals. Juan's supervision and support during the PhD short stay at UPC, Barcelona has been vital to get the expertise in Langmuir monolayer technique and analysis. His guidance was invaluable for developing the experimental plans and protocols which lead to fruitful outcomes in this thesis.

Thirdly, I would like to express my sincere thanks to Dr. Khashayar Khoshmanesh from Engineering group for all his help and advice for designing and fabricating the microfluidic devices for this research. His expertise in microfluidics was invaluable for suggesting an improved perfusion method through this thesis. I also use this opportunity to thank Mr. Hannes Hohn for his assistance in the fabrication of microfluidic devices.

Throughout the course of this project, I received the assistance of a number of staffs, scientists, colleagues and friends from RMIT, whose help has been much appreciated. I would like to thank Dr. Tamar Greaves, Mr. Asoka, Ms. Dilek Yalcin and Mrs. Radhika Arunkumar for their advice and assistance in DSC experiments; Dr. Zeyad Nasa, Dr. Amanda Abraham, Ms. Emma Wilson and Mr. Reece Nixon-Luke for their assistance in the cell culture training and experiments. I am also grateful to Dr. Arwen Pagon, Dr. Matthew Taylor, Dr. Lisa Dias and Emma Stockham for all their support throughout this journey.

Significant funding has also been received during my PhD which has been vital for conducting all of my experiments both locally and internationally for which I gratefully acknowledge; ARC (Australian Research Council) scholarship 2016, RRSS (RMIT Research Stipend

Scholarship 2017-2019) and European Union Erasmus plus grant 2018 for PhD short stay internship (4 months). I would also like to thank Gary for all his funding support internally from the supervisor funding, which has been vital for attending all the conferences and research tours. Those were really eye-opening opportunities for realizing the significance of my research area and helped a lot to the fruitful completion of this PhD.

I am sure there are very few tasks more tedious than writing a PhD thesis, but of course reading someone else's must be one of them. For that, I would like to again thank my principal supervisor, Gary for his assistance and patience in the multiple corrections, iterations and proof readings. I would also like to express my gratitude to all my associate supervisors for their proof reading and corrections.

I am greatly indebted to all my family members and parents especially my mother who always prayed for me and gave her generous support and love. Words cannot express how I am grateful to her!! A profound gratitude to my late father in law for his positive advice and encouragement during the very initial stages of my thought about doing a PhD.

I would like to express special appreciation to my beloved husband, who always stood by me especially during the period of this study to strive towards my goal in all the happy and stressful circumstances. Many thanks for your love, care, patience and encouragement!!

At the end, I would like to thank my "sweet little daughter - Hana" for her love, understanding and support along the way. Thank you so much and love you more than anything in the world my dear!!

Rekha Raju

Author publications

A list of journal articles

- Raju Rekha, Merl Theresa, Adam Madeleine K., Staykov Emiliyan, Ben Robert N., Bryant Gary, Wilkinson Brendan L. (2019) *n*-Octyl (Thio)glycosides as Potential Cryoprotectants: Glass Transition Behaviour, Membrane Permeability, and Ice Recrystallization Inhibition Studies*. *Australian Journal of Chemistry* **72**, 637-643; <https://doi.org/10.1071/CH19159>
- Rekha Raju, Hannes Höhn, Christian Karnutsch, Khashayar Khoshmanesh, and Gary Bryant. "Measuring volume kinetics of human monocytes in response to cryoprotectants using microfluidic technologies." *Applied Physics Letters* 114, no. 22 (2019): 223702; <https://doi.org/10.1063/1.5096199>
- Juan Torrent-Burgués and Rekha Raju., 2019., "Effect of lysozyme subphase and insertion on several lipid films." *Adv Mater Sci*, Volume 4: 1-7. ISSN: 2398- 6883., doi: 10.15761/AMS.1000149, <https://www.oatext.com/pdf/AMS-4-149.pdf>
- Rekha Raju, Juan Torrent Burgues and Gary Bryant (2019), "Interactions of cryoprotective agents with phospholipid membranes - a Langmuir monolayer study" (Under review)

Manuscripts under preparation

- Rekha Raju and Gary Bryant, "Review on the need for novel Cryoprotectants and cryopreservation protocols - Insights into the importance of biophysical investigation and cell permeability".
- Rekha Raju, Gary Bryant and Brendan Wilkinson, "Glass transition, Permeability and cryopreservation studies with novel potential cryoprotectant- Trehalose derivatives"
- Rekha Raju, Juan Torrent Burgues and Gary Bryant, "Interactions of cryoprotective agents (concentrated; 10% by volume) with phospholipid membranes - a Langmuir monolayer study"
- Radhika Arunkumar , Rekha Raju , Gary Bryant , Calum J. Drummond and Tamar L. Greaves, "Investigation of cell membrane permeability and cytotoxicity of Protic Ionic liquids towards THP1 cell line"

Awards and grants

- European Union Erasmus+ grant 2018
- RMIT (Royal Melbourne Institute of Technology) Research Scholarship 2017
- ARC (Australian Research Council) scholarship 2016

Table of contents

Declaration	i
Acknowledgements	ii
Author publications	iv
Awards and grants	v
Table of contents	vi
List of Figures	ix
List of Tables	xi
Abstract	1
Chapter 1	3
Introduction and Literature Review	3
1.1 Introduction	3
1.2 Cryobiological damage at the cellular level	5
1.3 Cryoprotective Agents	7
1.3.1 Penetrating (permeating) cryoprotectants	8
1.3.2 Non-penetrating (Non-permeating) cryoprotectants	8
1.3.3 Plant Vitrification Solutions (PVS)	8
1.4 Effect of cryoprotectants on cell membranes	9
1.5 Cryoprotectant toxicity and damage	10
1.5.1 Toxicity reduction by cryoprotectant combinations	11
1.5.2 Other means of reducing CPA toxicity	11
1.6 Biophysical properties of cells	11
1.6.1 Determination of osmotically inactive volume V_b using Boyle-Van't Hoff (BVH) plot	11
1.6.2 Cell membrane permeability of cryoprotectants	12
1.6.3 Estimation of permeability parameters	13
1.7 Methods and techniques used to measure cell permeability	14
1.8 Future cryoprotectants	14
1.9 Aims of the thesis and Research questions	15
1.10 Overview of the thesis	15
1.11 References	16
Chapter 2	25
Methodology	25

2.1	Langmuir monolayer technique	25
2.1.1	Materials used	26
2.1.2	Experiments and Equipments	27
2.2	Differential scanning calorimetry (DSC)	28
2.3	Single cell volume kinetics	30
2.3.1	Materials and methods used	30
2.4	Cryopreservation trials	33
2.4.1	Materials and methods	33
2.5	References	34
Chapter 3		36
Interactions of cryoprotective agents with phospholipid membranes - a Langmuir monolayer study		36
Author contributions:		36
Chapter 4		37
n-Octyl(thio)glycosides as Potential Cryoprotectants: Glass Transition Behaviour, Membrane Permeability, and Ice Recrystallization Inhibition Studies*		37
Author contributions:		37
Chapter 5		38
Glass transition, permeability and cryopreservation studies with novel potential cryoprotectants - trehalose derivatives		38
5.1	Introduction	38
5.2	Experimental: Materials and Methods	38
5.3	Results and Discussion	39
5.3.1	DSC thermograms – Phases observed on cooling and warming	39
5.4	Cell permeability- shrink-swell behavior of cells	41
5.5	Cryopreservation of THP-1 cells using Trehalose derivatives	43
5.6	Cryopreservation of THP-1 cells with Trehalose di pivotate using different cryopreservation protocols	45
5.7	Conclusions and future work	48
5.8	References	49
Chapter 6		51
Measuring volume kinetics of human monocytes in response to cryoprotectants using microfluidic technologies		51
Author contributions:		51
Chapter 7		52
General discussions, Conclusions and Future directions		52
7.1	General discussions and conclusions	52

7.2	Recommendations for the future work	55
7.3	References	56
	Appendix I: Supplementary material- Chapter 4	57
	Appendix II: Supplementary materials- Chapter 6	58
	Appendix III: Table showing the novelty of current study with THP-1 cells	59

List of Figures

<i>Fig.1.1: Schematic representation of some key aspects of cryopreservation</i>	6
<i>Fig.1.2: Differing actions of penetrating and non-penetrating CPAs:</i>	7
<i>Fig.1.3: Schematic representation of the effect of dehydration in the cell membrane lipid organization:</i>	9
<i>Fig.1.4: Schematic of BVH plot representing the osmotically inactive volume \mathcal{V}_b of the cell –</i>	12
<i>Fig.1.5: Shrink–swell behavior of an individual cell upon addition of a penetrating CPA (adapted from Reference⁹).</i>	13
<i>Fig.2.1: (A) schematic of a Langmuir trough with two movable barriers, monolayer film formed at the surface of the subphase, a wilhelmy paper plate and a pressure sensor. (B) shows the schematic of how the phospholipids are arranged in a monolayer (C) shows the schematic of how the monolayer lipids are compressed (Image source²).</i>	25
<i>Fig. 2.2: (A) Schematic of $\pi - A$ isotherm showing the various states achieved by the monolayer upon compression (B) Schematic of Cs-1 graph showing the various states achieved by the monolayer during compression (image source¹¹).</i>	26
<i>Fig. 2.3: Molecular structure of various phospholipids used as monolayers for the CPA-membrane lipid interaction studies.</i>	27
<i>Fig. 2.4: (A) Nima teflon trough used for the Langmuir monolayer experiments (B) Closer view of the trough showing pressure sensor and wilhelmy plate (C) Small teflon trough used for insertion experiments</i>	28
<i>Fig. 2.5: Schematic DSC thermogram showing the ice crystallization (T_c), glass transition (T_g) and ice melting (T_m) temperatures. Inset shows the glass transition part of the DSC thermogram</i>	29
<i>Fig. 2.6: Schematic of the DSC method used for the current study</i>	29
<i>Fig. 2.7: Schematic of the two microfluidic cell trap designs used for the current study</i>	31
<i>Fig. 2.8: Experimental set up for single cell trapping and permeability studies using microfluidic device- (A) Schematic experimental set up (B) Setup in the laboratory</i>	32
<i>Fig.5.1: Molecular structures of trehalose and its derivatives</i>	39
<i>Fig.5.2: DSC warming thermograms showing T_g of Trehalose and its derivatives: (A) Neat samples (B) aqueous samples, inset shows the T_g of 10 vol% DMSO for comparison</i>	40
<i>Fig.5.3: THP-1 cell perfusion with the two trehalose derivatives -</i>	42
<i>Fig.5.4: Cell volume excursion during perfusion by the two trehalose derivatives</i>	43

Fig.5.5: Cell images after 1 week of cryopreservation using DMSO and trehalose derivatives
..... 44

*Fig.5.6: Cell images after 1week cryopreservation using DMSO as well as trehalose
dipivotate in protocols P-1& P-2* 47

*Fig.5.7: Cell images after 1week cryopreservation using DMSO as well as trehalose
dipivotate in protocols P-3& P-4* 47

List of Tables

<i>Table 5.1: Tg values of Trehalose and it's derivatives</i>	41
<i>Table 5.2: Cell viabilities of the samples cryopreserved using CPAs as DMSO and trehalose derivatives</i>	44
<i>Table 5.3 Cell viabilities of the samples cryopreserved using protocol P-1</i>	46
<i>Table 5.4 Cell viabilities of the samples cryopreserved using protocol P-2</i>	46
<i>Table 5.5 Cell viabilities of the samples cryopreserved using protocol P-3</i>	46
<i>Table 5.6 Cell viabilities of the samples cryopreserved using protocol P-4</i>	46

Abstract

This thesis aims to examine the critical molecular properties that lead to good cryoprotective performance and use this knowledge to test novel non-toxic compounds which can be optimized to use as cryoprotectants (CPAs). The key properties needed to make a good CPA are: low toxicity; the ability to pass through membranes to get inside cells; the ability to form glasses at relatively high sub-zero temperatures; and the ability to inhibit ice recrystallisation during thawing (the growth of larger ice crystals from smaller ones). This thesis presents a systematic investigation of these important properties, for both traditional CPAs and novel compounds with cryoprotective potential. Cryopreservation trials with some of these compounds are carried out to assess their cryoprotective potential.

First, this thesis presents a Langmuir monolayer study of the effects of four common cryoprotective agents (dimethyl sulfoxide, ethylene glycol, glycerol and dimethyl formamide) on phospholipid monolayers. Four different phospholipids (DOPC, DPPC, POPC, POPE) are studied to determine if the headgroup and level of chain saturation influence the interactions. It is shown that the phospholipid species can have a significant effect. DMSO showed interesting lipid specific effects – causing expansion of DPPC monolayers but compression for POPC monolayers, while having little effect for DOPC and POPE. The results highlight the importance of studying more than one model lipid system as well as the need to study concentrations relevant to cryopreservation.

Second, this thesis investigates the potential of carbohydrate-based surfactants such as n-octyl(thio)glycosides to be a novel and accessible class of penetrating CPAs. A series of eight n-octyl (thio)glycosides ($1\alpha/\beta$ – $4\alpha/\beta$) with D-glucose or D-galactose-configured head groups and varying anomeric configurations were evaluated for glass transition behavior and membrane permeability. Of these, n-octyl β -D-glucopyranoside (2β) exhibited high glass transition temperature (T_g), both as a neat sample and 20wt-% aqueous solution. Membrane permeability studies of this compound revealed cellular uptake at concentrations relevant to the inhibition of intracellular ice formation, thus presenting a promising lead candidate for further biophysical and cryopreservation studies.

Third, this thesis presents similar studies on four trehalose derivatives in order to understand their cryoprotective potential. Permeability trials on these molecules showed that trehalose-di acetate has no cell permeability, whereas both trehalose di pivotate and trehalose tetra acetate have moderate permeability. The most promising candidate with high glass transition temperature and relatively good permeability was trehalose di pivotate, so this compound was used for further cryopreservation studies on THP-1 cells.

Finally, this thesis presents the development of a novel microfluidic cell trapping device for cell permeability studies, which has considerable advantages over traditional techniques. Two microfluidic cell trapping structures were produced, combining direct laser writing (DLW) and soft lithography techniques. These structures were used for the hydrodynamic capturing of single human monocyte (THP-1) cells and tested by studying the cell volume kinetics upon the

addition of DMSO. Compared to existing technologies, the method allowed: (i) rapid capture of single cells without surface functionalization; (ii) the rapid exchange of solvent to generate osmotic gradients across the cell membrane; and (iii) real-time imaging of cells during the shrinkage and swelling phases due to the imaging stability provided by the traps.

To date, the search for new CPAs has been reliant on educated guesswork and trial and error. This thesis systematically investigates the critical molecular properties relevant for cryopreservation and provides a systematic method for assessing novel molecules as alternative cryoprotectants.

Chapter 1

Introduction and Literature Review

1.1 Introduction

Cryopreservation¹ is the primary application of cryobiology and is a viable option for the preservation of a range of biological materials such as cells and simple tissues. Cryobiology fundamentally refers to understanding ultra-low temperature effects on biological systems and utilizing this knowledge to develop better cryopreservation protocols. Cryopreservation involves several steps during which cellular membranes are exposed to extreme conditions and severe stresses which may lead to cell death²⁻⁴. Adding chemicals called cryoprotective agents (CPAs) helps to minimize many of the stresses associated with freezing. CPAs help to preserve cell membranes, inhibit ice formation inside and outside the cells and promote vitrification (formation of glass)⁵.

Since glycerol and dimethyl sulphoxide (DMSO) were introduced as penetrating cryoprotectants⁶, cryopreservation methodologies have been developed for many different types of cells. For example, we can now successfully cryopreserve red and white blood cells, sperm, embryos, some cancer cells and stem cells⁷. However, current methods have two significant disadvantages: i) the CPAs used are highly toxic, and generally must be rapidly removed upon thawing, which is expensive and time consuming and so not ideal for many critical applications such as stem cell therapies, preservation of endangered species, reproductive technologies etc; and ii) despite years of research, most cell types (>hundreds) cannot be cryopreserved using existing CPAs. So, there is a need to develop novel cryopreservation protocols involving less toxic CPAs. Investigating the cell biophysical response to different potential CPAs is a key step in the development of “cell-type specific” novel protocols⁸. Given that most CPAs must enter the cell in order to provide cryoprotection, cell permeability is one of the critical parameters in a molecule’s cryobiological potential⁹⁻¹¹. Osmotic effects at the time of CPA addition may lead to cell damage, so understanding cell volume kinetics during the freezing process is important for the development of new protocols^{7,11-16}.

According to Mazur's “Two-Factor Hypothesis”, the cellular osmotic response is measured by the biophysical properties of the cells such as the cell membrane permeability to water (L_p) as well as CPAs (P_s)^{12,13,17,18} and the osmotically inactive cell volume (V_b). These fundamental properties are unknown for many cells. Cell permeability studies with various CPAs will help to understand the fundamental cryobiological characteristics and thus may allow the development of improved cryopreservation protocols¹⁹⁻²⁴. The search for novel and less toxic CPAs is ongoing, to enable the successful cryopreservation of a wider variety of cells, and reduce the toxicity associated with traditional media²⁵⁻³².

Advances in modern cryopreservation procedures could be divided into two themes:

- i) Optimization of cryopreservation protocols for particular cell types; and

ii) Improvement of the cryoprotective solutions by developing less toxic novel CPAs

This thesis focusses on the second theme, which requires investigating the single cell biophysical response to various cryoprotectants and understanding their fundamental cryobiological and biophysical properties. Exposing cells to (permeating) CPAs causes osmotic imbalances due to solute and water flux across the membranes, resulting in cell volume changes (cells initially shrink and then swell) leading to osmotically induced membrane stresses^{4,5,9,33}, which need to be minimized. In addition, cryoprotectants may interact with cell membrane lipids causing phase transitions which may lead to structural changes in the membrane^{2,3,34}. Moreover, the optimum protocols vary from cell type to cell type due to their variable sensitivity to the freezing process and the cell-type specific biophysical properties. So, the development of a successful cryopreservation protocol for each cell type involves identification of a suitable CPA and optimization of the CPA concentration in order to reduce the cytotoxicity^{5,9,35}.

Many solutes have been studied to determine if they might act as CPAs, reviewed in^{7,33}. The most widely used CPAs are DMSO and glycerol. However, these CPAs are toxic to cells and recovery rates can be low. The key properties needed to make a good CPA are: low toxicity; the ability to pass through membranes to get inside cells; the ability to form glasses at relatively high sub-zero temperatures; and the ability to inhibit ice recrystallization during thawing (the growth of larger ice crystals from smaller ones). The CPAs used to date usually have some of these properties, but not all. For example, DMSO³⁶ and glycerol have high glass transition temperatures and high membrane permeability, but are moderately toxic, causing membrane disruption at high concentration, and do not inhibit ice recrystallization upon thawing. So, novel materials that overcome the limitations of existing CPAs are desired to facilitate the effective preservation of not only cells but also (potentially) simple tissues and organs.

Simple sugars display effective cryoprotection that is correlated with their hydration³⁷, and sugars such as sucrose and trehalose are accumulated in nature by a number of plant and animal species to protect them from freezing and dehydration damage^{38,39}. In nature these sugars are accumulated inside cells, and so can perform their functions naturally. However, they are not membrane permeable so have limited use as artificial cryoprotectants. This has inspired a search for non-toxic, low molecular weight compounds based on carbohydrates that exhibit strong cryoprotection. It has been shown that among these, substituted aryl glycosides and amphiphilic carbohydrates, including surfactants and hydrogelators, are promising⁴⁰⁻⁴². These compounds display low cytotoxicity and can be readily synthesized from abundant and renewable starting materials. The importance of the carbohydrate head group and tail group hydrophobicity for tuning ice recrystallization inhibition (IRI) has recently been demonstrated^{43,44}. However, while IRI activity is desirable, it is not sufficient to make a good CPA – the primary requirements are the ability to permeate biological membranes and the ability to promote intracellular vitrification. Surprisingly, there has been very little work in understanding these aspects in potential synthetic CPAs. The importance of cell permeability has been highlighted in a recent review⁴⁵, and if the search for new CPAs is to be successful,

high quality characterization of both permeability and vitrification propensity are essential. In addition, it is also important to understand how potential cryoprotectants interact with the membrane lipids. Despite their importance, the interaction between penetrating cryoprotectants and membranes is poorly understood in contrast with non-penetrating cryoprotectants such as sugars whose mechanisms of action have been extensively studied^{34,46-50}.

The following sections (1.2-1.8) provide a detailed literature review about the fundamentals of cryobiology, the importance of cryoprotectants and their mechanisms of action.

1.2 Cryobiological damage at the cellular level

For many organisms and cells, moderately low temperatures *per se* are not particularly damaging. However, freezing is often lethal. The formation of an ice crystal is stochastic, which means that the probability of ice formation is proportional to the volume of water available - at a given sub-zero temperature, ice is more likely to form in a large volume than a small volume. As the volume of any individual cell is much lower than the volume of the extracellular aqueous environment, ice will normally form in the extracellular space first.

Ice, however, is a poor solvent – water molecules need to align very specifically with each other in order to form crystalline ice, and the inclusion of any contaminant (salts or other solutes) would disrupt the ice structure. Therefore when an ice crystal forms, it forms as very pure water ice, with very low concentrations of other molecules⁵¹. Thus, the formation of ice outside the cells leads to freeze-concentration of the solutes into a co-existing unfrozen fraction. This fraction will have a much higher concentration of salts, sugars, proteins etc than the isotonic solution.

As a consequence of the increased external concentration, water efflux occurs through the cell membrane in order to restore the osmotic equilibrium. The next step is determined by the cooling rate: if the cooling rate is low enough that the cells have time to expel water and re-equilibrate, the cells will be dehydrated, and will be exposed for long periods to high concentrations of solutes, which can be toxic. This situation is shown schematically in *Fig. 1.1*. Damage under this regime is often known as solution effects injury, as this leads to many irreversible changes, especially damage due to freeze-induced dehydration. On the other hand, if the cells are cooled too fast, the aqueous solution inside the cells becomes supercooled, and eventually ice will nucleate inside the cells. This is called “intracellular ice formation” and usually causes irreparable cell damage^{5,12,52}. Therefore, an intermediate cooling rate is usually ideal as it provides the best compromise between cytotoxicity and ice formation^{13,53,54}, as first proposed by Mazur – the “Two-factor hypothesis”^{12,17}. According to this model, there should be an optimum cooling rate where there is maximum cell viability.

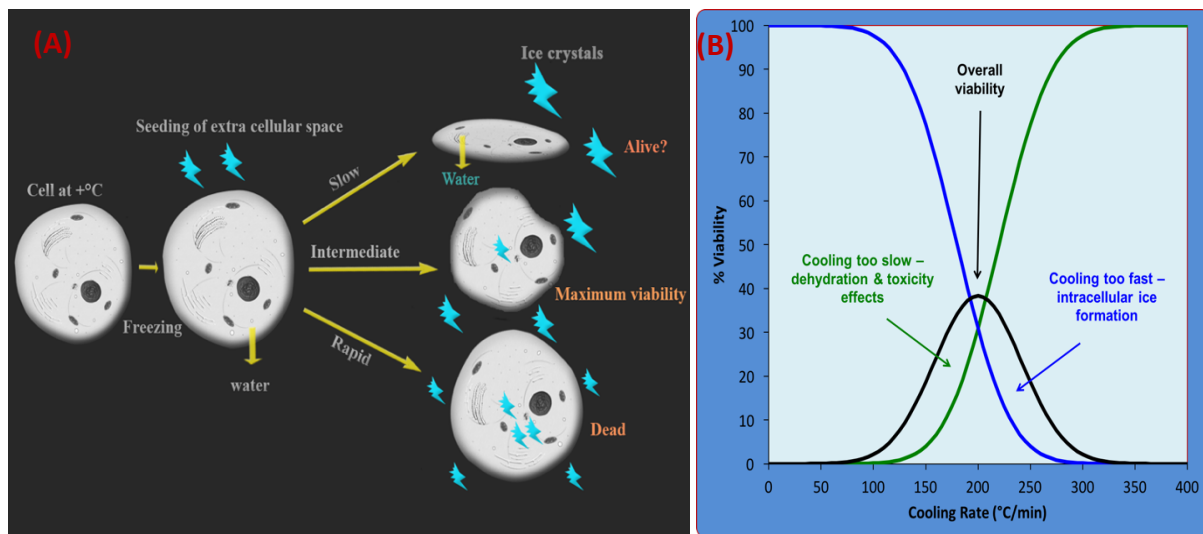


Fig.1.1: Schematic representation of some key aspects of cryopreservation: (A) cooling rate dependent cell viability during freezing: When the cells are cryopreserved, seeding of ice crystal happens initially in the extracellular space and the cells shrink depending on the cooling rate due to osmotic dehydration. With the addition of a suitable cryoprotectant, in many cases there is an intermediate cooling rate for maximum cell viability (adapted from Reference¹³) (B) Mazur's Two-factor hypothesis for maximum cell viability - "solution effects" at slow cooling rates and "Intracellular ice formation (IIF)" at high cooling rates, with maximum viability at some intermediate, optimum cooling rate^{4,17}.

The actual value of any optimal cooling rate is determined by the osmotic properties of the cells and can vary enormously with different cell types. This will be discussed in more detail later. If an optimum cooling rate is found, the cells will undergo moderate shrinking, concentrating the intracellular solutes. There is a minimum critical volume below which the cell can no longer respond osmotically which is called the osmotically inactive volume. Below this value, the cell is considered to be too dehydrated leading to irreversible damage. To prevent dehydration, measures have to be taken to stop the separation of water into pure ice and instead have the entire intracellular solution solidify, forming an amorphous glass (vitrification). Addition of CPAs helps to avoid IIF at rapid cooling rates, helps to depress the equilibrium freezing point and promote vitrification.

Thus, cryobiological damage at the cellular level can generally be split into three effects: (i) low temperature; (ii) direct freezing effects; and (iii) indirect freezing effects. In many cases low temperature *per se* is not a major cause of damage and is more closely related to chilling damage^{55,56}. Thus, in practical terms there are two major causes of damage: (i) intracellular ice formation (IIF); and the indirect effects of ice formation – the stress due to volume excursions and concentration effects as a result of cell osmotic responses. Most of these stresses

are related to dehydration and the transport of water across the cell membrane^{5,24}. Basic knowledge of the multifaceted nature of freezing damage and the discovery of prevention methods, has led to the long-term storage of a number of biological cells.

1.3 Cryoprotective agents

Cryoprotective agents are the substances used to protect biological materials from freezing damage. CPAs serve to prevent damage induced by the freezing process, in part by reducing ice crystal formation and by reducing stress resulting from osmotic shock and dehydration. Consequently, variables such as cell size and membrane permeability are important factors in selecting appropriate cryoprotectants³³. Based on their ability to diffuse across cell membranes, CPAs are usually classified into two broad categories: Penetrating (permeating) and non-penetrating (non-permeating) agents. Permeating cryoprotectants pass through the cell membrane whereas the non-permeating ones do not⁵⁷. Fig.1.2 gives a schematic representation of the manner by which penetrating and non-penetrating cryoprotectants (CPAs) exert their actions upon cells. Both cause the reduction of intracellular water, potentially protecting the cells from lethal intracellular ice³³.

Although many individual compounds have been reported to convey a protective effect in various cellular systems^{33,58,59}, current cryopreservation techniques are mainly based on using additives such as glycerol and dimethyl sulfoxide (DMSO). Polyethylene glycol, propylene glycol, polyvinyl pyrrolidone, sorbitol, dextran and trehalose are other CPAs that have been used occasionally, either alone or in combination. Common groups of penetrating and non-penetrating CPAs are discussed in the following sections^{33,58}.

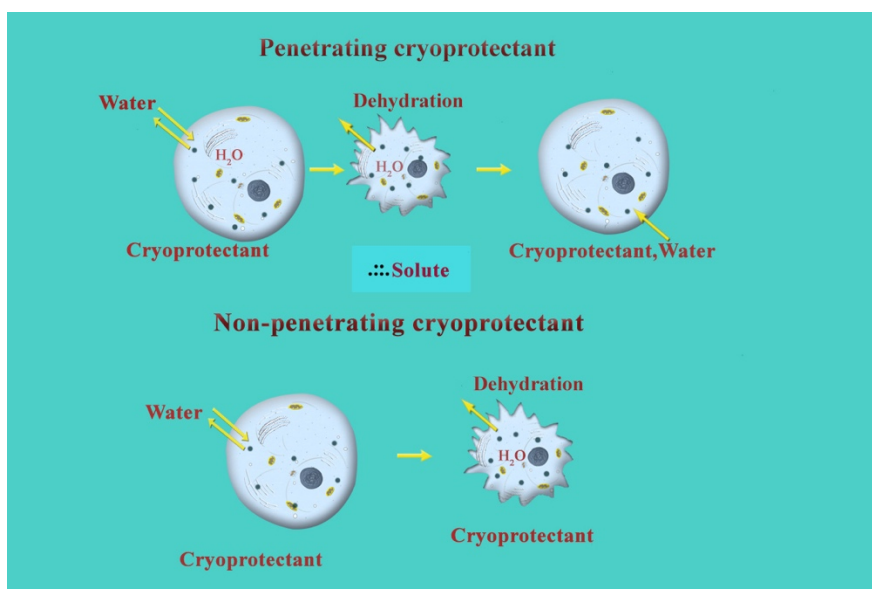


Fig.1.2: Differing actions of penetrating and non-penetrating CPAs:

Penetrating cryoprotectants make the cells contract first and then swell because of the initial movement of water out of the cell, followed by the influx of both cryoprotectant and water. By contrast, non-penetrating cryoprotectants cause the cells to contract, but because they do not penetrate, lead to dehydration³³.

1.3.1 Penetrating (permeating) cryoprotectants

Penetrating cryoprotectants are generally small, non-ionic molecules which are highly water soluble at low temperatures. Given time, these molecules can diffuse through cellular membranes, permeating the cell and reaching equilibrium in the cytoplasm without significant dehydrating. Penetrating cryoprotectants need to be able to both lower the freezing point and increase the glass transition temperature, while reducing the amount of IIF at a given temperature. Additionally, penetrating cryoprotectants act as a solvent and reduce the effective salt concentration in the remaining intracellular water fraction, thereby provide buffering against the salt-induced stress. Common groups of permeating CPAs include sulfoxides, alcohols and amides & imides^{33,58}.

1.3.2 Non-penetrating (Non-permeating) cryoprotectants

Non-penetrating cryoprotectants are generally sugars or long chain polymers and are too large to permeate cells. These compounds increase the osmolarity of the extracellular environment, which results in cellular dehydration (and therefore higher solute concentrations) which reduces the chance of intracellular ice crystal formation³³. It is also postulated that some non-permeating cryoprotectants may adsorb on membrane surfaces, inhibiting ice crystal formation in the immediate vicinity of the cell by keeping ice in the amorphous state^{33,58,60}. Additionally, non-penetrating cryoprotectants are often included in the cell thawing media to help avoid osmotic shock^{2,7,33,61}. Upon thawing, traumatic cell expansion and lysis can occur during the accompanying water influx. Common groups of non-permeating CPAs include sugars and macromolecules/polymers^{7,33,58,59}.

1.3.3 Plant Vitrification Solutions (PVS)

Since the discovery that certain cryoprotectants help the cell survival at ultra-low temperatures, various solution compositions combining many cryoprotectants have been developed for plant cells. Due to their role in preventing ice formation inside the cell by encouraging the formation of glass, these solutions are called “vitrification solutions” or “vitrifying” solutions⁶².

Vitrification Solutions (VSs) are aqueous cryoprotectant solutions which can be cooled slowly to temperatures below the glass transition temperature without appreciable ice formation, either intra or extracellularly. They thus allow the amorphous glass status to be conserved during cooling and thawing, thereby avoiding crystallization⁶³. They usually consist of a mixture of permeating and non-permeating CPAs in order to slightly dehydrate samples, while avoiding cytotoxicity and protecting cells from crystallization of remaining water molecules. Among the vitrification solutions developed for freezing plant tissues, PVS2 (Plant Vitrification Solution 2), designed by Sakai et al. for citrus callus⁶⁴, has been successfully used for the cryopreservation of many species⁶⁵. PVS2 is the most commonly used cryoprotectant solution for plants, and its glass transition temperature is observed to be -115 °C. Though the majority of studies employ PVS2, PVS3⁶⁶ has been notably used for cooling wasabi⁶⁷, asparagus⁶⁶ and garlic^{68,69} shoot apices. Suranthran, P., et al. evaluate the effect of five vitrification solutions (VSs) on the cryopreservation and viability of oil palm poly embryoids⁷⁰. In several studies,

alternative VSs are designed by increasing or decreasing the concentration of the constitutive cryoprotectants (mainly glycerol and sucrose) of the original PVS2 and PVS3^{71,72}.

The cryoprotectants most commonly used in vitrification protocols are dimethyl sulfoxide (DMSO), ethylene glycol (EG), glycerol and sucrose. DMSO, originally used to cryoprotect red blood cells and spermatozoa⁷³, is one of the most widely employed cryoprotectants for animals, plants and micro-organisms. It permeates cells very rapidly, even at low temperature, and has a good glass-forming tendency^{57,63}. EG is known for its rapid permeability and ice blocking tendency. Glycerol is less permeable than DMSO and EG, due to its higher molecular weight and viscosity. Sugars are often added in cryoprotectant mixtures as they aid dehydration and act as an osmotic buffer. They may also preserve the integrity of membranes in the dry state by substituting for water⁷⁴. In vitrification protocols, the duration of exposure of explants to PVS2 is usually very short due to its cytotoxicity⁷².

1.4 Effect of cryoprotectants on cell membranes

The basic structure of a cell membrane is a lipid bilayer which controls the movement of water and solute molecules in and out of the cell. In this way, cell membranes act as a selective permeability barrier between the intracellular space and the extra cellular environment. Cell viability is directly related to the proper functioning of this permeability barrier. Cellular dehydration caused by freezing leads to changes in the membrane lipid bilayer structure (*Fig.1.3*). This may affect the normal permeability barrier function of the membrane leading to cell death^{34,75-77}. There is evidence that some cryoprotectants may directly interact with cell membrane lipids and proteins and help to stabilize the membrane structure^{78,79}.

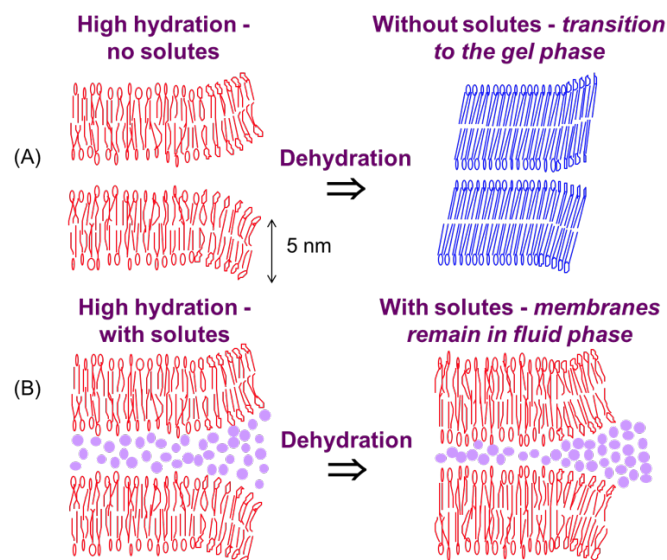


Fig.1.3: Schematic representation of the effect of dehydration in the cell membrane lipid organization:

(A) Without solutes cell membrane transition takes place from liquid to gel phase (B) Presence of solutes enables the cell membrane to remain in the fluid phase⁸⁰.

Several studies have been carried out on the effects of non-penetrating CPAs such as sugars especially disaccharides and their mechanisms of action are becoming clearer^{34,46,47,50,75,80-83}. During dehydration, these solutes are known to protect cellular membranes by lowering deleterious phase transition temperatures^{48,84,85} (*Fig.1.3*). The studies of the effects of sugars on membrane phase transitions at different hydrations suggest that these damaging effects are primarily due to non-specific osmotic and volumetric effects^{48,80}. In order to explain how sugar molecules help to protect from lethal phase transitions, two molecular scale theories have been proposed called water replacement hypothesis (WRH) and the hydration forces explanation (HFE)⁸⁰, which are not mutually exclusive, and are discussed in detail elsewhere^{34,50,81-83}.

The effects of penetrating cryoprotectants have been less widely studied, with most attention being given to DMSO and Glycerol^{61,86-92}. The interaction between DMSO and cell membrane lipids has been studied using Small angle X-ray scattering (SAXS), differential scanning calorimetry (DSC), nuclear magnetic resonance (NMR), small-angle neutron scattering (SANS), and infrared (IR) spectroscopy as well as molecular dynamics (MD) simulations and the findings have been summarized elsewhere⁹³. Many studies have shown that the influence of DMSO on membranes is concentration-dependent⁹⁴. Yu and Quinn conducted extensive studies of the interaction between DMSO and phospholipid membranes, demonstrating that DMSO destabilizes the lamellar liquid-crystal phase in favour of the gel phase, summarized in their review paper⁸⁶. It has also been shown that DMSO can penetrate across a lipid bilayer⁶¹ and can limit membrane compression by partitioning between intermembrane space and forming a physical barrier at appropriate concentrations⁹⁵. Cheng and co-workers reported from SAXS and NMR studies that DMSO causes dehydration near DPPC lipid membrane⁹⁶, and this DMSO-induced dehydration has also been studied using SAXS and SANS⁹⁴. Insights into the molecular mechanism of the interaction of DMSO with phosphocholine bilayers has been gained by MD simulation studies^{87,89,95,97} which showed that at low concentrations, DMSO caused membrane thinning as well as increased membrane fluidity whereas at high concentrations it caused pore formation. Similarly, Schrader and co-workers studied the effect of DMSO and Glycerol on DPPC membranes and found that they have contrasting effects on membrane surface hydration dynamics and forces⁹⁸. Gironi and co-workers measured the effects of DMSO on bilayers in the frozen state, and noted that the presence of DMSO significantly reduced the amount of unfrozen water, but also dehydrated the lipid headgroups⁹⁹.

1.5 Cryoprotectant toxicity and damage

Though the purpose of cryoprotectants is to prevent damage during freezing, some of these compounds, especially penetrating CPAs, can themselves result in cell damage. Thus, care is needed in the selection of an appropriate CPA, and its concentration, to achieve effective cryoprotection⁹. The various types of CPAs, their general classification, mechanism of action, toxicity etc. are detailed in several publications^{7,33,58-60,100-106}. In addition, innovative approaches that integrate bio-inspired and dynamic-hydrogel cryoprotectants at high concentrations in tissue and organ preservation have been proposed to alleviate the existing toxicity problems^{26,30}. In particular, two recent reviews of cryoprotectant toxicity by Fahy¹⁰⁴ and Best¹⁰⁶ summarize the major issues around cryoprotectant toxicity and toxicity

reduction. There are two primary mechanisms of toxicity: toxicity to the cell membrane; and damage due to the oxidative effect of CPAs. The toxicity of cryoprotectants is related to the temperature at which they are added, the exposure time and the concentration³³, so cryopreservation protocols try to minimize damage by optimizing these conditions.

1.5.1 Toxicity reduction by cryoprotectant combinations

It has been found in several studies that toxicity can be reduced by combining CPAs - multiple CPAs interact with each other, neutralizing the toxic effects^{107,108}. Penetrating CPAs are used with non-penetrating CPAs because extra cellular ice formation (EIF) happens more rapidly than IIF¹⁰⁹. Sugar molecules show low toxicity and are often used as extracellular CPAs. Very early examples of this are in cryopreservation of embryos of mice¹¹⁰ and cows¹¹¹. Both of these landmark papers utilized a protocol that combined DMSO, sucrose, and poly vinyl pyrrolidone. Combining multiple cryoprotectants may also alleviate, or at least reduce, toxicity by one cryoprotectant counteracting the negative effects of another. Many successful cryopreservation protocols now utilize a combination of permeating and non-permeating CPAs in conjunction with macromolecule supplementation, and this approach is undoubtedly a large reason for improved efficacy.

1.5.2 Other means of reducing CPA toxicity

Permeating CPAs may be added at lower temperatures in order to reduce toxicity. Different equilibration times may be required based on the speed of permeation of the CPAs and the cell type. Normally, equilibration periods are longer at lower temperatures than at higher temperatures³³. Stepwise addition of cryoprotective agents, or gradually increasing concentrations, has also been used to reduce toxicity^{112,113}. Additionally, stepwise removal of these compounds upon warming/thawing helps to minimize osmotic stress^{112,113}. Furthermore, altering the ionic composition of the carrier solution in which the cryoprotectant is dissolved offers another means of mitigating damage^{33,114}.

1.6 Biophysical properties of cells

Cell biophysical properties include the osmotically inactive volume (V_b), water permeability (hydraulic conductivity) and the CPA/solute permeability^{22,115}. These properties can be determined using mathematical equations which were first described by Jacobs¹¹⁶ and later modified.

1.6.1 Determination of osmotically inactive volume V_b using Boyle-Van't Hoff (BVH) plot

V_b (osmotically inactive volume / the osmotic ballast) is the portion of the cell volume that does not respond to osmotic pressure. This can be determined by exposing the cell to different concentrations of anisotonic solutions containing an impermeable solute and allowing for equilibration. The cell volume before and after exposure are calculated, assuming the cells are spherical. Normalized cell volumes are calculated, plotted against the inverse osmolality and the fitted straight line is extrapolated to find the volume at infinite osmolality which is V_b (see *Fig. 1.4*).

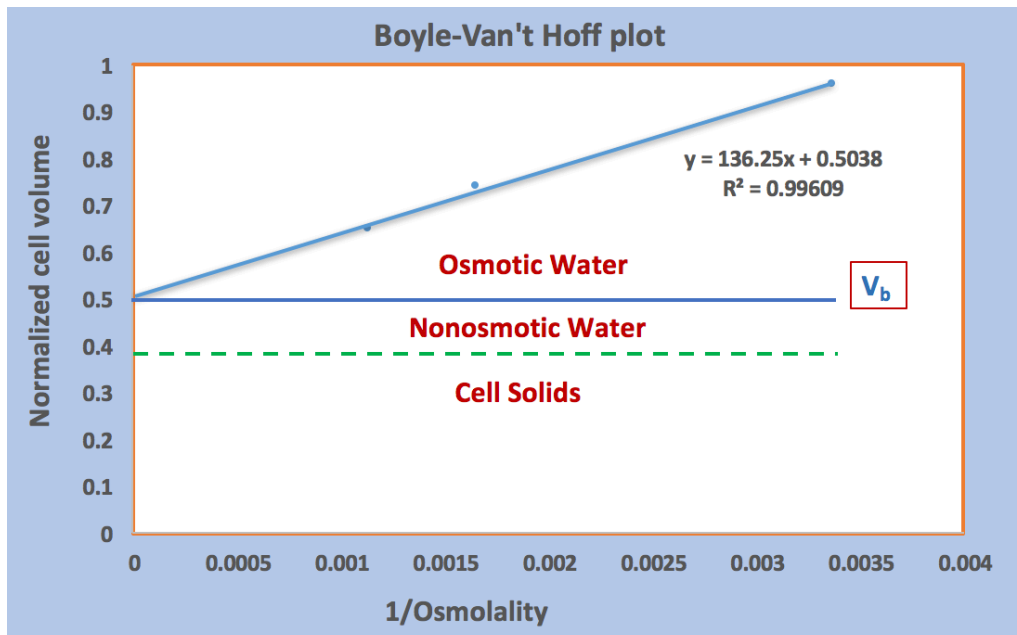


Fig.1.4: Schematic of BVH plot representing the osmotically inactive volume V_b of the cell –

Here in the example, V_b is 50% of the cell volume out of which 10% is non-osmotic water (also called bound water) and the remaining 40% is composed of cell solids. 10% of cell water is bound by hydrogen bonding with macromolecules, as has been experimentally confirmed through differential scanning calorimetry (DSC)^{117,118}. This is often called “unfreezable” water, though this terminology has been questioned¹¹⁹.

1.6.2 Cell membrane permeability of cryoprotectants

CPAs must enter the cell in order to provide cryoprotection, so cell permeability is widely known to be one of the most important parameters that determines the cryobiological potential of a molecule⁹⁻¹¹. Osmotic effects at the time of CPA addition have significant effects on the cell volume kinetics during the freezing process¹¹⁻¹⁵. The permeability of a cell membrane is generally determined by analyzing the volume response of the cells to a change in the osmotic environment. As the cell membrane is more permeable to water than anything else, cells initially expel water in an attempt to restore osmotic balance when they are treated with hypertonic solutions. As a result, cells begin to shrink. If the hypertonic medium does not contain permeating molecules (such as salts or sugars) then it reaches a new equilibrium size. However, if the medium contains a permeable cryoprotectant, it slowly begins to penetrate the cell, and the cell responds by taking up both cryoprotectant and water and swelling back approximately to its initial volume^{9,11}. This total response of the cells can be described as “shrink-swell behavior” as shown in Fig.1.5. A reverse process occurs at the time of CPA removal after thawing.

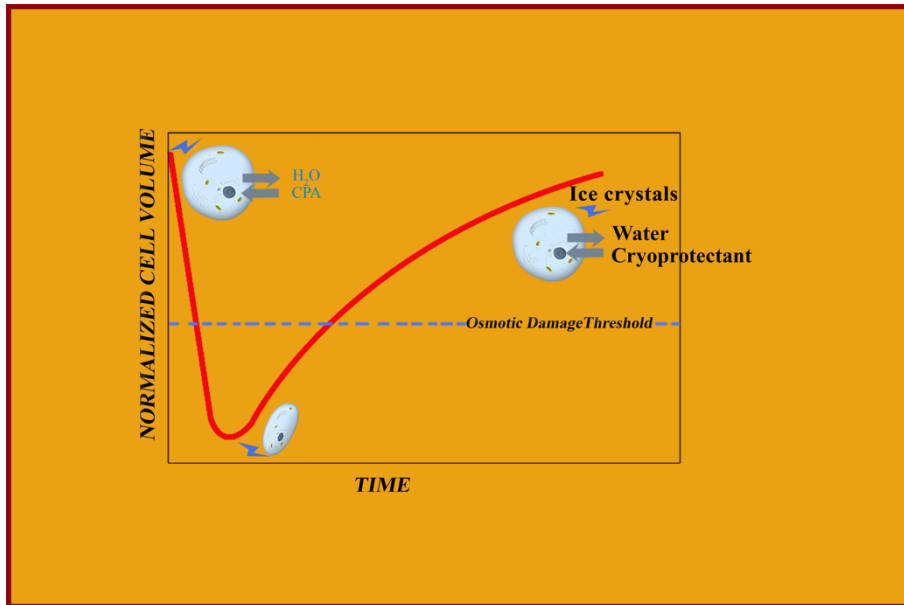


Fig.1.5: Shrink–swell behavior of an individual cell upon addition of a penetrating CPA (adapted from Reference⁹).

Permeability parameters can be determined using the standard estimation techniques by fitting the mathematical model to measurements of cell volume response during a shrink–swell experiment. For these experiments to be accurate, large single spherical cells are required, and the most efficient method is to trap single cells using a microfluidic perfusion device^{22,23}, which also helps to rapidly change the cell osmotic environment. Recent work by Shu and co-workers²⁰ aimed to find better cryopreservation protocols for human vaginal immune cells through shrink-swell experiments using a microfluidic perfusion device.

1.6.3 Estimation of permeability parameters

There are several formalisms to find the membrane permeability parameters. Mazur and colleagues^{120,121} introduced the first one-parameter model for calculating solute permeability. This was refined to a two-parameter model called 2P^{116,122} for finding water and solute permeability. Kedem and Katchalsky¹²² developed the three-parameter model (also called the Kedem–Katchalsky (KK) formalism) which is most commonly used today. The KK formalism adds a ‘ σ ’ term to the 2P, which is the term representing the interaction between solute and solvent¹²³. An Arrhenius plot is used to find the activation energies of these permeability parameters¹²³. It has been shown that the knowledge of these so-called “fundamental cryobiological characteristics” of the cell membranes may enable the design of protocols to minimize freezing damage^{124,125}.

1.7 Methods and techniques used to measure cell permeability

A number of methods have been used to measure cell permeability, including stopped-flow light scattering¹²⁶⁻¹²⁸, electronic particle counters¹²⁹, differential scanning calorimetry¹³⁰ and micropipette perfusion¹³¹. However, many of these methods have their own disadvantages described elsewhere¹¹.

The simplest method for studying cell permeability is to microscopically measure the cell volume change of isolated large spherical cells. Cells must not overlap and should not move during the osmotic excursion. A simple method of cell immobilization is the surface coating of the experimental device (usually coverslips) with chemicals that can provide cell attachment as described by Xu et al.,^{132,133}. One disadvantage of this method is that the spherical shape of the cells can be lost due to surface attachment in some cases.

Innovations in microfluidic technologies offer a tremendous potential to revolutionize cryopreservation. In recent years, several microfluidic devices with perfusion chambers²³ or single cell traps^{11,134,135} have been developed, some of them specifically for the measurement of cell permeability^{10,23,45,136,137}. Microfluidic devices are now considered essential technology in cell biology, as they enable the user to: (i) monitor the changes of cellular conditions following the perfusion of various media; (ii) confine cells within a chamber/trap and preventing imaging ambiguity due to the overlapping of cells or their movement out of the focal plane; (iii) study the single cell response to osmotic pressure and calculate the cell membrane parameters; (iv) use low cell numbers and reagent volumes; and (v) perform kinetic analysis of non-adherent suspension cells by maintaining their position in place over long times without any dislodgement during image acquisition^{23,134}. Technological advances in high-resolution three dimensional (3D) printing with direct laser writing (DLW) using multi-photon polymerization has enabled the fabrication of microfluidic devices in a single step¹³⁸⁻¹⁴¹. Compared to conventional lithography techniques, DLW accelerates the fabrication procedure, and more importantly, enables the fabrication of arbitrary 3D structures with high resolution¹⁴²⁻¹⁴⁶.

1.8 Future cryoprotectants

Currently researchers are looking to develop novel cryoprotective agents (CPAs) for the preservation of wide variety of cells with maximum viability and avoiding the toxicity associated with traditional cryopreservation media used today. Some of those recent studies are summarized below.

A new study by Zylberberg and co-workers²⁵ investigated non-toxic, bio-inspired DMSO-free CPAs. These novel compounds are based on mixtures of natural compounds with antioxidative and cell preserving properties. Preliminary cryopreservation trials with these novel compounds have been carried out and the results were promising. Cell viabilities were tested, and results were comparable to standard cryoprotectants based on DMSO. Another study by Demirci & Assal²⁶ has reported the preservation of human red blood cells with bio-inspired CPAs based on natural cryo-inks, such as trehalose solutions and ectoine. Briard and coworkers^{27,28} have examined various natural antifreeze (glyco) proteins (AF(G)Ps) found in the inhabitants of cold and sub-zero environments, and these also gave promising results. Their early work led to

developing the analogues of carbon-linked glycoprotein (C-AFGP) that shows custom-tailored antifreeze behaviour. These C-AFGPs are also efficient ice recrystallization inhibitors and have been used for the effective cryopreservation of human liver cells with reduced DMSO concentrations. Detailed structural and functional studies on these compounds revealed that several classes of carbohydrate-based molecules are very effective ice recrystallization inhibitors as well as effective cryoprotectants at very low concentrations. Leclere, M. et al.,²⁹ also published the effect of C-AFGP analogues as novel cryoprotectants.

Another study by Mark and co-workers³⁰ introduced dynamic-hydrogel cryoprotectants for the preservation of tissue and organs. Nakagawa et al.,³¹ examined the cryoprotective ability of betaine-type metabolite analogs. Verdanova et al.,³² recently published an evaluation of Sericin as a Fetal Bovine Serum (FBS) - replacing cryoprotectant. The allergic reaction of FBS is problematic for its use in medical applications. Sericin when used as a substitute for DMSO and FBS in the cryopreservation medium has provided satisfactory results. The search for alternative cryoprotectants is thus a very active research field.

1.9 Aims of the thesis and Research questions

In the context articulated above, the study of the behavior of individual cells to CPAs provides a starting point for analysis of how they can protect the cells from freezing damage during cryopreservation. So, the aims of this project are:

- To understand the physical mechanisms of membrane protection by traditional cryoprotectants.
- To develop techniques to investigate the critical molecular properties that lead to good cryoprotective performance.
- To use this knowledge to test novel non-toxic compounds which can be optimized for use as CPAs

In line with the above aims, this research aims to answer the following questions.

- How do traditional cryoprotectants interact with cell membrane lipids?
- Can we develop methods to more efficiently characterize the important biophysical parameters of potential new CPAs?
- Is there a link between permeability of different cryoprotectants and their protective effects?

1.10 Overview of the thesis

This thesis is organized in 7 Chapters.

Chapter 2 presents the materials and methods, and outlines the relevant experimental techniques used: Langmuir studies, DSC and cell volume kinetics; as well as the design and application of cryopreservation protocols.

Chapter 3 presents Langmuir studies of the effects of traditional penetrating cryoprotectants on cell membrane lipids.

Chapter 4 reports glass transition and cell permeability studies of novel carbohydrate derivatives (n-Octyl glycosides and thioglycosides) to assess their potential as novel cryoprotectants.

Chapter 5 presents the results of glass transition, cell membrane permeability and cryopreservation studies of modified trehalose derivatives.

Chapter 6 presents an improved method for measuring cell permeability using microfluidic technologies.

Chapter 7 integrates the work in the thesis and presents conclusions and suggestions for future work.

1.11 References

- 1 Kaczmarczyk, A., Rokka, V.-M. & Keller, E. J. Potato shoot tip cryopreservation. A review. *Potato Research* **54**, 45-79 (2011).
- 2 Elliott, G. D., Wang, S. & Fuller, B. J. Cryoprotectants: A review of the actions and applications of cryoprotective solutes that modulate cell recovery from ultra-low temperatures. *Cryobiology* **76**, 74-91, doi:<https://doi.org/10.1016/j.cryobiol.2017.04.004> (2017).
- 3 Wolkers, W. F. *et al.* Factors affecting the membrane permeability barrier function of cells during preservation technologies. *Langmuir* **35**, 7520-7528 (2018).
- 4 Mazur, P. Cryobiology: the freezing of biological systems. *Science* **168**, 939-949, doi:10.1126/science.168.3934.939 (1970).
- 5 Wolfe, J. & Bryant, G. Cellular cryobiology: thermodynamic and mechanical effects. *International Journal of Refrigeration-Revue Internationale Du Froid* **24**, 438-450, doi:10.1016/s0140-7007(00)00027-x (2001).
- 6 Polge, C., Smith, A. U. & Parkes, A. Revival of spermatozoa after vitrification and dehydration at low temperatures. *Nature* **164**, 666 (1949).
- 7 Fuller, B. J. Cryoprotectants: the essential antifreezes to protect life in the frozen state. *CryoLetters* **25**, 375-388 (2004).
- 8 Zheng, Y., Zhao, G., Zhang, Y. & Gao, R. On-chip loading and unloading of cryoprotectants facilitate cell cryopreservation by rapid freezing. *Sensors and Actuators B: Chemical* **255**, 647-656 (2018).
- 9 Toner, J. O. M. K. a. M. in *Principles of Tissue Engineering (Second Edition)* (eds Robert Langer & Joseph Vacanti) 293-307 (Academic Press, 2000).
- 10 Zhao, G. & Fu, J. Microfluidics for cryopreservation. *Biotechnology Advances* **35**, 323-336, doi:<http://dx.doi.org/10.1016/j.biotechadv.2017.01.006> (2017).
- 11 Weng, L. *et al.* A highly-occupied, single-cell trapping microarray for determination of cell membrane permeability. *Lab on a Chip* **17**, 4077-4088 (2017).

- 12 Mazur, P. Kinetics of water loss from cells at subzero temperatures and the likelihood of Intracellular freezing. *The Journal of General Physiology* **47**, 347-369 (1963).
- 13 Mazur, P. Freezing of living cells: mechanisms and implications. *American Journal of Physiology-Cell Physiology* **247**, C125-C142 (1984).
- 14 Weng, L., Li, W. & Zuo, J. Kinetics of osmotic water flow across cell membranes in non-ideal solutions during freezing and thawing. *Cryobiology* **61**, 194-203 (2010).
- 15 Weng, L., Li, W., Chen, C. & Zuo, J. Kinetics of coupling water and cryoprotectant transport across cell membranes and applications to cryopreservation. *The Journal of Physical Chemistry B* **115**, 14721-14731 (2011).
- 16 Levin, R. L. & Miller, T. W. An optimum method for the introduction or removal of permeable cryoprotectants: Isolated cells. *Cryobiology* **18**, 32-48, doi:[http://dx.doi.org/10.1016/0011-2240\(81\)90004-3](http://dx.doi.org/10.1016/0011-2240(81)90004-3) (1981).
- 17 Mazur, P., Leibo, S. & Chu, E. A two-factor hypothesis of freezing injury: evidence from Chinese hamster tissue-culture cells. *Experimental Cell Research* **71**, 345-355 (1972).
- 18 Mazur, P. Equilibrium, quasi-equilibrium, and nonequilibrium freezing of mammalian embryos. *Cell Biophysics* **17**, 53-92 (1990).
- 19 Kleinhans, F. W. & Mazur, P. Determination of the water permeability (Lp) of mouse oocytes at -25 degrees C and its activation energy at subzero temperatures. *Cryobiology* **58**, 215-224, doi:10.1016/j.cryobiol.2008.12.008 (2009).
- 20 Shu, Z. *et al.* A study of the osmotic characteristics, water permeability, and cryoprotectant permeability of human vaginal immune cells. *Cryobiology* **72**, 93-99, doi:10.1016/j.cryobiol.2016.03.003 (2016).
- 21 Tseng, H.-Y. *et al.* A microfluidic study of megakaryocytes membrane transport properties to water and dimethyl sulfoxide at suprazero and subzero temperatures. *Biopreservation and Biobanking* **9**, 355-362 (2011).
- 22 Chen, H.-h. *et al.* A microfluidic study of mouse dendritic cell membrane transport properties of water and cryoprotectants. *International Journal of Heat and Mass Transfer* **51**, 5687-5694, doi:10.1016/j.ijheatmasstransfer.2008.04.013 (2008).
- 23 Chen, H. H., Purtteman, J. J., Heimfeld, S., Folch, A. & Gao, D. Development of a microfluidic device for determination of cell osmotic behavior and membrane transport properties. *Cryobiology* **55**, 200-209, doi:10.1016/j.cryobiol.2007.08.001 (2007).
- 24 Lyu, S.-R., Chen, W.-J. & Hsieh, W.-H. Measuring transport properties of cell membranes by a PDMS microfluidic device with controllability over changing rate of extracellular solution. *Sensors and Actuators B: Chemical* **197**, 28-34 (2014).
- 25 Zylberberg, C., Pasley, S. & Matosevic, S. Novel bio-inspired DMSO-free cryoprotectants for hard-to-preserve cell. *Cytotherapy* **17**, S75 (2015).
- 26 Demirci, U. & Assal, R. E. 53. Bio-inspired cryoprotectants and microfluidics for cryopreservation. *Cryobiology* **71**, 178, doi:<http://dx.doi.org/10.1016/j.cryobiol.2015.05.059> (2015).
- 27 Briard, J. G. *et al.* Small molecule ice recrystallization inhibitors – A novel class of cryoprotectants. *Cryobiology* **71**, 540-541, doi:10.1016/j.cryobiol.2015.10.018 (2015).

- 28 Briard, J. *et al.* Carbohydrate-based small molecule ice recrystallization inhibitors as cryopreservatives for red blood cells. *Cryobiology* **71**, 554, doi:10.1016/j.cryobiol.2015.10.072 (2015).
- 29 Leclere, M., Kwok, B. K., Wu, L. K., Allan, D. S. & Ben, R. N. C-linked antifreeze glycoprotein (C-AFGP) analogues as novel cryoprotectants. *Bioconjugate Chemistry* **22**, 1804-1810 (2011).
- 30 Kline, M., Dreyer, M., Gyring, P., Lifson, M. & Assal, R. E. 60. Innovative cryoprotectants for tissue and organ preservation. *Cryobiology* **71**, 180, doi:10.1016/j.cryobiol.2015.05.066 (2015).
- 31 Nakagawa, Y., Sota, M. & Koumoto, K. Cryoprotective ability of betaine-type metabolite analogs during freezing denaturation of enzymes. *Biotechnology Letters* **37**, 1607-1613 (2015).
- 32 Verdanova, M., Pytlik, R. & Kalbacova, M. H. Evaluation of sericin as a fetal bovine serum-replacing cryoprotectant during freezing of human mesenchymal stromal cells and human osteoblast-like cells. *Biopreservation and Biobanking* **12**, 99-105 (2014).
- 33 Chian, R.-C. & Quinn, P. *Fertility cryopreservation*. (Cambridge University Press, 2010).
- 34 Garvey, C. J., Lenne, T., Koster, K. L., Kent, B. & Bryant, G. Phospholipid membrane protection by sugar molecules during dehydration-insights into molecular mechanisms using scattering techniques. *Int J Mol Sci* **14**, 8148-8163, doi:10.3390/ijms14048148 (2013).
- 35 Wolfe, J. & Bryant, G. *Cryobiology and anhydrobiology of cells*. Sydney: University of New South Wales (2004).
- 36 Yu, Z.-W. & Quinn, P. J. Solvation effects of dimethyl sulphoxide on the structure of phospholipid bilayers. *Biophysical Chemistry* **70**, 35-39 (1998).
- 37 Balcerzak, A. K., Capicciotti, C. J., Briard, J. G. & Ben, R. N. Designing ice recrystallization inhibitors: From antifreeze (glyco) proteins to small molecules. *RSC Advances* **4**, 42682-42696 (2014).
- 38 Storey, K. B. & Storey, J. M. Natural freezing survival in animals. *Annual Review of Ecology and Systematics* **27**, 365-386, doi:10.1146/annurev.ecolsys.27.1.365 (1996).
- 39 Tarkowski, t. P. & Van den Ende, W. Cold tolerance triggered by soluble sugars: a multifaceted countermeasure. *Frontiers in Plant Science* **6**, 203 (2015).
- 40 Capicciotti, C. J. *et al.* Potent inhibition of ice recrystallization by low molecular weight carbohydrate-based surfactants and hydrogelators. *Chemical Science* **3**, 1408-1416 (2012).
- 41 Capicciotti, C. J. *et al.* O-aryl-glycoside ice recrystallization inhibitors as novel cryoprotectants: A structure–function study. *ACS Omega* **1**, 656-662 (2016).
- 42 Davies, P. L., Baardsnes, J., Kuiper, M. J. & Walker, V. K. Structure and function of antifreeze proteins. *Philosophical Transactions of the Royal Society of London. Series B: Biological Sciences* **357**, 927-935 (2002).
- 43 Adam, M. K. *et al.* Photoswitchable carbohydrate-based fluorosurfactants as tuneable ice recrystallization inhibitors. *Carbohydrate Research* **439**, 1-8, doi:10.1016/j.carres.2016.12.004 (2017).
- 44 Adam, M. K. *et al.* Carbohydrate-based surfactants as photocontrollable inhibitors of ice recrystallization. *Rsc Advances* **6**, 39240-39244, doi:10.1039/c6ra07030b (2016).

- 45 Edashige, K. Permeability of the plasma membrane to water and cryoprotectants in mammalian oocytes and embryos: Its relevance to vitrification. *Reproductive Medicine and Biology* **16**, 36-39 (2017).
- 46 Kent, B. *et al.* Direct Comparison of Disaccharide Interaction with Lipid Membranes at Reduced Hydrations. *Langmuir* **31**, 9134-9141, doi:10.1021/acs.langmuir.5b02127 (2015).
- 47 Lenné, T., Garvey, C. J., Koster, K. L. & Bryant, G. Effects of Sugars on Lipid Bilayers during Dehydration – SAXS/WAXS Measurements and Quantitative Model. *The Journal of Physical Chemistry B* **113**, 2486-2491, doi:10.1021/jp808670t (2009).
- 48 Koster, K. L., Lei, Y. P., Anderson, M., Martin, S. & Bryant, G. Effects of vitrified and nonvitrified sugars on phosphatidylcholine fluid-to-gel phase transitions. *Biophysical Journal* **78**, 1932-1946 (2000).
- 49 Lenné, T., Bryant, G., Holcomb, R. & Koster, K. L. How much solute is needed to inhibit the fluid to gel membrane phase transition at low hydration? *Biochimica et Biophysica Acta (BBA)-Biomembranes* **1768**, 1019-1022 (2007).
- 50 Kent, B. *et al.* Measurement of glucose exclusion from the fully hydrated DOPE inverse hexagonal phase. *Soft Matter* **6**, 1197, doi:10.1039/b919086d (2010).
- 51 Oughton, J., Xu, S. & Battino, R. The purification of water by freeze-thaw or zone melting. *J. Chem. Educ* **78**, 1373 (2001).
- 52 Fuller, B. J., Lane, N., Benson, E. E. & Mazur, P. in *Life in the frozen state* 3-65 (CRC Press, 2004).
- 53 Campbell, L. H. & Brockbank, K. G. M. *Cryopreservation of adherent cells on a fixed substrate*. (2014).
- 54 Taylor, M. *Sub-zero preservation and the prospect of long-term storage of multicellular tissues and organs*. (Oxford University Press, Oxford, 1984).
- 55 MacMillan, H. A., Baatrup, E. & Overgaard, J. Concurrent effects of cold and hyperkalaemia cause insect chilling injury. *Proceedings of the Royal Society B: Biological Sciences* **282**, 20151483, doi:10.1098/rspb.2015.1483 (2015).
- 56 Atwell, B. J., Kriedemann, P. E. & Turnbull, C. G. *Plants in action: Adaptation in nature, performance in cultivation*. (Macmillan Education AU, 1999).
- 57 Taylor, R., Adams, G., Boardman, C. & Wallis, R. Cryoprotection—permeant vs nonpermeant additives. *Cryobiology* **11**, 430-438 (1974).
- 58 Hubálek, Z. Protectants used in the cryopreservation of microorganisms. *Cryobiology* **46**, 205-229, doi:10.1016/s0011-2240(03)00046-4 (2003).
- 59 KAROW, A. M. Cryoprotectants—a new class of drugs. *Journal of Pharmacy and Pharmacology* **21**, 209-223 (1969).
- 60 Sieme, H., Oldenhof, H. & Wolkers, W. F. Mode of action of cryoprotectants for sperm preservation. *Animal Reproduction Science* **169**, 2-5, doi:<http://dx.doi.org/10.1016/j.anireprosci.2016.02.004> (2016).
- 61 Anchoroguy, T. J., Rudolph, A. S., Carpenter, J. F. & Crowe, J. H. Modes of interaction of cryoprotectants with membrane phospholipids during freezing. *Cryobiology* **24**, 324-331 (1987).
- 62 Volk, G. M. & Walters, C. Plant vitrification solution 2 lowers water content and alters freezing behavior in shoot tips during cryoprotection. *Cryobiology* **52**, 48-61 (2006).

- 63 Fahy, G. M., Levy, D. & Ali, S. Some emerging principles underlying the physical properties, biological actions, and utility of vitrification solutions. *Cryobiology* **24**, 196-213 (1987).
- 64 Sakai, A., Kobayashi, S. & Oiyama, I. Cryopreservation of nucellar cells of navel orange (*Citrus sinensis* Osb. var. *brasiliensis* Tanaka) by vitrification. *Plant Cell Reports* **9**, 30-33 (1990).
- 65 Sakai, A. & Engelmann, F. Vitrification, encapsulation-vitrification and droplet-vitrification: A review. *CryoLetters* **28**, 151-172 (2007).
- 66 Nishizawa, S., Sakai, A., Amano, Y. & Matsuzawa, T. Cryopreservation of asparagus (*Asparagus officinalis* L.) embryogenic suspension cells and subsequent plant regeneration by vitrification. *Plant Science* **91**, 67-73 (1993).
- 67 Matsumoto, T., Sakai, A., Takahashi, C. & Yamada, K. Cryopreservation of in vitro-grown apical meristems of wasabi (*Wasabia japonica*) by encapsulation-vitrification method. *Cryo-letters (United Kingdom)* (1995).
- 68 Makowska, Z., Keller, J. & Engelmann, F. Cryopreservation of apices isolated from garlic (*Allium sativum* L.) bulbils and cloves. *Cryo-letters* **20**, 175-182 (1999).
- 69 Huang, H. *et al.* Thermostabilization by foam drying of a recombinant anthrax vaccine. *Cryobiology* **71**, 550, doi:10.1016/j.cryobiol.2015.10.057 (2015).
- 70 Suranthran, P. *et al.* Effect of loading and vitrification solutions on survival of cryopreserved oil palm polyembryoids. *Plant Growth Regulation* **66**, 101-109, doi:10.1007/s10725-011-9633-7 (2012).
- 71 Kim, H.-H. *et al.* Cryopreservation of garlic bulbil primordia by the droplet-vitrification procedure. *CryoLetters* **27**, 143-153 (2006).
- 72 Kim, H.-H. *et al.* Development of alternative plant vitrification solutions in droplet-vitrification procedures. *CryoLetters* **30**, 320-334 (2009).
- 73 Lovelock, J. & Bishop, M. Prevention of freezing damage to living cells by dimethyl sulphoxide. (1959).
- 74 Potts, M. Desiccation tolerance of prokaryotes. *Microbiological Reviews* **58**, 755-805 (1994).
- 75 Wolfe, J. & Bryant, G. Freezing, drying, and/or vitrification of membrane-solute-water systems. *Cryobiology* **39**, 103-129, doi:10.1006/cryo.1999.2195 (1999).
- 76 Maurel, C. Aquaporins and water permeability of plant membranes. *Annual Review of Plant Biology* **48**, 399-429 (1997).
- 77 Koster, K. & Bryant, G. Dehydration in model membranes and protoplasts: contrasting effects at low, intermediate and high hydrations. *Cold hardiness in plants. CAB International Press, Wallingford*, 219-234 (2006).
- 78 Timasheff, S. Preferential interactions in protein-water-cosolvent systems. *Biophysics of Water, Wiley, New York*, 70-72 (1982).
- 79 Anchooguy, T. J., Cecchini, C. A., Crowe, J. H. & Crowe, L. M. Insights into the cryoprotective mechanism of dimethyl sulfoxide for phospholipid bilayers. *Cryobiology* **28**, 467-473 (1991).
- 80 Bryant, G., Koster, K. L. & Wolfe, J. Membrane behaviour in seeds and other systems at low water content: the various effects of solutes. *Seed Science Research* **11**, 17-25 (2001).
- 81 Kent, B. *et al.* Localization of trehalose in partially hydrated DOPC bilayers: insights into cryoprotective mechanisms. *J R Soc Interface* **11**, 20140069, doi:10.1098/rsif.2014.0069 (2014).

- 82 Lenne, T., Garvey, C. J., Koster, K. L. & Bryant, G. Kinetics of the lamellar gel-fluid transition in phosphatidylcholine membranes in the presence of sugars. *Chem Phys Lipids* **163**, 236-242, doi:10.1016/j.chemphyslip.2009.12.001 (2010).
- 83 Kent, B., Garvey, C. J., Cookson, D. & Bryant, G. The inverse hexagonal – inverse ribbon – lamellar gel phase transition sequence in low hydration DOPC:DOPE phospholipid mixtures. *Chemistry and Physics of Lipids* **157**, 56-60, doi:<http://dx.doi.org/10.1016/j.chemphyslip.2008.10.003> (2009).
- 84 Koster, K. L., Maddocks, K. J. & Bryant, G. Exclusion of maltodextrins from phosphatidylcholine multilayers during dehydration: effects on membrane phase behaviour. *European Biophysics Journal* **32**, 96-105 (2003).
- 85 Bryant, G. & Koster, K. L. Dehydration of solute–lipid systems: hydration forces analysis. *Colloids and Surfaces B: Biointerfaces* **35**, 73-79 (2004).
- 86 Yu, Z.-W. & Quinn, P. J. The modulation of membrane structure and stability by dimethyl sulphoxide (Review). *Molecular membrane biology* **15**, 59-68 (1998).
- 87 Gurtovenko, A. A. & Anwar, J. Modulating the structure and properties of cell membranes: The molecular mechanism of action of dimethyl sulfoxide. *The Journal of Physical Chemistry B* **111**, 10453-10460 (2007).
- 88 Hammerstedt, R., Graham, J. K. & Nolan, J. P. Cryopreservation of mammalian sperm: what we ask them to survive. *J Androl* **11**, 73-88 (1990).
- 89 Notman, R., Noro, M., O'Malley, B. & Anwar, J. Molecular basis for dimethylsulfoxide (DMSO) action on lipid membranes. *Journal of the American Chemical Society* **128**, 13982-13983 (2006).
- 90 Yu, Z.-W. & Quinn, P. J. Dimethyl sulphoxide: A review of its applications in cell biology. *Bioscience Reports* **14**, 259-281 (1994).
- 91 De Leeuw, F., De Leeuw, A., Den Daas, J., Colenbrander, B. & Verkleij, A. Effects of various cryoprotective agents and membrane-stabilizing compounds on bull sperm membrane integrity after cooling and freezing. *Cryobiology* **30**, 32-44 (1993).
- 92 Simonin, H., Winckler, P., Gros, A., Perrier-Cornet, J.-M. & Gervais, P. How dehydration with glycerol protects bacteria cell membranes against deleterious effects of supercooling. *Cryobiology* **71**, 549, doi:10.1016/j.cryobiol.2015.10.051 (2015).
- 93 Chen, X., Huang, Z., Hua, W., Castada, H. & Allen, H. C. Reorganization and caging of DPPC, DPPE, DPPG, and DPPS monolayers caused by dimethylsulfoxide observed using Brewster angle microscopy. *Langmuir* **26**, 18902-18908 (2010).
- 94 Kiselev, M., Lesieur, P., Kiselev, A., Grabielle-Madmond, C. & Ollivon, M. DMSO-induced dehydration of DPPC membranes studied by X-ray diffraction, small-angle neutron scattering, and calorimetry. *Journal of Alloys and Compounds* **286**, 195-202 (1999).
- 95 Malajczuk, C. J., Hughes, Z. E. & Mancera, R. L. Molecular dynamics simulations of the interactions of DMSO, mono- and polyhydroxylated cryosolvents with a hydrated phospholipid bilayer. *Biochimica et Biophysica Acta (BBA)-Biomembranes* **1828**, 2041-2055 (2013).
- 96 Cheng, C.-Y., Song, J., Pas, J., Meijer, L. H. & Han, S. DMSO induces dehydration near lipid membrane surfaces. *Biophysical Journal* **109**, 330-339 (2015).
- 97 Hughes, Z. E., Mark, A. E. & Mancera, R. L. Molecular dynamics simulations of the interactions of DMSO with DPPC and DOPC phospholipid membranes. *The Journal of Physical Chemistry B* **116**, 11911-11923 (2012).

- 98 Schrader, A. M., Cheng, C.-Y., Israelachvili, J. N. & Han, S. (AIP Publishing, 2016).
- 99 Gironi, B., Paolantoni, M., Morresi, A., Foggi, P. & Sassi, P. The Influence of Dimethyl Sulfoxide on the Low-Temperature Behavior of Cholesterol-Loaded Palmitoyl-oleyl-phosphatidylcholine Membranes. *The Journal of Physical Chemistry B* (2018).
- 100 Meryman, H. Cryoprotective agents. *Cryobiology* **8**, 173-183 (1971).
- 101 Fahy, G. M. The relevance of cryoprotectant "toxicity" to cryobiology. *Cryobiology* **23**, 1-13 (1986).
- 102 Cordeiro, R. M., Stirling, S., Fahy, G. M. & de Magalhaes, J. P. Insights on cryoprotectant toxicity from gene expression profiling of endothelial cells exposed to ethylene glycol. *Cryobiology* **71**, 405-412, doi:10.1016/j.cryobiol.2015.10.142 (2015).
- 103 Fahy, G. Cryoprotectant toxicity neutralizers reduce freezing damage. *Cryo-letters* **4**, 309-314 (1983).
- 104 Fahy, G. M. Cryoprotectant toxicity neutralization. *Cryobiology* **60**, S45-53, doi:10.1016/j.cryobiol.2009.05.005 (2010).
- 105 Fahy, G. M., Lilley, T. H., Linsdell, H., Douglas, M. S. J. & Meryman, H. T. Cryoprotectant toxicity and cryoprotectant toxicity reduction: In search of molecular mechanisms. *Cryobiology* **27**, 247-268 (1990).
- 106 Best, B. P. Cryoprotectant Toxicity: Facts, Issues, and Questions. *Rejuvenation Research* **18**, 422-436, doi:10.1089/rej.2014.1656 (2015).
- 107 Ruwart, M., Holland, J. & Haug, A. Fluorimetric evidence of interactions involving cryoprotectants and biomolecules. *Cryobiology* **12**, 26-33 (1975).
- 108 Chian, R.-C. *et al.* High survival rate of bovine oocytes matured in vitro following vitrification. *Journal of Reproduction and Development* **50**, 685-696 (2004).
- 109 Meryman, H. T. Cryopreservation of living cells: principles and practice. *Transfusion* **47**, 935-945, doi:10.1111/j.1537-2995.2007.01212.x (2007).
- 110 Wilmut, I. The effect of cooling rate, warming rate, cryoprotective agent and stage of development of survival of mouse embryos during freezing and thawing. *Life Sciences* **11**, 1071-1079 (1972).
- 111 Wilmut, I. & Rowson, L. The successful low-temperature preservation of mouse and cow embryos. *Journal of Reproduction and Fertility* **33**, 352 (1973).
- 112 Mukherjee, I. N., Song, Y. C. & Sambanis, A. Cryoprotectant delivery and removal from murine insulinomas at vitrification-relevant concentrations. *Cryobiology* **55**, 10-18 (2007).
- 113 Davidson, A. F., Glasscock, C., McClanahan, D. R., Benson, J. D. & Higgins, A. Z. Toxicity minimized cryoprotectant addition and removal procedures for adherent endothelial cells. *PLoS One* **10**, e0142828, doi:10.1371/journal.pone.0142828 (2015).
- 114 Stachecki, J. J., Cohen, J. & Willadsen, S. M. Cryopreservation of unfertilized mouse oocytes: the effect of replacing sodium with choline in the freezing medium. *Cryobiology* **37**, 346-354 (1998).
- 115 Shu, Z. Q. *et al.* A study of the osmotic characteristics, water permeability, and cryoprotectant permeability of human vaginal immune cells. *Cryobiology* **72**, 93-99, doi:10.1016/j.cryobiol.2016.03.003 (2016).
- 116 Jacobs, M. H. The simultaneous measurement of cell permeability to water and to dissolved substances. *Journal of Cellular and Comparative Physiology* **2**, 427-444, doi:10.1002/jcp.1030020405 (1933).

- 117 Schreuders, P. D., Smith, E. D., Cole, K. W., Laughinghouse, A. & Mazur, P. Characterization of intraembryonic freezing in *Anopheles gambiae* embryos. *Cryobiology* **33**, 487-501 (1996).
- 118 Sun, W. Q. State and phase transition behaviors of *Quercus rubra* seed axes and cotyledonary tissues: Relevance to the desiccation sensitivity and cryopreservation of recalcitrant seeds. *Cryobiology* **38**, 372-385 (1999).
- 119 Wolfe, J., Bryant, G. & Koster, K. L. What is 'unfreezable water', how unfreezable is it and how much is there? *Cryoletters* **23**, 157-166 (2002).
- 120 Mazur, P. & Miller, R. H. Permeability of the human erythrocyte to glycerol in 1 and 2 M solutions at 0 or 20 °C. *Cryobiology* **13**, 507-522, doi:[http://dx.doi.org/10.1016/0011-2240\(76\)90144-9](http://dx.doi.org/10.1016/0011-2240(76)90144-9) (1976).
- 121 Mazur, P., Leibo, S. P. & Miller, R. H. Permeability of the bovine red cell to glycerol in hyperosmotic solutions at various temperatures. *The Journal of Membrane Biology* **15**, 107-136, doi:10.1007/BF01870084 (1974).
- 122 Kedem, O. & Katchalsky, A. Thermodynamic analysis of the permeability of biological membranes to non-electrolytes. *Biochimica et Biophysica Acta* **27**, 229-246 (1958).
- 123 Kleinhans, F. Membrane permeability modeling: Kedem–Katchalsky vs a two-parameter formalism. *Cryobiology* **37**, 271-289 (1998).
- 124 Benson, C. *et al.* Hydraulic conductivity (L_p) and its activation Energy (E_a), cryoprotectant agent permeability (P_s) and its E_a , and reflection Coefficients (σ) for Golden hamster individual pancreatic islet cell membranes. *Cryobiology* **37**, 290-299 (1998).
- 125 Newton, H., Pegg, D., Barrass, R. & Gosden, R. Osmotically inactive volume, hydraulic conductivity, and permeability to dimethyl sulphoxide of human mature oocytes. *Journal of Reproduction and Fertility* **117**, 27-33 (1999).
- 126 Chen, P. Y., Pearce, D. & Verkman, A. S. Membrane water and solute permeability determined quantitatively by self-quenching of an entrapped fluorophore. *Biochemistry* **27**, 5713-5718 (1988).
- 127 Verkman, A. & Ives, H. E. Water permeability and fluidity of renal basolateral membranes. *American Journal of Physiology-Renal Physiology* **250**, F633-F643 (1986).
- 128 Worman, H. J., Brasitus, T. A., Dudeja, P. K., Fozzard, H. A. & Field, M. Relationship between lipid fluidity and water permeability of bovine tracheal epithelial cell apical membranes. *Biochemistry* **25**, 1549-1555 (1986).
- 129 Gilmore, J. *et al.* Effect of cryoprotectant solutes on water permeability of human spermatozoa. *Biology of reproduction* **53**, 985-995 (1995).
- 130 Mori, S., Choi, J., Devireddy, R. V. & Bischof, J. C. Calorimetric measurement of water transport and intracellular ice formation during freezing in cell suspensions. *Cryobiology* **65**, 242-255, doi:10.1016/j.cryobiol.2012.06.010 (2012).
- 131 Gao, D. *et al.* Membrane transport properties of mammalian oocytes: A micropipette perfusion technique. *Journal of Reproduction and Fertility* **102**, 385-392 (1994).
- 132 Xu, X., Cui, Z. & Urban, J. P. Measurement of the chondrocyte membrane permeability to Me₂SO, glycerol and 1, 2-propanediol. *Medical Engineering & Physics* **25**, 573-579 (2003).
- 133 Xu, Y., Zhang, L., Xu, J., Wei, Y. & Xu, X. Membrane permeability of the human pluripotent stem cells to Me₂SO, glycerol and 1, 2-propanediol. *Archives of Biochemistry and Biophysics* **550**, 67-76 (2014).

- 134 Wlodkowic, D., Faley, S., Zagnoni, M., Wikswo, J. P. & Cooper, J. M. Microfluidic single-cell array cytometry for the analysis of tumor apoptosis. *Analytical Chemistry* **81**, 5517-5523 (2009).
- 135 Tan, W.-H. & Takeuchi, S. A trap-and-release integrated microfluidic system for dynamic microarray applications. *Proceedings of the National Academy of Sciences* **104**, 1146-1151 (2007).
- 136 Zhao, G. *et al.* A microfluidic perfusion approach for on-chip characterization of the transport properties of human oocytes. *Lab on a Chip* **17**, 1297-1305 (2017).
- 137 Fang, C., Ji, F., Shu, Z. & Gao, D. Determination of the temperature-dependent cell membrane permeabilities using microfluidics with integrated flow and temperature control. *Lab on a Chip* **17**, 951-960 (2017).
- 138 Kitson, P. J., Rosnes, M. H., Sans, V., Dragone, V. & Cronin, L. Configurable 3D-Printed millifluidic and microfluidic 'lab on a chip' reactionware devices. *Lab on a Chip* **12**, 3267-3271 (2012).
- 139 Lee, M. P. *et al.* Development of a 3D printer using scanning projection stereolithography. *Scientific Reports* **5**, 9875 (2015).
- 140 Temiz, Y., Lovchik, R. D., Kaigala, G. V. & Delamarche, E. Lab-on-a-chip devices: How to close and plug the lab? *Microelectronic Engineering* **132**, 156-175 (2015).
- 141 Au, A. K., Huynh, W., Horowitz, L. F. & Folch, A. 3D-printed microfluidics. *Angewandte Chemie International Edition* **55**, 3862-3881 (2016).
- 142 Reza, A. *et al.* 3D-printed microfluidic devices. *Biofabrication* **8**, 022001 (2016).
- 143 Kamei, K.-i. *et al.* 3D printing of soft lithography mold for rapid production of polydimethylsiloxane-based microfluidic devices for cell stimulation with concentration gradients. *Biomedical Microdevices* **17**, 36, doi:10.1007/s10544-015-9928-y (2015).
- 144 Erkal, J. L. *et al.* 3D Printed Microfluidic Devices with Integrated Versatile and Reusable Electrodes. *Lab on a chip* **14**, 2023-2032, doi:10.1039/c4lc00171k (2014).
- 145 Anderson, K. B., Lockwood, S. Y., Martin, R. S. & Spence, D. M. A 3D Printed Fluidic Device that Enables Integrated Features. *Analytical Chemistry* **85**, 5622-5626, doi:10.1021/ac4009594 (2013).
- 146 Cotteleer, M. & Joyce, J. 3D opportunity: Additive manufacturing paths to performance, innovation, and growth. *Deloitte Review* **14**, 5-19 (2014).

Chapter 2

Methodology

2.1 Langmuir monolayer technique

The Langmuir monolayer technique is a well-established technique for studying the interactions between soluble molecules and lipids, and is described in detail elsewhere¹. Fig. 2.1 shows the schematic of a Langmuir trough. A monolayer of lipid is placed on the liquid subphase which can be water or any other solution of interest. In this study, water and CPA solutions are used as the subphases. Two movable barriers are used to compress the monolayer. As the monolayer is compressed, the surface area decreases and the corresponding increase in surface pressure is measured through a Wilhelmy plate electro balance connected to a pressure sensor. Initially the molecules will be spread unevenly (in the 2D equivalent of the gaseous state) and as the film is compressed the molecules become more ordered, transitioning through other phases.

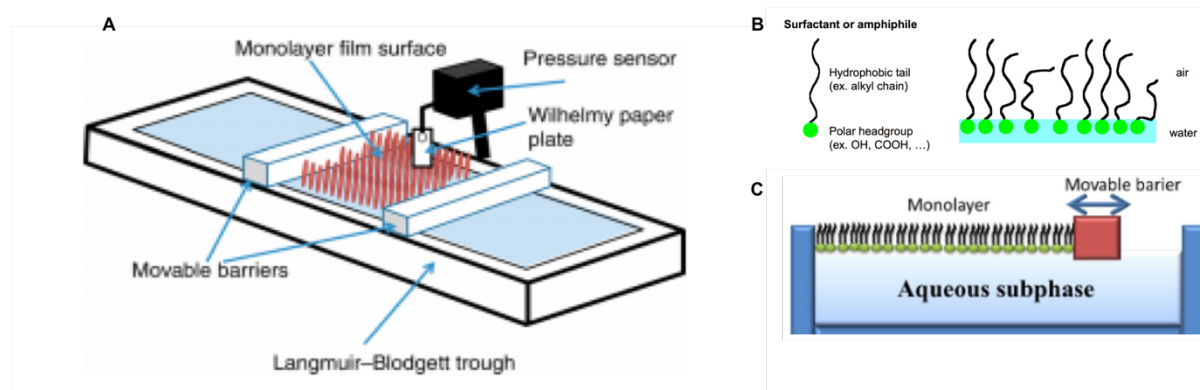


Fig.2.1: (A) schematic of a Langmuir trough with two movable barriers, monolayer film formed at the surface of the subphase, a wilhelmy paper plate and a pressure sensor. (B) shows the schematic of how the phospholipids are arranged in a monolayer (C) shows the schematic of how the monolayer lipids are compressed (Image source²).

The results are visualised in Pressure-Area ($\pi - A$) isotherms (Fig.2.2A). The effects of solutes on lipid organization can be assessed in terms of the changes in the area per lipid molecule and the pressures at which phase transitions take place. The fluid and gel phases of a bilayer are analogous to the liquid expanded and liquid condensed phases of a monolayer respectively. These phases can be more clearly understood by calculating the inverse compressibility modulus (also called the Elasticity modulus) from the slope of the isotherm which is represented by C_s^{-1} (Eq. 2.1)^{1,3-9}.

$$C_s^{-1} = -A \left(\frac{d\pi}{dA} \right)_T \quad (\text{Eq. 2.1})$$

The value of C_s^{-1} allows one to assign the monolayer physical state during compression: C_s^{-1} values between 12.5-100 mN.m⁻¹ correspond to the liquid expanded (LE) phase, $100 < C_s^{-1} < 250$ mN.m⁻¹ corresponds to the liquid condensed (LC) phase, and $C_s^{-1} > 250$ mN.m⁻¹ corresponds to the solid (S) phase¹⁰. Fig. 2.2 (B) shows a schematic of the C_s^{-1} graph.

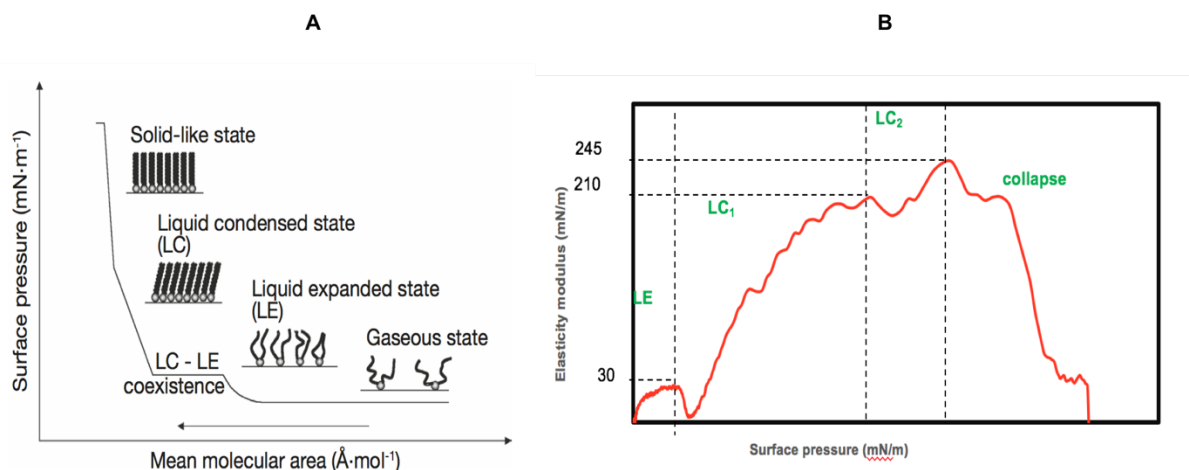


Fig. 2.2: (A) Schematic of $\pi - A$ isotherm showing the various states achieved by the monolayer upon compression (B) Schematic of C_s^{-1} graph showing the various states achieved by the monolayer during compression (image source¹¹).

The results of the current study provide insights into the interactions of various cryoprotectants with biological cell membrane lipids which are discussed in detail in *chapter 3*.

2.1.1 Materials used

Fig. 2.3 shows the molecular structure of the phospholipids (DOPC, POPC, DPPC and POPE) which are commonly found in biological membranes and used in the current study for forming the monolayers. DOPC was purchased from Sigma-Aldrich Chemistry (Madrid, Spain) and the other lipids were purchased from Avanti Polar Lipids (Alabaster, AL, USA). These lipids were used without further purification by dissolving in chloroform (PA-ACS-ISO grade, PANREAC (Barcelona, Spain)) to a final concentration of 1mg.ml⁻¹ and kept in the refrigerator. Other than ultrapure water (Milli Q®, 18.3 MΩcm resistivity), various penetrating CPAs (DMSO, glycerol, ethylene glycol and dimethyl formamide) were used as subphases for forming the Langmuir films. All CPA subphases were prepared as 5% v/v in ultrapure water and the chemicals were PA-ACS-ISO grade (PANREAC).

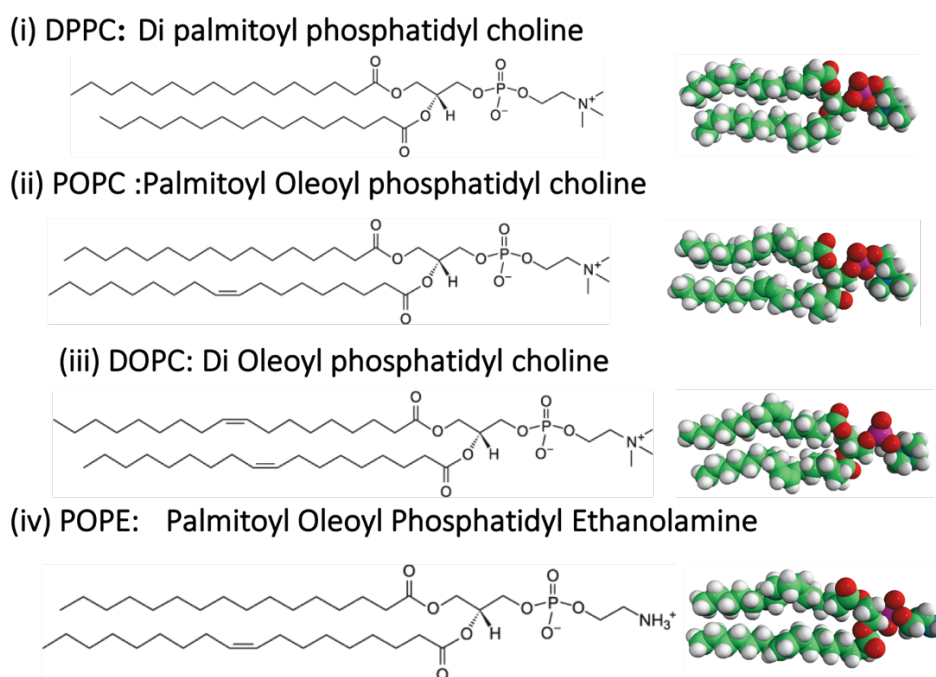


Fig. 2.3: Molecular structure of various phospholipids used as monolayers for the CPA-membrane lipid interaction studies.

(Image source: <https://www.sigmaaldrich.com/>)

2.1.2 Experiments and Equipments

Two kinds of experiments were carried out - compression isotherms and insertion experiments. Langmuir compression isotherms were carried out on a NIMA teflon trough (Nima Technology, Coventry, UK), model 1232D1D2 (area 1200 cm²), equipped with two movable barriers (see Fig. 2.4 A, B), and the surface pressure was measured using a pressure sensor with a Wilhelmy plate (10 mm × 50 mm filter paper; Whatman International, Maidstone, UK). The linear velocity of the barriers was 2.5 cm.min⁻¹, which corresponds to an area change of 50 cm².min⁻¹ in the trough used. The trough was placed on a vibration-isolated table (Newport, Irvine, CA, USA) and enclosed in an environmental chamber. In the insertion experiments the effect of inserting the CPA directly into the subphase was measured by the change in surface pressure of the lipid monolayer. The experiments were carried out using a NIMA Langmuir film balance equipped with a wilhelmy plate and a small teflon trough (see Fig. 2.4 C) that was rinsed with chloroform and ultrapure water before use. All experiments were performed at 22±1°C. See *chapter 3* for more details about the experimental procedure.

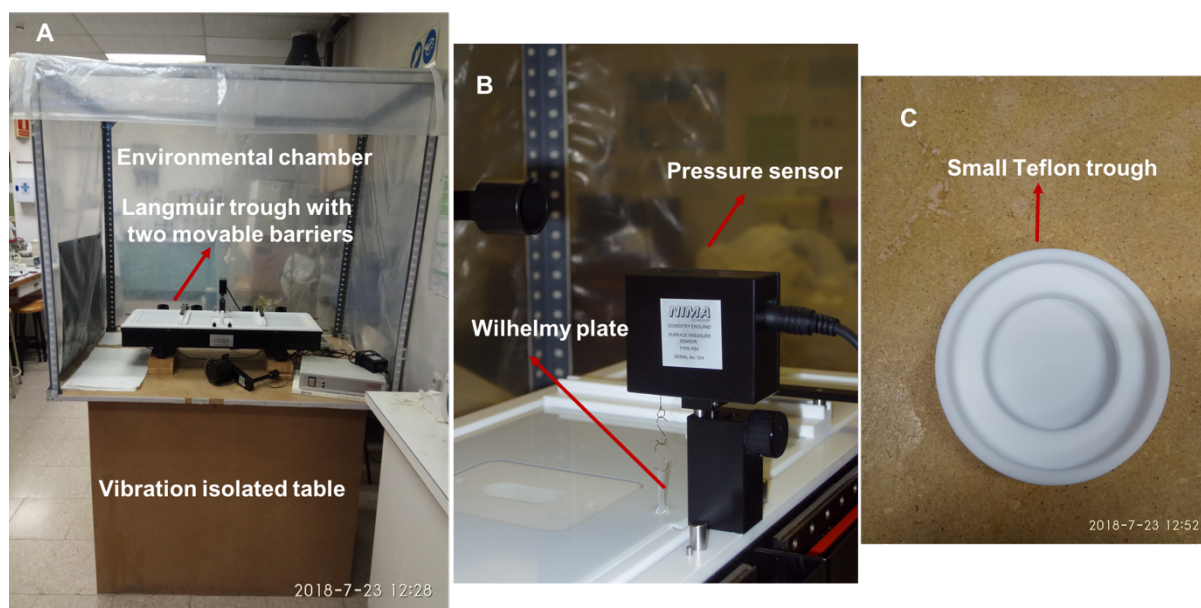


Fig. 2.4: (A) Nima teflon trough used for the Langmuir monolayer experiments (B) Closer view of the trough showing pressure sensor and wilhelmy plate (C) Small teflon trough used for insertion experiments.

2.2 Differential scanning calorimetry (DSC)

DSC is used to analyze the phase transition behavior of materials. In a DSC thermogram, generally, the high temperature peak (large exothermic peak) in the cooling cycle represents ice crystallization (T_c). The inflections in the thermogram represent vitrification (glass transitions T_g) which is usually most clearly visible on warming cycles. Following glass melting in the warming run the super cooled solution undergoes freezing and a devitrification peak can sometimes be observed in the warming run ^{12,13}. The ice subsequently melts as it reaches the freezing point and the corresponding large endothermic peak represents the melting temperature T_m . *Fig. 2.5* shows a schematic DSC thermogram. In this study, thermograms on warming and cooling were obtained with Mettler Toledo DSC 3+ STARe system differential scanning calorimeter with a few milligrams of samples (2-10mg). Method used for the study is shown in *Fig. 2.6*.

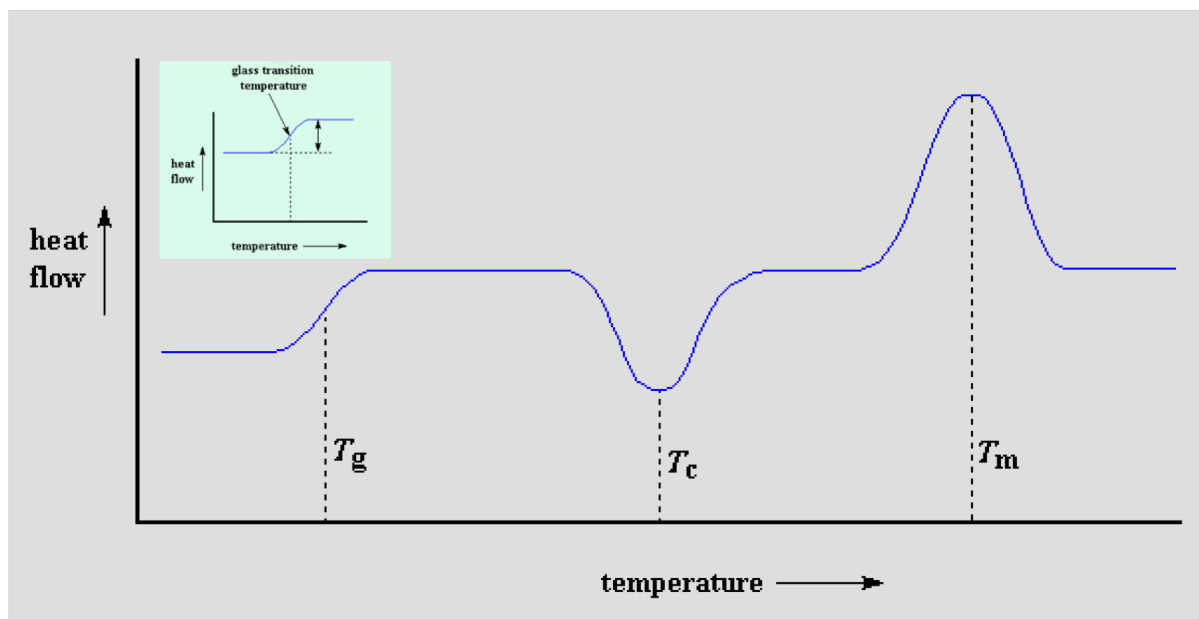


Fig. 2.5: Schematic DSC thermogram showing the ice crystallization (T_c), glass transition (T_g) and ice melting (T_m) temperatures. Inset shows the glass transition part of the DSC thermogram (Image source: <https://pslc.ws/macrog/dsc.htm>).

Except where stated, samples were cooled and warmed between -160°C and $+25^{\circ}\text{C}$. For all samples, measurements were made on several (at least 3) successive cooling/warming runs to confirm the consistency in thermal behavior. Between each run the samples were held for approximately 1 min at 25°C . All scanning measurements were performed at a cooling/heating rate of $10^{\circ}\text{C}/\text{min}$ and the thermograms were analyzed to determine the glass transition temperature. More details about the thermograms and interpretations of results are discussed in the upcoming experimental chapters (*chapters 4&5*).

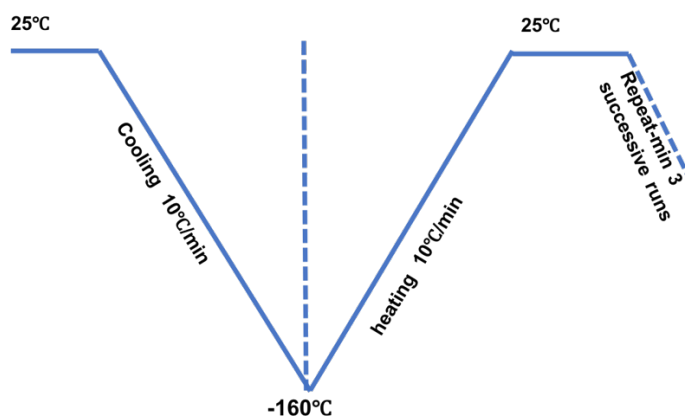


Fig. 2.6: Schematic of the DSC method used for the current study

2.3 Single cell volume kinetics

Cell permeability¹⁴⁻¹⁶ studies were conducted microscopically in standard media. The solute concentrations were rapidly increased, and the cells expel water to restore osmotic balance, resulting in cell shrinkage. Cell volume excursions were recorded, the volume was calculated as a function of time and the results were plotted. A second series of experiments were conducted with a permeating CPA – the cell initially shrinks as water is expelled, but the CPA slowly permeates, and then as the water re-entered the cell and the cell is expanded allowing the determination of the CPA permeability¹⁷. So, addition of a CPA to a cell suspension resulted in the characteristic “shrink–swell” behavior (*Fig. 1.5*).

2.3.1 Materials and methods used

The two main criteria for cell permeability studies are (i) requirement of large and spherical single cells and (ii) Cell immobilization without overlapping or dislodgement during image acquisition. For the current study, human monocyte leukemia cells (THP-1) were used which are spherical and large with diameters in the range of 12-18 μ m. Cell lines were purchased from ATCC (American Type Culture Collection, MANASSAS, VA). Cells were revived from liquid nitrogen and cultured according to ATCC standard protocol. Briefly, the cell culture consisted of RPMI 1640 medium (ATCC, 30-2001) supplemented with 10% FBS (Fetal Bovine Serum) (ATCC, 30-2020) and 1% antibiotic (Penstrep). The cells were cultured in T25 flasks (Corning) and incubated at 37°C in a humidified atmosphere containing 5% CO₂. The cells were allowed to grow for 2-3 weeks with medium renewal and sub culturing. The viability of cells was measured using a Trypan blue exclusion test¹⁸ and found to be in the range of 96-98% before experiments. The cells were collected, centrifuged at 200g for 5 min, and then re-suspended in RPMI 1640 medium at a density of 2.5×10^5 cells/mL, and used for experiments within 3 hours.

For cell immobilization, two techniques were used:

(i) Coating coverslips with Poly-L-Lysin:

The cells were immobilized on a 15 mm diameter cover slip coated with poly-L-lysine (Sigma, USA) and placed in a tissue culture dish. The cell solution (50-100 μ L) was then loaded onto the cover slip for up to 15 min. Once the cells were immobilized on the cover slip, the medium was completely replaced by the prepared CPA solutions to achieve a rapid extracellular osmotic change^{19,20}. For each experiment, new cell solutions were loaded onto the cover slips freshly from the incubator.

(ii) Trapping of single cells using microfluidic devices

The microfluidic trapping structures were fabricated at the Micro Nano Research Facility (MNRF) of RMIT by the author and co-workers. Structures were designed with the help of Dr. Khashayar Khoshmanesh from the engineering group. Schematic of the two types of cell trap designs (cup shaped and serpentine shaped traps) used for the current study is shown in *Fig. 2.7*.

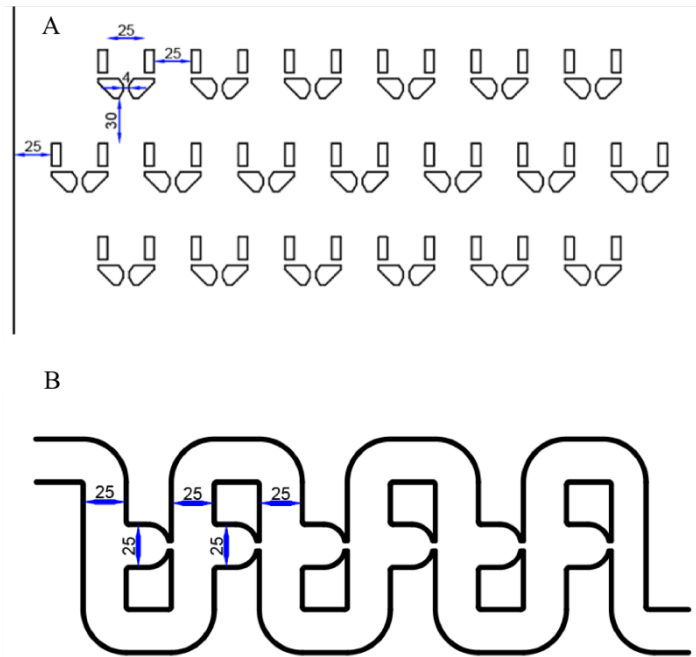


Fig. 2.7: Schematic of the two microfluidic cell trap designs used for the current study – (A) cup-shaped cell traps (B) serpentine shaped cell traps

The fabrication was done by the author and Mr. Hannes Hohn (who worked as an intern student at RMIT from University of Applied Sciences Karlsruhe, Germany), combining Direct Laser Writing (DLW) and soft lithography techniques. Using DLW, a master mould can be made which can be repeatedly used for creating Poly di methyl siloxane (PDMS) replicas with soft lithography²¹. Fabricated microfluidic trapping devices were used for cell trapping and CPA perfusion studies. A schematic of the experimental setup for the cell trapping and CPA perfusion studies is shown in *Fig. 2.8*. An aliquot of cell suspension ($\sim 30\text{-}50\mu\text{L}$) was added gently to the inlet of the microfluidic device and allowed to flow through the channel using a syringe pump (PHD 2000 Infusion, Harvard Apparatus) with a flow rate of $200\mu\text{L}/\text{h}$ in order to allow the hydrodynamic trapping of cells. After enough cells were trapped, the CPA (DMSO) solution was added for cell perfusion and permeability experiments. More details about the fabrication techniques and permeability studies can be found in *chapter 6*. Microfluidic cell trapping devices eliminate the limitations associated with traditional single cell sorting methods, such as cell overlapping, loss of sphericity due to surface attachment as well as the possibility of cell toxicity associated with the chemicals used for surface coating.

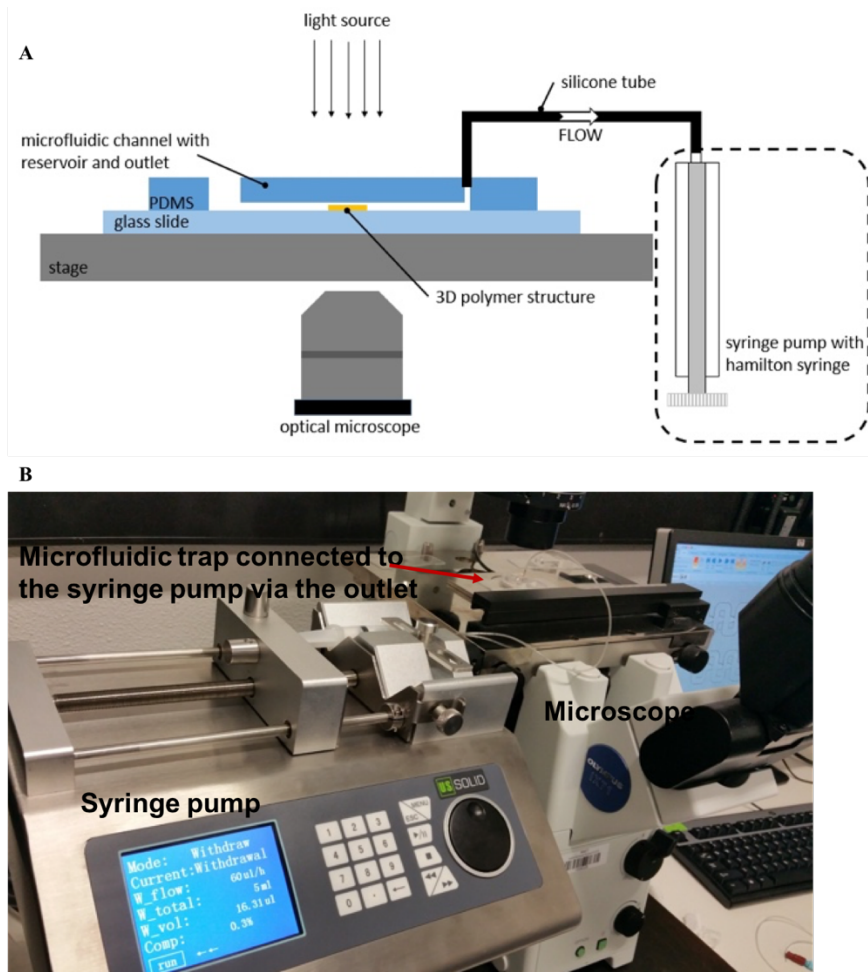


Fig. 2.8: Experimental set up for single cell trapping and permeability studies using microfluidic device- (A) Schematic experimental set up (B) Setup in the laboratory

An inverted microscope (Olympus IX71 inverted optical microscope) equipped with a CCD camera at 1024×1024 resolution and a CMOS sensor (Mikrotron MC1362) was utilized for visualization. Automated time-lapse image acquisition was used for periods of up to 15 min under the control of streampix software to capture the cell volume excursion history. The captured video was converted into image frames by exporting the full sequence at 1 frame/sec. Individual cells were cropped from each frame for image analysis. Images were extracted and processed using ImageJ (<https://imagej.nih.gov/ij/>). A few images were analyzed at regular time intervals to understand the volume response (shrinking and swelling) of the cells. The areas of the selected cells were manually measured using oval/free hand selections. Radii and normalized volumes were calculated assuming the cell to be a sphere. The sphericity of THP-1 cells was evaluated as $2\pi R_{cell}/P_{cell}$, where, P_{cell} is the actual cell perimeter and R_{cell} is the equivalent cell radius calculated with the two-dimensional cell area based on image analysis.

2.4 Cryopreservation trials

Carbohydrate based (sugar) surfactants which showed promising cryoprotective behavior were used for cryopreservation studies of THP-1 cells. Cells were cryopreserved with DMSO as a control. The basic protocol was the standard protocol for DMSO cryopreservation.

2.4.1 Materials and methods

The cell suspension was diluted to $\sim 1 \times 10^6$ cells per mL using complete media (RPMI1640 + 10% FBS +1% antibiotic-Penstrep). The cryo-tubes were labelled, cell samples and the CPAs were added to each vial in microliter (μL) amounts in order to attain the final desired CPA concentration. In the current studies, molar concentrations of 1.3M and 0.65M were used which are osmotically equivalent to the 10% and 5% by volume DMSO used in standard cryopreservation protocols. All procedures were carried out at room temperature. Samples were immediately placed in a freezing box and transferred into the -20°C freezer for 1 hour and then transferred to the -80°C freezer. The next day, the samples were transferred to Liquid Nitrogen (LN). After 1 week, cell viabilities were measured using a Trypan blue exclusion test¹⁸ after revival from LN. Initial viabilities were noted, and all cell samples were cultured in T25 flasks and incubated at 37°C in a humidified atmosphere containing 5% CO_2 . The cells were allowed to grow for 2 weeks with medium renewal and sub-culturing. Cell viability tests were repeated at each sub-culturing time.

After the initial trials, final cryopreservation experiments were carried out only with the most promising cryoprotective candidates which showed relatively good cell viability, with slight variations in the basic optimized DMSO protocol described above. Four different protocols were tried:

P-1: Bypassing the first step (transferring to freezing box), otherwise keeping the protocol the same.

P-2: Bypassing the first step (transferring to freezing box) and then transferring directly to -80°C freezer and then to LN.

P-3: As for P-1 except all procedures were carried out at 4°C instead of room temperature.

P-4: As for P-2 except all procedures were carried out at 4°C instead of room temperature.

More details on the cryopreservation trials and outcomes are explained in *chapter 5*.

2.5 References

- 1 Giner-Casares, J. J., Brezesinski, G. & Möhwald, H. Langmuir monolayers as unique physical models. *Current Opinion in Colloid & Interface Science* **19**, 176-182 (2014).
- 2 Larsen, M. C. Binary phase diagrams at the air–water interface: An experiment for undergraduate physical chemistry students. *Journal of Chemical Education* **91**, 597-601 (2014).
- 3 Bianco, I. D., Fidelio, G. D. & Maggio, B. Effect of glycerol on the molecular properties of cerebrosides, sulphatides and gangliosides in monolayers. *Biochemical Journal* **251**, 613 (1988).
- 4 Domènech, Ò. *et al.* Surface thermodynamics study of monolayers formed with heteroacid phospholipids of biological interest. *Colloids and Surfaces B: Biointerfaces* **41**, 233-238, doi:<https://doi.org/10.1016/j.colsurfb.2004.12.012> (2005).
- 5 Nowotarska, S. W., Nowotarski, K. J., Friedman, M. & Situ, C. Effect of structure on the interactions between five natural antimicrobial compounds and phospholipids of bacterial cell membrane on model monolayers. *Molecules* **19**, 7497-7515 (2014).
- 6 Wnętrzak, A., Łątka, K. & Dynarowicz-Łątka, P. Interactions of alkylphosphocholines with model membranes—The langmuir monolayer study. *The Journal of Membrane Biology* **246**, 453-466 (2013).
- 7 Torrent-Burgués, J. Phase separation in mixed monolayers of arachidic acid and a phthalocyanine of zinc. *Colloids and Surfaces A: Physicochemical and Engineering Aspects* **396**, 137-143 (2012).
- 8 Torrent-Burgués, J. Langmuir films study on lipid-containing artificial tears. *Colloids and Surfaces B: Biointerfaces* **140**, 185-188 (2016).
- 9 Torrent-Burgués, J., Cea, P., Giner, I. & Gaus, E. Characterization of Langmuir and Langmuir–Blodgett films of an octasubstituted zinc phthalocyanine. *Thin Solid Films* **556**, 485-494 (2014).
- 10 Vitovič, P., Nikolelis, D. & Hianik, T. Study of calix [4] resorcinarene–dopamine complexation in mixed phospholipid monolayers formed at the air–water interface. *Biochimica et Biophysica Acta (BBA)-Biomembranes* **1758**, 1852-1861 (2006).
- 11 Eeman, M. & Deleu, M. From biological membranes to biomimetic model membranes. *Biotechnologie, Agronomie, Société et Environnement* **14**, 719 (2010).
- 12 Baudot, A., Alger, L. & Boutron, P. Glass-forming tendency in the system water–dimethyl sulfoxide. *Cryobiology* **40**, 151-158 (2000).
- 13 Baudot, A. & Boutron, P. Glass-forming tendency and stability of aqueous solutions of diethylformamide and dimethylformamide. *Cryobiology* **37**, 187-199, doi:<http://dx.doi.org/10.1006/cryo.1998.2112> (1998).
- 14 Toner, J. O. M. K. a. M. in *Principles of Tissue Engineering (Second Edition)* (eds Robert Langer & Joseph Vacanti) 293-307 (Academic Press, 2000).
- 15 Zhao, G. & Fu, J. Microfluidics for cryopreservation. *Biotechnology Advances* **35**, 323-336, doi:<http://dx.doi.org/10.1016/j.biotechadv.2017.01.006> (2017).
- 16 Weng, L. *et al.* A highly-occupied, single-cell trapping microarray for determination of cell membrane permeability. *Lab on a Chip* **17**, 4077-4088 (2017).
- 17 Shu, Z. Q. *et al.* A study of the osmotic characteristics, water permeability, and cryoprotectant permeability of human vaginal immune cells. *Cryobiology* **72**, 93-99, doi:10.1016/j.cryobiol.2016.03.003 (2016).

- 18 Strober, W. Trypan blue exclusion test of cell viability. *Current Protocols in Immunology* **21**, A. 3B. 1-A. 3B. 2 (1997).
- 19 Xu, Y., Zhang, L., Xu, J., Wei, Y. & Xu, X. Membrane permeability of the human pluripotent stem cells to Me₂SO, glycerol and 1, 2-propanediol. *Archives of Biochemistry and Biophysics* **550**, 67-76 (2014).
- 20 Xu, X., Cui, Z. & Urban, J. P. Measurement of the chondrocyte membrane permeability to Me₂SO, glycerol and 1, 2-propanediol. *Medical Engineering & Physics* **25**, 573-579 (2003).
- 21 LaFratta, C. N., Simoska, O., Pelse, I., Weng, S. & Ingram, M. A convenient direct laser writing system for the creation of microfluidic masters. *Microfluidics and Nanofluidics* **19**, 419-426, doi:10.1007/s10404-015-1574-4 (2015).

Chapter 3

Interactions of cryoprotective agents with phospholipid membranes - a Langmuir monolayer study

Rekha Raju^{a,b}, Juan Torrent Burgues^{b,*} and Gary Bryant^{a,*}

^a *Centre for Molecular and Nanoscale Physics, School of Science, RMIT University
Melbourne, Australia.*

^b *Universitat Politècnica de Catalunya (UPC), C/ Colom 1, E08222 Terrassa, Barcelona,
Spain*

This work has been compiled into a journal manuscript and is currently undergoing peer-review. This work was completed by the author of this thesis at UPC, Barcelona, Spain under the guidance of Prof. Juan Torrent Burgues and Prof. Gary Bryant.

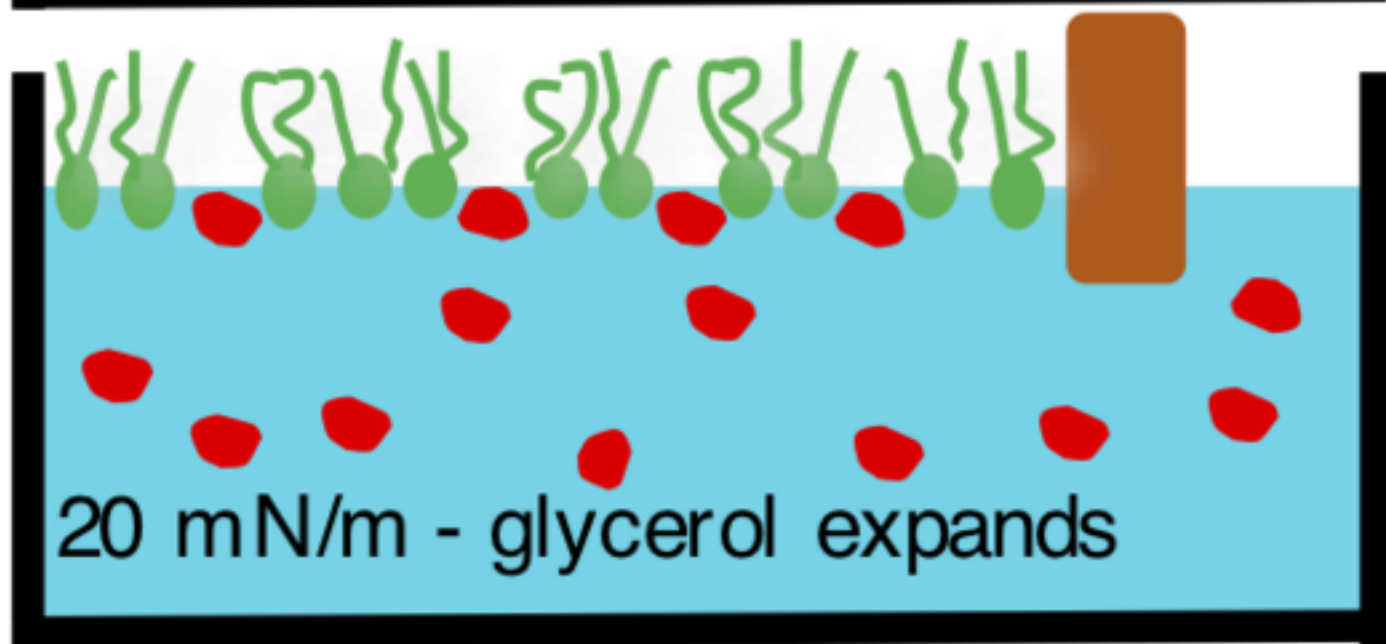
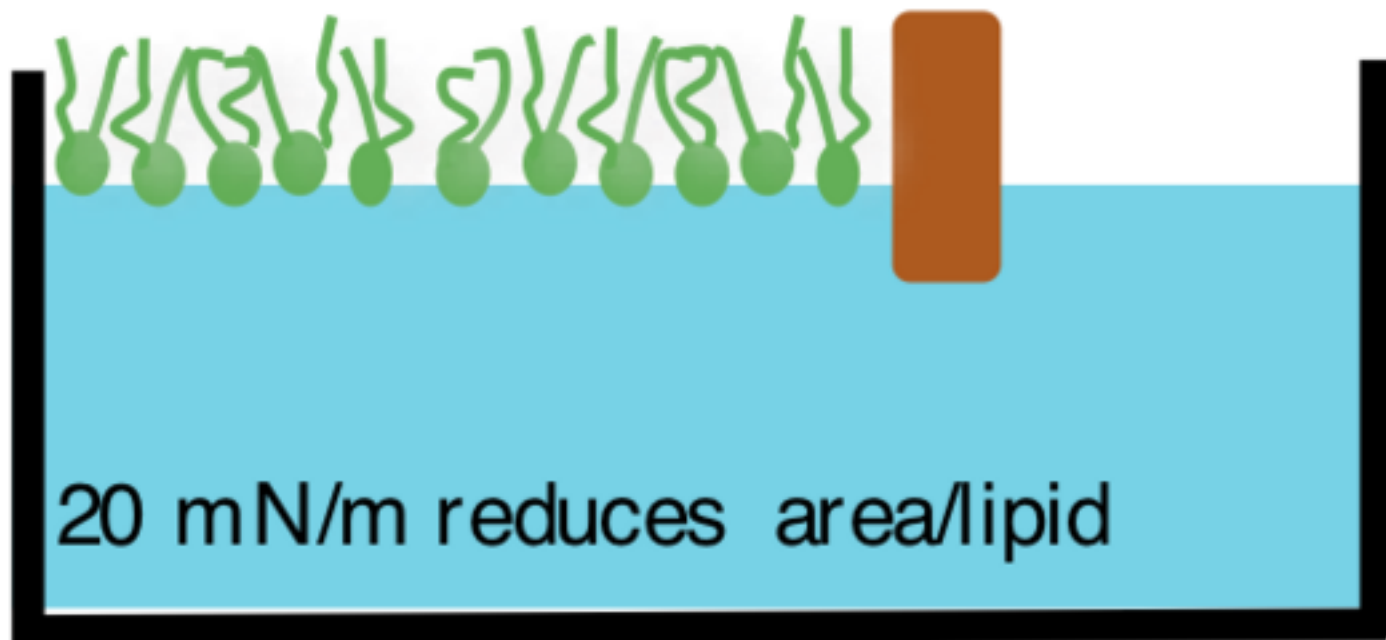
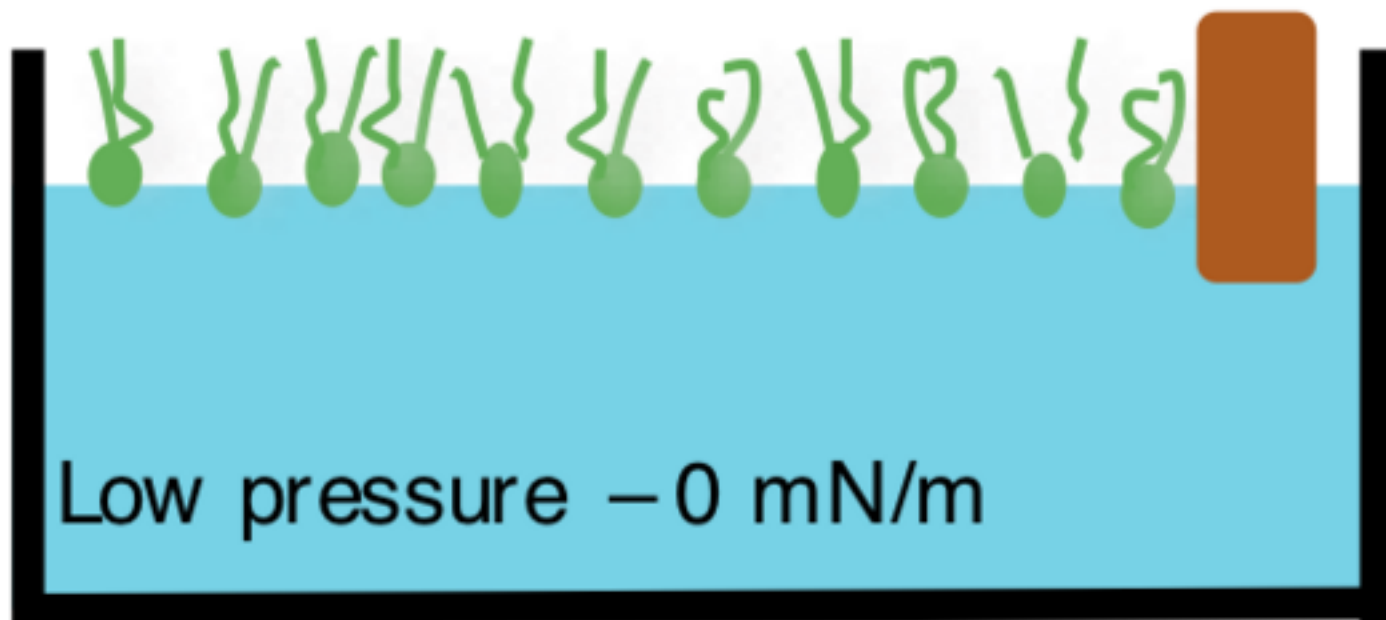
Author contributions:

- I carried out the experiments, measurements, analysis, initial interpretations of the results as well as the writing of initial manuscript draft.
- I received extensive training in the Langmuir monolayer technique from Prof. Juan Torrent Burgues who has also helped in experimental planning, results interpretation and manuscript corrections.
- Theoretical guidance for the Langmuir monolayer experiments were given by Prof. Gary Bryant. Further interpretation of results and the final manuscript corrections were also done with the guidance of Prof. Gary Bryant.

I would like to use this opportunity to thank the European Union and the Erasmus grant for the PhD short stay at UPC, Barcelona.

Candidate's Name:	Ms. Rekha Raju	Date
		11/11/2019

Principal Supervisor's Name:	Prof. Gary Bryant	Date
		11/11/2019



Interactions of cryoprotective agents with phospholipid membranes - a Langmuir monolayer study

Rekha Raju^{a,b}, Juan Torrent-Burgués^{b,*} and Gary Bryant^{a,*}

^a Centre for Molecular and Nanoscale Physics, School of Science, RMIT University
Melbourne, Australia.

^b Universitat Politècnica de Catalunya (UPC), C/ Colom 1, E08222 Terrassa, Barcelona,
Spain

*Corresponding authors: gary.bryant@rmit.edu.au ; juan.torrent@upc.edu

Abstract

The influence of four common cryoprotectants (dimethyl sulfoxide, glycerol, ethylene glycol and dimethylformamide) on monolayers of four common phospholipids (DPPC, DOPC, POPC and POPE) have been studied using Langmuir isotherms and monolayer insertion experiments. The cryoprotectant concentrations were chosen to be directly relevant to cryoprotection. We show that DMSO causes an expansion of the DPPC area per lipid (in contrast to previous work at higher concentrations). However, it caused compression for POPC, and had little effect for POPE or DOPC. As most previous studies have involved only DPPC, this highlights the importance of studying different lipid types as these may have a significant effect on the interactions. We show that both ethylene glycol and glycerol cause a small expansion of the monolayer at fixed pressure, implying that they insert into the headgroup regions, regardless of lipid species, and consistent with their ability to penetrate membranes. By contrast, dimethylformamide causes monolayer compression for all lipid species, implying it dehydrates the lipid head groups. Membrane insertion experiments at physiological values of lateral pressure highlight that DPPC is the most difficult lipid to penetrate, implying that the penetrating action of cryoprotectants may only occur for unsaturated phospholipids. Thus extrapolations of results based solely on the DPPC need to be made with care.

1 Introduction

Cryopreservation is a viable option for the long-term storage of biological material. In cryopreservation, samples are stored in a vitrified state at liquid nitrogen temperatures (-196 °C). One requirement of a successful cryopreservation protocol is an effective cryoprotective agent (CPA). CPAs reduce cellular damage by limiting the formation of intra- and extra-cellular ice, minimizing cell dehydration, and inhibiting membrane phase changes ¹⁻⁵.

When a cell suspension is frozen, ice tends to form external to the cells. Solutes are excluded from the ice structure, which leads to an increase in the extra-cellular solute concentration, resulting in cell shrinkage due to the efflux of water via osmosis ⁵. Thus, the formation of ice removes liquid water – ie, it causes dehydration, which can damage cell membranes ^{1,6}. By contrast, if a cell suspension is cooled rapidly, cells become supercooled, leading to the formation of intracellular ice, which is almost always lethal to cells ⁷. Thus, optimal cryopreservation usually involves cooling at an intermediate rate, to avoid the formation of

intracellular ice, and limit freeze-induced dehydration. If cells can be cooled below the glass transition, then further growth of ice is inhibited, and biochemical processes effectively cease.

The addition of penetrating CPAs is generally essential for successful cryopreservation. CPAs need to have the following properties: they should depress the equilibrium freezing point and encourage supercooling; they should have a relatively high glass transition temperature; and they must permeate cell membranes so that intracellular vitrification can be achieved^{3,5}. The proposed mechanisms of action and toxicity of a range of CPAs, are discussed in the literature^{8,9}. Several studies have been carried out to understand the membrane protection effects of natural CPAs such as sugars, especially disaccharides, and the mechanisms are becoming clearer^{6,10-13}. The mechanisms of action of penetrating cryoprotectants have been less widely studied, with the exception of dimethyl sulphoxide (DMSO) and glycerol¹⁴⁻²¹. However, these molecules are toxic to cells and cryopreservation involves balancing these two effects⁵. Other classes of potential penetrating CPAs include sulfoxides, alcohols, amides and imides^{22,23}, including dimethyl formamide (DMF) and ethylene glycol (EG). These compounds offer an alternative to more conventional cryoprotectants, such as DMSO and glycerol, and may have lower toxicity, so are also worth exploring.

The various factors affecting membrane permeability of cells during preservation are reviewed in a recent study by Wolkers et al.²⁴ The interaction of DMSO with membranes has been studied using a range of techniques summarized elsewhere²⁵. DMSO can diffuse across a lipid bilayer²¹ and can partition within an intermembrane space to limit membrane compression by forming a physical barrier between lipid headgroups⁴. However, DMSO has also been reported to dehydrate lipid membranes^{26,27}. Molecular Dynamics simulations show that DMSO induces membrane thinning and increased membrane fluidity at low concentrations and causes the formation of pores across the bilayer at higher concentrations^{4,15-17}. Schrader and co-workers found that DMSO reduces the repulsive forces between bilayers, whereas glycerol increases them²⁸, and proposed that the differences in hydrogen bonding capability of the two solutes leads DMSO to dehydrate the lipid head groups, while glycerol affects surface hydration only as much as it affects the bulk water properties.

One approach to studying the interactions of molecules with biological membranes is to use model systems of monolayers. Lipid monolayers have been widely accepted as ideal model systems to mimic biological membranes (reviewed for example in²⁹⁻³⁴) as they represent exactly half a bilayer. They have particular advantages in examining the interactions of biomolecules with lipid membranes, and have been used to study such diverse systems as sugars³⁵, cryoprotectants^{36,37}, proteins²⁹, amphiphilic drugs³¹ and antimicrobial peptides³². The conditions under which monolayers and bilayers may be directly compared has also been examined³⁸. The key advantage over bilayer (or multilamellar) systems is that in monolayer studies temperature is constant and the lateral pressure is varied – this enables us to directly probe interactions with water soluble molecules. By contrast the lateral pressure in lamellar systems can only be changed by dehydration (eg^{39,40}). The effects of solutes on lipid organization can be assessed in terms of the changes in the area per lipid molecule, phase transition pressures and inverse compressibility modulus values^{34,41-43}. These can be directly related to the properties of bilayers: for example, the gel and fluid phases of a bilayer are analogous to the liquid condensed and liquid expanded phases, respectively, of a monolayer.

Despite the relevance of monolayer techniques, the interaction between penetrating cryoprotectants and lipid monolayers has not been widely studied except for some early studies using DMSO and glycerol. Williams and Harris⁴⁴ found that DMSO and glycerol are excluded

from the lipid-water interface. Bianco et al.⁴⁵ observed that the presence of glycerol modifies the molecular area, surface potential and thermodynamic properties of monolayers of various lipids. Dabkowska et al.³⁶ found that the presence of DMSO dehydrates the phosphatidylcholine headgroup. Chen and co-workers found similar effects using Vibrational Sum Frequency Generation (VSFG)⁴⁶ and Brewster angle microscopy (BAM)²⁵ and found that the effect of DMSO is concentration dependent. These authors suggest that DMSO-induced condensing and caging is the molecular mechanism that may account for the enhanced permeability of membranes upon exposure to DMSO.

In this paper we present the first comprehensive study of the effects of four common CPAs (DMSO, glycerol, ethylene glycol and dimethyl formamide) on phospholipid monolayers. We study four different phospholipids to determine if the headgroup or level of chain saturation influences the interaction.

2 Materials and methods

2.1 Materials

1,2-dioleoyl-sn-glycero-3-phosphocholine (DOPC) from Sigma-Aldrich Chemistry (Madrid, Spain), 1-Palmitoyl-2-oleoyl-sn-glycero-3-phosphoethanolamine (POPE), 1,2-dipalmitoyl-sn-glycero-3-phosphocholine (DPPC), and 1-palmitoyl-2-oleoyl-glycero-3-phosphocholine (POPC) from Avanti Polar Lipids (Alabaster, AL, USA) were used without further purification. Both of the lipids were dissolved in chloroform, PA-ACS-ISO grade, purchased from PANREAC (Barcelona, Spain) to a final concentration of $1\text{mg}\cdot\text{mL}^{-1}$ and kept in the refrigerator. The subphase used for preparing the Langmuir films was mainly Ultrapure water (Milli Q®, $18.3\text{ M}\Omega\text{cm}$ resistivity). Other than water, various sub-phases such as dimethyl sulphoxide (DMSO), glycerol, ethylene glycol and dimethyl formamide (DMF) (all 5% v/v in ultrapure water) were used. All of the above chemicals, PA-ACS-ISO grade, were purchased from PANREAC.

2.2 Techniques and equipment

2.2.1 Experiment 1 – compression isotherms using standard Langmuir trough.

Langmuir compression isotherms were carried out on a NIMA teflon trough (Nima Technology, Coventry, UK), model 1232D1D2 (area 1200 cm^2), equipped with two movable barriers, and the surface pressure was measured using a pressure sensor with a Wilhelmy plate ($10\text{ mm} \times 50\text{ mm}$ filter paper; Whatman International, Maidstone, UK). The linear velocity of the barriers was $2.5\text{ cm}\cdot\text{min}^{-1}$, which corresponds to an area change of $50\text{ cm}^2\cdot\text{min}^{-1}$ in the trough used.

The trough was placed on a vibration-isolated table (Newport, Irvine, CA, USA) and enclosed in an environmental chamber. The resolution of surface pressure measurement was $\pm 0.1\text{ mN m}^{-1}$. In all experiments, the temperature was controlled at $22.0 \pm 1^\circ\text{C}$. In each experiment, the trough and barriers were cleaned twice with chloroform and once with MilliQ® quality water before the subphase addition. In order to ensure the cleanliness of the subphase, the following

procedure was implemented prior to each run: the trough area was compressed to the minimum surface area, and any surface contaminants were removed by aspiration until zero surface pressure was measured. This procedure was repeated at least 3 times prior to each measurement. Other than MilliQ® quality water, several different CPA sub-phases were used at 5% v/v (dimethyl sulphoxide (DMSO), glycerol, ethylene glycol (EG) and dimethyl formamide (DMF)). 5% v/v was chosen as it is a common concentration used in cryoprotective solutions. This is with the assumption that the slight difference in molarity won't make much difference in the interaction as the molecular weights of the compounds under investigation are not vastly varying.

A 100 μL aliquot of lipid dissolved in chloroform (concentration $0.5 \text{ mg}\cdot\text{mL}^{-1}$) was spread on the surface of the subphase solution with a Hamilton microsyringe (Bonaduz, Switzerland). An equilibration time of 15 min was allowed before starting the experiment, to allow lipid spreading and solvent evaporation. Every Pressure-Area isotherm was repeated at least twice, and the isotherms showed satisfactory reproducibility. As the concentration and trough area are known, the area per lipid molecule can be calculated.

2.2.2 Experiment 2 - insertion experiments

In these experiments, the effect of inserting the CPA directly into the subphase was measured by the change in surface pressure of the lipid monolayer. The experiments were carried out using a NIMA Langmuir Film Balance equipped with a Wilhelmy plate and a small teflon trough that was rinsed with chloroform and ultrapure water before use. All experiments were performed at $22\pm 1^\circ\text{C}$.

For these experiments, a lipid stock solution was prepared and added dropwise on the water subphase until the desired surface pressure was achieved. After 15 min, when equilibrium was reached, the desired cryoprotectant was injected into the subphase to attain a concentration of 5% (v/v). The surface pressure changes were monitored as a function of time for 15 min. For the control experiment the same procedure was followed without using lipid. For each lipid, up to four lipid concentrations were measured (corresponding to different initial pressures). The change in pressure upon addition of the cryoprotectant is a direct measure of the effect of the cryoprotectant on the structure of the monolayer.

3 Results and Discussion

3.1 Surface behavior of cryoprotectants

The surface activity of the cryoprotectants is measured in this section. Initially the surface tension, γ , of the water subphase was measured and found to be $72.6 \text{ mN}\cdot\text{m}^{-1}$. CPAs were then added to give a final concentration of 5% by volume, and the surface tension remeasured. Table 1 shows the measured surface tensions, and the CPA concentration in both $\text{mol}\cdot\text{L}^{-1}$, and mass fraction X_{CPA} . It is seen that DMF has significant surface activity, while the other molecules have minimal activity.

Table1: Surface tension of water and CPA subphases

Sub-phase solutions (5% v/v)	γ (mN.m ⁻¹)	C _{CPA} (mol/L)	X _{CPA}
Water	72.6		
Glycerol	74.8	0.683	0.0128
EG	72.8	0.894	0.0167
DMF	67	0.646	0.0121
DMSO	72.6	0.706	0.0132

3.2 Influence of cryoprotectants on lipid monolayers - Compression Isotherms

The phase behavior can be characterized by surface pressure-area isotherms. Figure 1(a-d) shows the surface pressure-area isotherms of monolayers of the 4 lipids DOPC, POPE, DPPC and POPC on subphases consisting of water, or aqueous solutions with 5% CPA (v/v). The isotherms were reproducible on successive runs. The following parameters are extracted from these isotherms: the lift off area (where the surface pressure rises above zero); the inflection points (where there is a phase change); and the collapse pressure (where pressure reaches a maximum, and further compression leads to collapse of the monolayer). These parameters are provided in Table 2.

The first thing to note from these isotherms is that each pure lipid has slightly different behavior, with DOPC and POPC showing continuous isotherms up to the collapse pressure, whereas both DPPC and POPE show inflections corresponding to a phase change. In all cases, the behavior is not qualitatively changed by the presence of the CPAs, though there are quantitative changes in the values of key parameters.

For all lipids studied, DMF causes a significant compression, shifting the isotherms to the left, whereas glycerol and EG both cause an expansion. This means that at the same surface pressure, DMF causes a reduction in area per molecule, whereas glycerol and EG cause an increase in the area per molecule. A compression of the monolayer implies that the presence of DMF is effectively dehydrating the headgroups, forcing them closer together. By contrast, the behaviour of glycerol and EG implies that they are inserting between the lipids, thus increasing the average area per lipid molecule at fixed surface pressure. This effect of glycerol agrees with that reported in literature²⁸. These different behaviors have important implications for the mechanisms of cryoprotection. The behavior of glycerol and EG are consistent with their behavior as membrane penetrating cryoprotectants - these must reside between lipids during the passage across the membrane, so the observed expansion is consistent with this behavior. The fact that this effect is fairly similar for all four lipids implies that the effect is not strongly dependent on lipid headgroup or chain configuration.

DMSO shows different behavior. For DPPC (saturated) it causes a clear expansion, whereas for POPC (singly unsaturated) it induces a small compression. For POPE and DOPC, the presence of DMSO has little effect. How do we interpret these conflicting results? First, the clear expansion in the presence of DPPC implies significant DMSO penetration into the monolayer. For POPC on the other hand there appears to be some dehydration. For DOPC, there is little effect. So, it appears that DMSO has both a membrane penetration effect, and a

headgroup dehydration effect, which leads to subtle differences depending on the packing of the headgroups. We will return to this point later. Finally, we note that there is only a small difference between POPC and POPE, which implies only a small headgroup dependence.

It is known that these molecules are cell permeable, and so must interact with and pass through the bilayer. The permeability of cells to a particular cryoprotectant is generally termed the cryoprotectant permeability⁴⁷, and has been observed in previous work for glycerol, EG, and DMSO⁴⁸⁻⁴⁹. These papers found that glycerol has much lower permeability than DMSO and EG. This is interesting in the light of the isotherm results – glycerol expands the monolayer, and so must enter into the headgroup region. The low measured permeability implies that it may take a long time to cross the hydrocarbon region of the bilayer. To the best of the authors’ knowledge, there are no measurements of DMF cell permeability. The monolayer studies suggest that DMF dehydrates the headgroups as it causes a net compression. However, DMF has been successfully applied as a cryoprotectant (eg²²).

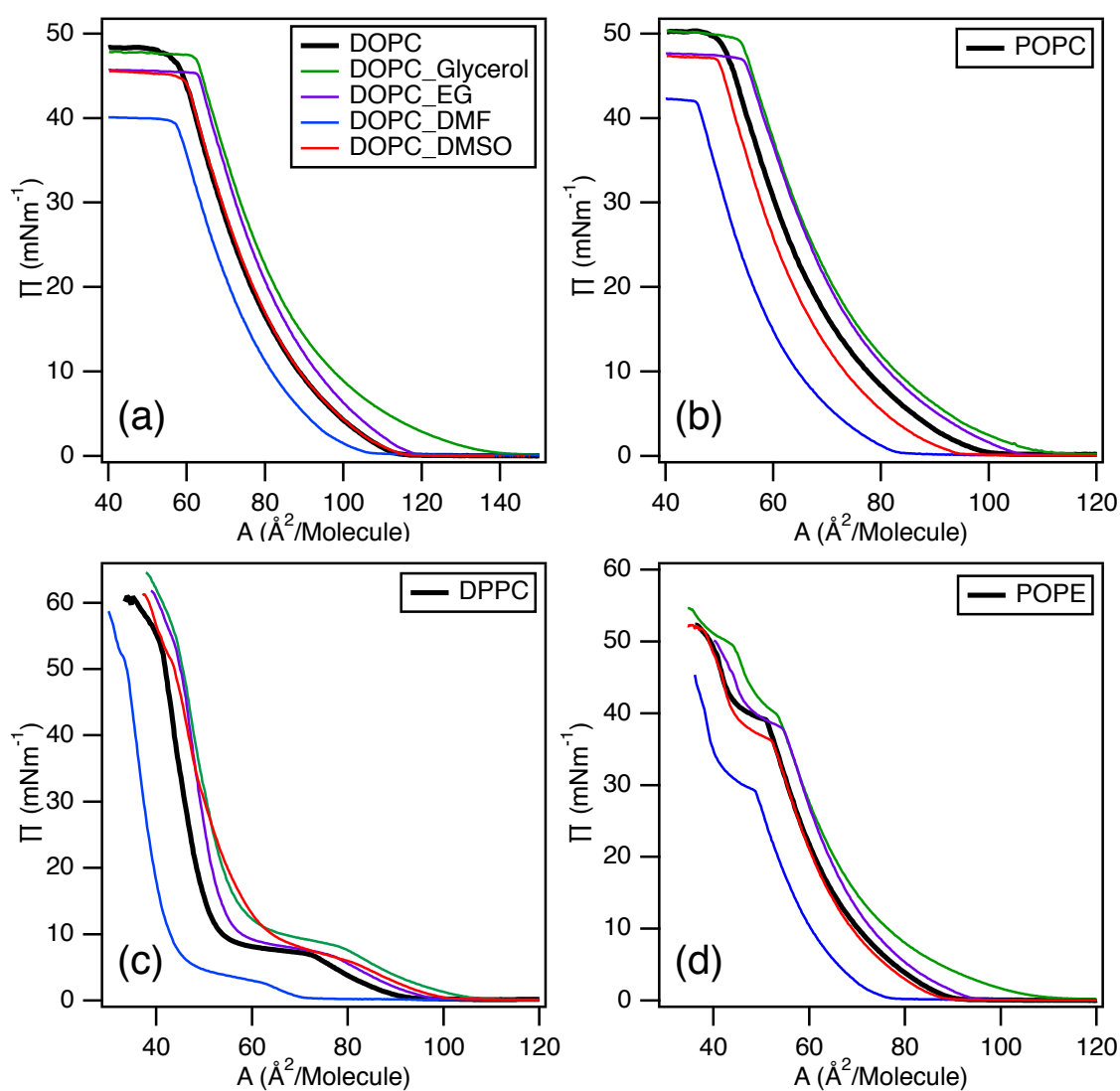


Figure 1: Surface pressure vs. area per molecule for (a) DOPC, (b) POPC, (c) DPPC, (d) POPE with subphases as shown in the legend to (a). Note that the scales are different for each lipid.

In order to further understand these data, Figure 2 shows the calculated inverse compressibility modulus (C_s^{-1})^{43,50}:

$$C_s^{-1} = -A \left(\frac{d\Pi}{dA} \right)_T \quad \text{Eq. (1)}$$

for the data in figure 1. The values of C_s^{-1} allows one to assign the monolayer physical state during compression: C_s^{-1} values between 12.5-100 $\text{mN}\cdot\text{m}^{-1}$ correspond to the liquid expanded (LE) state, $100 < C_s^{-1} < 250 \text{ mN}\cdot\text{m}^{-1}$ corresponds to the liquid condensed (LC) state, and $C_s^{-1} > 250 \text{ mN}\cdot\text{m}^{-1}$ corresponds to the solid (S) state⁵¹.

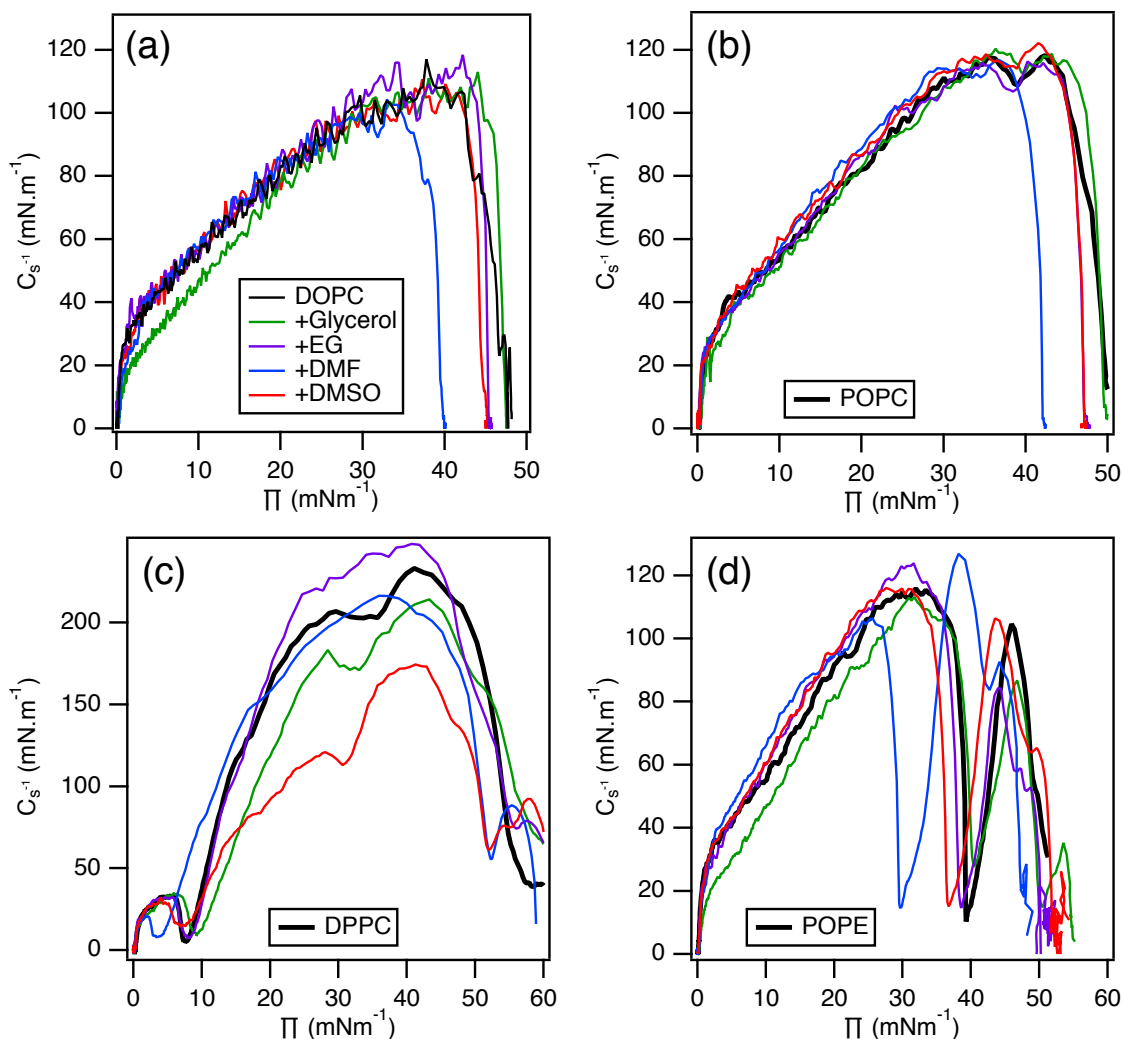


Figure 2: Inverse compressibility modulus vs. surface pressure for the data in figure 1.

DOPC and POPC exhibit the LE state over the whole range, with collapse occurring as the value of C_s^{-1} approaches that of the LC phase. POPE show a clear inflection corresponding to a phase change, but collapse occurs immediately afterwards, so again a stable LC phase is not seen. POPE has its transition temperature at 25 °C, above the working temperature of 22 °C. A result of this is the phase transition around 40 mN/m in the isotherm. Similarly, DPPC exhibits a clear inflection corresponding to a phase change, with C_s^{-1} value rising to above 200 $\text{mN}\cdot\text{m}^{-1}$, corresponding to the LC phase. This is due to the fact that the transition temperature

is 41 °C, above the working temperature of 22 °C. By contrast POPC (transition temperature of -2 °C) and DOPC (transition temperature of -17 °C) do not show phase transition as the corresponding transition temperatures are below 22 °C.

For DOPC and POPC (figures 2a, b) the Cs^{-1} values for DMSO, EG and glycerol subphase are practically the same as that of water subphase until the collapse, with DMF inducing collapse at a slightly lower surface pressure. Interestingly, for DOPC glycerol exhibits slightly lower Cs^{-1} values at lower surface pressures (figure 2a).

For DPPC (figure 2c) the Cs^{-1} values of the CPA and water subphases shows a similar value until the inflection ($\sim 8 \text{ mN.m}^{-1}$). Above the inflection, there is a notable influence of the CPA subphases, with Cs^{-1} values for DMSO and glycerol significantly lower than that of the water subphase, whereas the EG subphase shows higher values of Cs^{-1} than water subphase.

Finally, for POPE (figure 2d), DMSO shows similar Cs^{-1} values to that of water. Glycerol exhibits lower values at low surface pressures, whereas DMF shows a significantly lower transition.

The key parameters extracted from Figures 1 and 2 are summarized in table 2 and discussed here. DOPC (Fig 1a, 2a) shows a lift off area of $118.7 \text{ \AA}^2/\text{molecule}$, with a liquid expanded (LE) state until the collapse (area $\sim 58.7 \text{ \AA}^2/\text{molecule}$, $\Pi \sim 45.4 \text{ mN.m}^{-1}$, $Cs^{-1}_{\text{max}} = 108 \text{ mN.m}^{-1}$). Similar behavior was observed for POPC (Fig 1b, 2b) where the lift-off is at $102.5 \text{ \AA}^2/\text{molecule}$, with a LE state until 50.1 mN.m^{-1} ($Cs^{-1}_{\text{max}} = 118.2 \text{ mN.m}^{-1}$).

The DPPC isotherm (Fig 1c, 2c) behaves very differently. After the lift-off at $\sim 95.5 \text{ \AA}^2/\text{molecule}$, it exhibits LE state until 6.4 mN.m^{-1} , then there is a marked inflection followed by a regular increase in surface pressure corresponding to a Liquid condensed state (LC), and finally a collapse at $\sim 59.9 \text{ mN.m}^{-1}$. Similarly, the POPE monolayer on pure water (Fig 1d, 2d) shows several phases such as the liquid expanded (LE_1) state but with a maximum Cs^{-1} value around 118 mN.m^{-1} at $\Pi \sim 32.3 \text{ mN.m}^{-1}$, which is followed by a phase transition to what is either another liquid expanded (LE_2) state, or to a liquid condensed state (LC) till the collapse at $\Pi \sim 51.1 \text{ mN.m}^{-1}$ - the proximity between the inflection and the collapse do not permit a unique determination of monolayer state in this region.

Table 2: Parameters extracted from figures 1 & 2: lift off area (A_0), collapse area (A_c), collapse pressure (Π_c), Cs^{-1} and Π in the maximum of Cs^{-1} (Cs^{-1}_{max} , Π_{max}).

Lipids/ Subphase	A_0 ($\text{\AA}^2/\text{molecule}$)	A_c ($\text{\AA}^2/\text{molecule}$)	Π_c (mN.m^{-1})	Cs^{-1}_{max} (mN.m^{-1})	Π_{max} (mN.m^{-1})
DOPC	118.7	58.7	45.4	108	39.5
-Glycerol	142	63.3	45.9	108	43.1
-EG	121.2	63.3	45.9	113	41.8
-DMF	108.5	58.2	38.3	103	33.8
-DMSO	117.7	60.5	43.4	106	41.4
POPC	102.5	50.1	49.0	118.2	42.4
-Glycerol	114.7	54.8	47.7	119	36.7
-EG	108.0	55.7	44.9	116	40.2
-DMF	85.7	46.2	40.9	117	36.7

-DMSO	97.5	50.5	45.6	121	42.0
DPPC	95.5	36.1	59.9	29.3/233	6.4/41.1
-Glycerol	107.5	39.3	62.9	32.4/211	7.2/44.1
-EG	100.5	39.9	60.7	29.2/247	6.3/41.8
-DMF	72.4	30.7	57.3	20.5/216	2.2/35.9
-DMSO	102.5	38.6	59.8	29.3/174	4.6/41.3
POPE	92.0	38.2	51.1	118/106	32.3/45.9
-Glycerol	114.3	36.5	53.5	112/86.7	32.2/46.7
-EG	98.5	41.3	48.9	124/84.1	31.6/44.3
-DMF	78.6	35.8	46.1	106/127	25.6/38.1
-DMSO	90.4	39.2	49.6	116/106	31.3/43.5

We now turn to the effects of the CPAs on the lipid monolayer behavior. Looking first at the different headgroups (POPC vs POPE) it can be observed that each of CPAs induces similar changes in the isotherms and compressibility moduli for the two lipids – in other words, there are no significant effects which are specific to the lipid headgroup. As most previous studies have only been carried out on PC headgroups, this is an important finding.

Considering now the individual CPAs, it is observed that the compounds with hydroxyl groups (glycerol and EG) cause an expansion of the monolayer across the whole pressure range for all four lipids, but with no significant effect on the collapse or transition surface pressures, as evidenced by the similarity of the C_s^{-1} plots. Glycerol, with 3 hydroxyl groups, causes a slightly greater expansion of the monolayer than EG, with 2 hydroxyl groups.

The CPA that shows the largest effect is DMF, which induces a compression for all four lipids and also causes significant reductions in the collapse surface pressures and transition surface pressures - this decrease in the π_c may be related in part to the small surface-active character of DMF, as it competes with the lipid at the interface.

Finally, DMSO has almost no effect on the position of the isotherms for DOPC, POPC or POPE except for a slightly lower collapse surface pressure and/or transition surface pressure. Similarly, there is little effect on the C_s^{-1} plots for these lipids. By contrast, DMSO has a significant effect on the fully saturated lipid DPPC (Fig 1c & 2c) – the presence of DMSO shifts the isotherm to the right *ie* it provokes an area increase over the whole range. Both the lift off area and the area of the transition from LE to LC are significantly higher with DMSO than for the pure DPPC lipid. However, the cryoprotectant effects follow the same trends (figure 1C) both below and above the transition from liquid expanded to liquid condensed states (analogous to the fluid and gel states in a bilayer). This implies that headgroup interactions dominate over chain packing effects.

3.3 Insertion experiments

The insertion ability of CPAs into the lipid monolayers was monitored by measuring the variation in surface pressure, $\Delta\Pi$, as a function of the initial surface pressure. The results are shown in Figure 3 (a-d). For all lipids and all CPAs, it is observed that the change in pressure upon insertion, $\Delta\Pi$, decreases linearly as the initial surface pressure Π_i is increased. This is not surprising - higher initial surface pressure means lower area per lipid, and therefore less room

for the CPAs to insert between the lipids. However, although the CPAs follow the same trend, there are significant quantitative differences, with the slope and $\Delta\Pi$ values generally higher for DMF, and to a lesser extent glycerol.

In order to examine these differences, linear fits to the data yield two parameters, the slope and the extrapolation to $\Delta\Pi = 0$, called the Maximum insertion pressure (MIP). According to the treatment of Calvez et al.,⁵² (eq 2), the slope is $(a-1)$ where a is called the “synergy factor”. Values of a and MIP are given in Table 3.

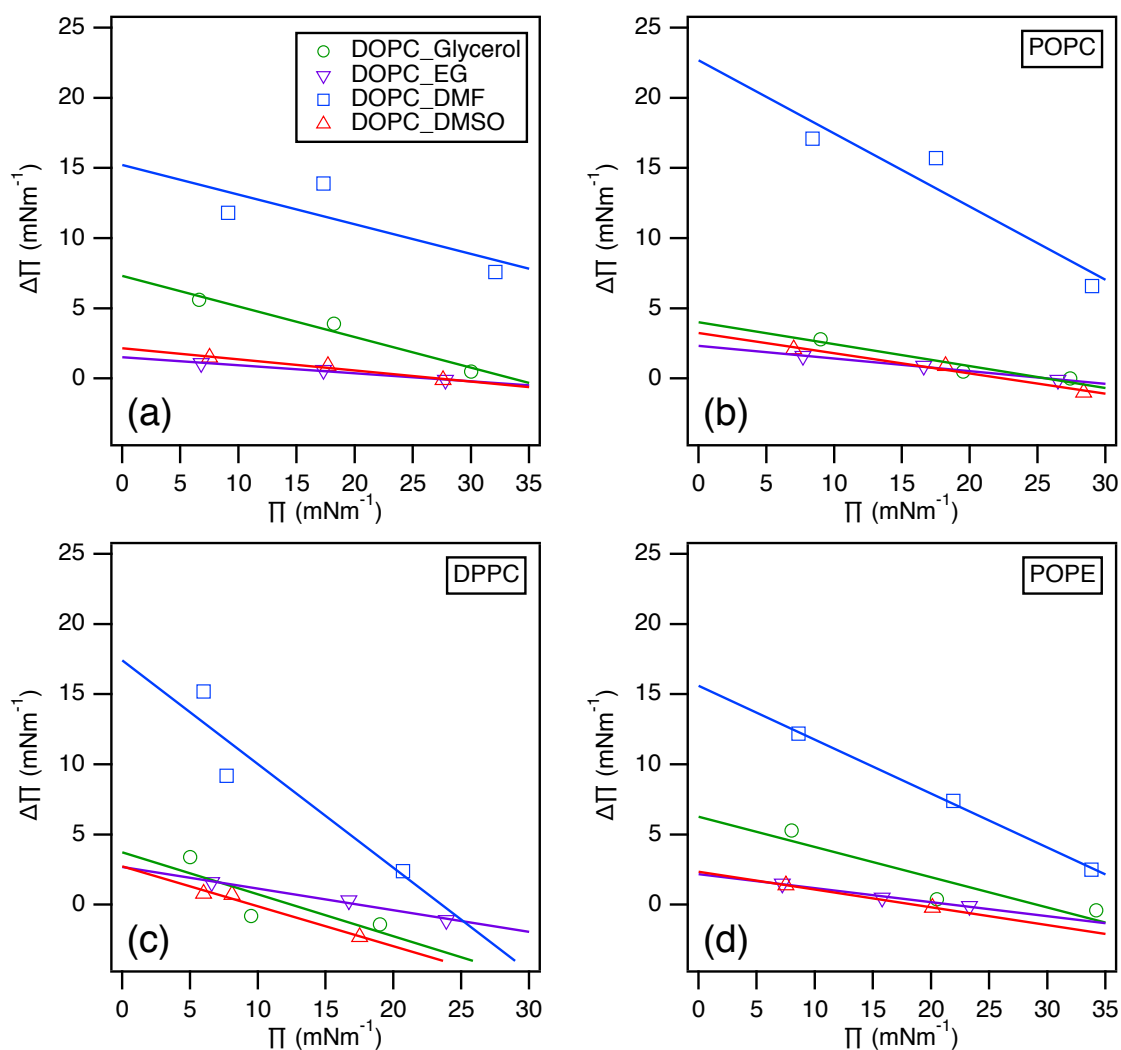


Figure 3: Variation in surface pressure Vs initial pressure in insertion experiments

Table 3: Values of the Maximum Insertion Pressure (MIP) and the synergy factor (a) for the data in figure 3.

LIPIDS	DPPC		POPC		DOPC		POPE	
	MIP	a	MIP	a	MIP	a	MIP	a
Glycerol	12.5	0.70	25.7	0.84	33.5	0.78	29.1	0.79
EG	17.5	0.85	25.8	0.91	26.7	0.94	21.8	0.90

DMF	23.6	0.26	43.5	0.48	71.9	0.79	40.6	0.62
DMSO	9.6	0.72	22.5	0.86	27.2	0.92	18.5	0.87

In all cases $a > 0$, which corresponds to favorable conditions for molecule monolayer binding, with higher values indicating more favorable binding of the CPA into the phospholipid monolayer. A number of trends can be identified from the table. First, for all lipids DMF has the highest MIP, and with the exception of DOPC the lowest value of a . The MIP is the maximum surface pressure, beyond which the molecules cannot insert into the monolayer (ie they would be squeezed out at surface pressures higher than this). Clearly DMF can remain within the monolayer to higher surface pressures. Conversely, the fact that DMF has the highest slope means that changes in surface pressure have a larger effect on the insertion.

The results shown in Table 3 are instructive for comparing the different lipids. Clearly the MIP is lower for DPPC than the other lipids – this makes sense given that DPPC has saturated chains, and a smaller inherent area per molecule, attaining an LC state. Comparing the MIP and values of a for POPC and POPE, which only differ in the headgroup, shows relatively small effects, as also seen in figures 3 b, d. The largest difference is for DMF, where the slope is significantly larger for POPC (ie the values of a are lower) – this means small increases in surface pressure excludes DMF more strongly for POPC than POPE.

For the unsaturated lipids, glycerol, EG and DMSO have similar parameters. However, for DPPC, the MIP is lowest for DMSO, then glycerol. Clearly the reduced area per lipid due to the saturated chains has a role in excluding these molecules.

Considering physiological values of lateral pressure (around 33 mN.m^{-1}), and looking at the MIP values, it is seen that EG and DMSO do not penetrate the phospholipid monolayers of DOPC, glycerol is at the limit, and only DMF clearly penetrates. For POPC and POPE only DMF penetrates at the physiological values of lateral pressure, and for DPPC none of the studied CPAs penetrate at the physiological values of lateral pressure. These results agree with Williams and Harris²⁷ who reported that DMSO and glycerol are excluded from the lipid-water interface.

From these results it is seen that, in general, DPPC is the most difficult to penetrate due to its rigidity and compactness (no unsaturation in the acyl chains), while DOPC is, in general, the most facile to penetrate due to its lower rigidity and compactness (two double bonds in the acyl chains). Consequently, penetration of CPAs needs the presence of phospholipids with unsaturation, as is commonly the case in natural membranes.

4 Discussion

There have been relatively few studies of the effects of artificial cryoprotectants on monolayer isotherms, and most studies that exist have concentrated on DMSO and DPPC. Both Krasteva et al.³⁷ and Chen et al.^{25,46} found that DMSO compresses DPPC isotherms. This effect is the opposite of that found in the current study, where DMSO was observed to expand the DPPC monolayer slightly. Those previous studies used higher concentrations than here, and Chen et al., noted a significant concentration dependence, which may explain the differences observed in the present study. Both studies concluded that DMSO leads to lipid dehydration. Recently, Dabkowska et al.³⁶ performed Neutron reflectivity on DPPC monolayers in the presence of

DMSO, and did not find a significant effect on the surface pressure, but found strong evidence to support the idea of that at high concentrations, DMSO dehydrates the headgroups by displacing water molecules bound to the choline group. Clearly concentration is a key factor – the concentrations chosen for the present study are relevant for cryopreservation.

It is clear that the effects of DMSO are subtle and concentration dependent – the variability seen for the effect of DMSO on the different lipids highlights this. At the concentration studied here, DMSO caused expansion for DPPC, compression for POPC, and had little effect for POPE or DOPC. Clearly further work is needed to understand these effects.

The authors are aware of no previous studies of the effects of glycerol, EG or DMF on phospholipid monolayers. However, while there are no monolayer studies, computer simulations studying the interactions of CPAs on bilayers can provide useful information, as the technique allows for the detailed study of the location of the molecules near the headgroups. Sum et al.⁵³ found that DMSO penetrates more deeply into the bilayer than water – indeed they found that the DMSO sequesters beneath the headgroup, rather than interacting directly with the polar groups, leading to an increase in area per headgroup. Due to the strong DMSO-water interaction they also found that DMSO dehydrates the headgroups.

Malajazuck et al.⁴ examined the effects of DMSO, glycerol and ethylene glycol on DPPC in the fluid phase. They found that each solvent induced lateral expansion of the membrane, consistent with the results found here. These simulations found that EG and glycerol induced less expansion than DMSO, contrary to what was found in this study. Again, the simulation trends were observed for much higher CPA concentrations than are used here, so the differences may be due to the concentration.

5 Conclusions

The influence of four common CPAs (DMSO, glycerol, EG and DMF) on monolayers of four common phospholipids (DPPC, POPC, DOPC and POPE), have been studied using compression surface pressure-area isotherms and insertion experiments. The CPA concentrations were chosen to be directly relevant to cryoprotection. To the best of the authors' knowledge, there has no previous studies of the effects of glycerol, EG or DMF on phospholipid monolayers although they are widely used as membrane penetrating cryoprotectants. These are also the first membrane insertion experiments reported for these molecules.

The main conclusions from this study are:

The effects of DMSO are subtle and concentration dependent – the variability observed for the effect of DMSO on the different lipids highlights this. At the concentration studied here (of relevance to cryopreservation), DMSO caused an expansion of the DPPC area per lipid. This is in contrast to previous studies from Krasteva et al.³⁷ and Chen et al.^{25,46}, which reported compression. However, those studies used higher CPA concentrations, so this highlights the importance of understanding concentration dependent effects, and of studying concentrations relevant to the application (in this case cryopreservation).

The effects of DMSO are strongly dependent on the lipid species – while DMSO caused expansion for DPPC (in both the liquid expanded and condensed phases), it caused

compression for POPC, and had little effect for POPE or DOPC. As most previous studies have involved only DPPC, this highlights the importance of studying different lipid types as these may have a significant effect on the interactions.

This study showed that both EG and glycerol cause a small expansion of the monolayer at fixed pressure, implying that they insert into the headgroup regions. This effect is similar for all lipid species studied and is consistent with their ability to penetrate membranes.

By contrast, DMF causes monolayer compression for all lipid species, implying it dehydrates the lipid head groups. This is perhaps related to the small inherent surface activity of DMF, which reduced the surface tension by 5.6 mN.m^{-1} compared to pure water. This surface activity may also be responsible for the fact that DMF had the highest maximum insertion pressure (ie showed the strongest affinity to stay in the monolayer). DMF has been used as a cryoprotectant, but there have been very few studies of its lipid interactions – clearly more work needs to be done here.

However, all four CPAs are known to penetrate into cells. Understanding the mechanisms of this penetration in more detail is the goal of future work using neutron membrane diffraction in lamellar systems ^{2,11,12}.

The insertion studies showed that the phospholipid species has a notable impact on the interactions with the CPAs. DPPC was the most difficult to penetrate (as expected due to the tighter chain packing) while DOPC was the most facile. These studies imply that at physiological values of lateral pressure, the penetrating action of CPAs may only occur for unsaturated phospholipids (as are present in natural membranes). Thus, extrapolations of results based solely on the saturated lipid DPPC need to be made with care.

While previous studies have been conducted overwhelmingly with model membranes (often DPPC) it is clear that the lipid species has a significant effect – more studies are needed with membrane models which more closely mimic biological membranes. In particular, almost all previous studies have been conducted with zwitterionic (neutral) lipids. However, one might expect charged lipids (such as phosphatidylinositol) to play a significant role in interactions with polarizable molecules such as CPAs, and effects of salts and pH may also play a significant role. Further studies of such systems are clearly needed.

Conflicts of Interest: The authors declare no conflicts of interest.

Acknowledgements: RR thanks the European Union and UPC for an Erasmus-K7 grant and acknowledges the support of an Australian Government Research Training Program Scholarship from RMIT. GB acknowledges funding from the Australian Research Council under Linkage Grant (Nos. LP140100993 and LP160101496).

References

- 1 Bryant, G., Koster, K. L. & Wolfe, J. Membrane behaviour in seeds and other systems at low water content: the various effects of solutes. *Seed Science Research* **11**, 17-25 (2001).

- 2 Garvey, C. J., Lenne, T., Koster, K. L., Kent, B. & Bryant, G. Phospholipid membrane protection by sugar molecules during dehydration-insights into molecular mechanisms using scattering techniques. *Int J Mol Sci* **14**, 8148-8163, doi:10.3390/ijms14048148 (2013).
- 3 Wolfe, J. & Bryant, G. Cellular cryobiology: thermodynamic and mechanical effects. *International Journal of Refrigeration-Revue Internationale Du Froid* **24**, 438-450, doi:10.1016/s0140-7007(00)00027-x (2001).
- 4 Malajczuk, C. J., Hughes, Z. E. & Mancera, R. L. Molecular dynamics simulations of the interactions of DMSO, mono-and polyhydroxylated cryosolvents with a hydrated phospholipid bilayer. *Biochimica et Biophysica Acta (BBA)-Biomembranes* **1828**, 2041-2055 (2013).
- 5 Wolfe, J. & Bryant, G. Freezing, drying, and/or vitrification of membrane-solute-water systems. *Cryobiology* **39**, 103-129, doi:10.1006/cryo.1999.2195 (1999).
- 6 Lenne, T., Garvey, C. J., Koster, K. L. & Bryant, G. Kinetics of the lamellar gel-fluid transition in phosphatidylcholine membranes in the presence of sugars. *Chem Phys Lipids* **163**, 236-242, doi:10.1016/j.chemphyslip.2009.12.001 (2010).
- 7 Mazur, P. Freezing of living cells: mechanisms and implications. *American Journal of Physiology-Cell Physiology* **247**, C125-C142 (1984).
- 8 Fahy, G. M. Cryoprotectant toxicity neutralization. *Cryobiology* **60**, S45-53, doi:10.1016/j.cryobiol.2009.05.005 (2010).
- 9 Fuller, B. J., Lane, N., Benson, E. E. & Mazur, P. in *Life in the frozen state* 3-65 (CRC Press, 2004).
- 10 Kent, B. *et al.* Measurement of glucose exclusion from the fully hydrated DOPE inverse hexagonal phase. *Soft Matter* **6**, 1197, doi:10.1039/b919086d (2010).
- 11 Kent, B. *et al.* Direct Comparison of Disaccharide Interaction with Lipid Membranes at Reduced Hydrations. *Langmuir* **31**, 9134-9141, doi:10.1021/acs.langmuir.5b02127 (2015).
- 12 Kent, B. *et al.* Localization of trehalose in partially hydrated DOPC bilayers: insights into cryoprotective mechanisms. *J R Soc Interface* **11**, 20140069, doi:10.1098/rsif.2014.0069 (2014).
- 13 Stewart, S. & He, X. Intracellular Delivery of Trehalose for Cell Banking. *Langmuir* (2018).
- 14 De Leeuw, F., De Leeuw, A., Den Daas, J., Colenbrander, B. & Verkleij, A. Effects of various cryoprotective agents and membrane-stabilizing compounds on bull sperm membrane integrity after cooling and freezing. *Cryobiology* **30**, 32-44 (1993).
- 15 Gurtovenko, A. A. & Anwar, J. Modulating the structure and properties of cell membranes: the molecular mechanism of action of dimethyl sulfoxide. *The journal of physical chemistry B* **111**, 10453-10460 (2007).
- 16 Hughes, Z. E., Mark, A. E. & Mancera, R. L. Molecular dynamics simulations of the interactions of DMSO with DPPC and DOPC phospholipid membranes. *The Journal of Physical Chemistry B* **116**, 11911-11923 (2012).
- 17 Notman, R., Noro, M., O'Malley, B. & Anwar, J. Molecular basis for dimethylsulfoxide (DMSO) action on lipid membranes. *Journal of the American Chemical Society* **128**, 13982-13983 (2006).
- 18 Simonin, H., Winckler, P., Gros, A., Perrier-Cornet, J.-M. & Gervais, P. How dehydration with glycerol protects bacteria cell membranes against deleterious

- effects of supercooling. *Cryobiology* **71**, 549, doi:10.1016/j.cryobiol.2015.10.051 (2015).
- 19 Yu, Z.-W. & Quinn, P. J. The modulation of membrane structure and stability by dimethyl sulphoxide (Review). *Molecular membrane biology* **15**, 59-68 (1998).
- 20 Anchooguy, T. J., Cecchini, C. A., Crowe, J. H. & Crowe, L. M. Insights into the cryoprotective mechanism of dimethyl sulfoxide for phospholipid bilayers. *Cryobiology* **28**, 467-473 (1991).
- 21 Anchooguy, T. J., Rudolph, A. S., Carpenter, J. F. & Crowe, J. H. Modes of interaction of cryoprotectants with membrane phospholipids during freezing. *Cryobiology* **24**, 324-331 (1987).
- 22 Alvarenga, M. A., Papa, F. O., Landim-Alvarenga, F. & Medeiros, A. Amides as cryoprotectants for freezing stallion semen: a review. *Animal reproduction science* **89**, 105-113 (2005).
- 23 Hubálek, Z. Protectants used in the cryopreservation of microorganisms. *Cryobiology* **46**, 205-229, doi:10.1016/s0011-2240(03)00046-4 (2003).
- 24 Wolkers, W. F. *et al.* Factors Affecting the Membrane Permeability Barrier Function of Cells during Preservation Technologies. *Langmuir* **35**, 7520-7528 (2018).
- 25 Chen, X., Huang, Z., Hua, W., Castada, H. & Allen, H. C. Reorganization and caging of DPPC, DPPE, DPPG, and DPPS monolayers caused by dimethylsulfoxide observed using Brewster angle microscopy. *Langmuir* **26**, 18902-18908 (2010).
- 26 Kiselev, M., Lesieur, P., Kiselev, A., Grabielle-Madmond, C. & Ollivon, M. DMSO-induced dehydration of DPPC membranes studied by X-ray diffraction, small-angle neutron scattering, and calorimetry. *Journal of alloys and compounds* **286**, 195-202 (1999).
- 27 Cheng, C.-Y., Song, J., Pas, J., Meijer, L. H. & Han, S. DMSO induces dehydration near lipid membrane surfaces. *Biophysical journal* **109**, 330-339 (2015).
- 28 Schrader, A. M., Cheng, C.-Y., Israelachvili, J. N. & Han, S. (AIP Publishing, 2016).
- 29 Brockman, H. Lipid monolayers: why use half a membrane to characterize protein-membrane interactions? *Current Opinion in Structural Biology* **9**, 438-443, doi:[https://doi.org/10.1016/S0959-440X\(99\)80061-X](https://doi.org/10.1016/S0959-440X(99)80061-X) (1999).
- 30 Eeman, M. & Deleu, M. From biological membranes to biomimetic model membranes. **v. 14** (2010).
- 31 Hac-Wydro, K. & Dynarowicz-Latka, P. Biomedical applications of the Langmuir monolayer technique. *Annales Umcs, Chemistry* **63**, 47-60, doi:10.2478/v10063-008-0027-2 (2008).
- 32 Maget-Dana, R. The monolayer technique: a potent tool for studying the interfacial properties of antimicrobial and membrane-lytic peptides and their interactions with lipid membranes. *Biochimica et Biophysica Acta (BBA)-Biomembranes* **1462**, 109-140 (1999).
- 33 Siontorou, C. G., Nikoleli, G.-P., Nikolelis, D. P. & Karapetis, S. K. Artificial Lipid Membranes: Past, Present, and Future. *Membranes (Basel)* **7**, 38, doi:10.3390/membranes7030038 (2017).
- 34 Giner-Casares, J. J., Brezesinski, G. & Möhwald, H. Langmuir monolayers as unique physical models. *Current Opinion in Colloid & Interface Science* **19**, 176-182 (2014).
- 35 Arnett, E. M., Harvey, N., Johnson, E., Johnston, D. S. & Chapman, D. No phospholipid monolayer-sugar interactions. *Biochemistry* **25**, 5239-5242 (1986).

- 36 Dabkowska, A. P. *et al.* Modulation of dipalmitoylphosphatidylcholine monolayers by dimethyl sulfoxide. *Langmuir* **30**, 8803-8811 (2014).
- 37 Krasteva, N., Vollhardt, D., Brezesinski, G. & Möhwald, H. Effect of sugars and dimethyl sulfoxide on the structure and phase behavior of DPPC monolayers. *Langmuir* **17**, 1209-1214 (2001).
- 38 Marsh, D. Lateral pressure in membranes. *Biochimica et Biophysica Acta (BBA) - Reviews on Biomembranes* **1286**, 183-223, doi:[https://doi.org/10.1016/S0304-4157\(96\)00009-3](https://doi.org/10.1016/S0304-4157(96)00009-3) (1996).
- 39 Bryant, G. & Koster, K. L. Dehydration of solute–lipid systems: hydration forces analysis. *Colloids and Surfaces B: Biointerfaces* **35**, 73-79 (2004).
- 40 Lenne, T., Bryant, G., Holcomb, R. & Koster, K. L. How much solute is needed to inhibit the fluid to gel membrane phase transition at low hydration? *Biochimica Et Biophysica Acta-Biomembranes* **1768**, 1019-1022, doi:10.1016/j.bbamem.2007.01.008 (2007).
- 41 Nowotarska, S. W., Nowotarski, K. J., Friedman, M. & Situ, C. Effect of structure on the interactions between five natural antimicrobial compounds and phospholipids of bacterial cell membrane on model monolayers. *Molecules* **19**, 7497-7515 (2014).
- 42 Torrent-Burgués, J. Phase separation in mixed monolayers of arachidic acid and a phthalocyanine of zinc. *Colloids and Surfaces A: Physicochemical and Engineering Aspects* **396**, 137-143 (2012).
- 43 Torrent-Burgués, J. Langmuir films study on lipid-containing artificial tears. *Colloids and Surfaces B: Biointerfaces* **140**, 185-188 (2016).
- 44 Meryman, H., Williams, R. & Douglas, M. S. J. Freezing injury from “solution effects” and its prevention by natural or artificial cryoprotection. *Cryobiology* **14**, 287-302 (1977).
- 45 Bianco, I. D., Fidelio, G. D. & Maggio, B. Effect of glycerol on the molecular properties of cerebroside, sulphatides and gangliosides in monolayers. *Biochemical Journal* **251**, 613 (1988).
- 46 Chen, X. & Allen, H. C. Interactions of dimethylsulfoxide with a dipalmitoylphosphatidylcholine monolayer studied by vibrational sum frequency generation. *The Journal of Physical Chemistry A* **113**, 12655-12662 (2009).
- 47 Vian, A. M. & Higgins, A. Z. Membrane permeability of the human granulocyte to water, dimethyl sulfoxide, glycerol, propylene glycol and ethylene glycol. *Cryobiology* **68**, 35-42, doi:<http://dx.doi.org/10.1016/j.cryobiol.2013.11.004> (2014).
- 48 PEDRO, P. B. *et al.* Permeability of mouse oocytes and embryos at various developmental stages to five cryoprotectants. *Journal of Reproduction and Development* **51**, 235-246 (2005).
- 49 Shu, Z. Q. *et al.* A study of the osmotic characteristics, water permeability, and cryoprotectant permeability of human vaginal immune cells. *Cryobiology* **72**, 93-99, doi:10.1016/j.cryobiol.2016.03.003 (2016).
- 50 Patterson, M., Vogel, H. J. & Prenner, E. J. Biophysical characterization of monofilm model systems composed of selected tear film phospholipids. *Biochimica et Biophysica Acta (BBA)-Biomembranes* **1858**, 403-414 (2016).
- 51 Vitovič, P., Nikolelis, D. & Hianik, T. Study of calix [4] resorcinarene–dopamine complexation in mixed phospholipid monolayers formed at the air–water interface. *Biochimica et Biophysica Acta (BBA)-Biomembranes* **1758**, 1852-1861 (2006).

- 52 Calvez, P., Demers, E. r., Boisselier, E. l. & Salesse, C. Analysis of the contribution of saturated and polyunsaturated phospholipid monolayers to the binding of proteins. *Langmuir* **27**, 1373-1379 (2011).
- 53 Benson, J. D., Woods, E. J., Walters, E. M. & Critser, J. K. The cryobiology of spermatozoa. *Theriogenology* **78**, 1682-1699, doi:<http://dx.doi.org/10.1016/j.theriogenology.2012.06.007> (2012).

Chapter 4

n-Octyl(thio)glycosides as Potential Cryoprotectants: Glass Transition Behaviour, Membrane Permeability, and Ice Recrystallization Inhibition Studies*

This work has been published as a research communication in the Australian Journal of Chemistry. Citation of the paper is:

Raju Rekha, Merl Theresa, Adam Madeleine K., Staykov Emiliyan, Ben Robert N., Bryant Gary, Wilkinson Brendan L. (2019) *n-Octyl (Thio)glycosides as Potential Cryoprotectants: Glass Transition Behaviour, Membrane Permeability, and Ice Recrystallization Inhibition Studies**. *Australian Journal of Chemistry* **72**, 637-643; <https://doi.org/10.1071/CH19159>

Author contributions:

- I conducted the glass transition and cell permeability studies with n-octyl-(thio)glycosides. I have carried out the analysis and interpretation of the results and wrote the initial draft of the manuscript.
- Synthesis of the glycosides and their purity testing has been done by Dr. Brendan Wilkinson and Theresa Merl at their lab in University of New England, Sydney.
- Ice recrystallization inhibition studies of these compounds were carried out by Madeleine Adam, Emiliyan Staykov and Prof. Robert Ben at their lab in University of Ottawa, Canada.
- Manuscript corrections and modification to final form has been done with the guidance of Dr. Brendan Wilkinson and Prof. Gary Bryant.

See Appendix I for the supplementary material from this paper.

Candidate's Name:	Ms. Rekha Raju	Date
		11/11/2019

Principal Supervisor's Name:	Prof. Gary Bryant	Date
		11/11/2019

n-Octyl (Thio)glycosides as Potential Cryoprotectants: Glass Transition Behaviour, Membrane Permeability, and Ice Recrystallization Inhibition Studies*

Rekha Raju,^A Theresa Merl,^B Madeleine K. Adam,^C Emiliyan Staykov,^C Robert N. Ben,^C Gary Bryant,^{A,D} and Brendan L. Wilkinson^{B,D}

^ACentre for Molecular and Nanoscale Physics, School of Science, RMIT University, Melbourne, Vic. 3000, Australia.

^BSchool of Science and Technology, University of New England, Armidale, NSW 2351, Australia.

^CDepartment of Chemistry and Biomolecular Sciences, University of Ottawa, Ottawa, ON K1N 6N5, Canada.

^DCorresponding authors. Email: gary.bryant@rmit.edu.au; brendan.wilkinson@une.edu.au

A series of eight *n*-octyl (thio)glycosides (**1** α , **2** α , **3** α , **4** α , **1** β , **2** β , **3** β , **4** β) with D-glucose or D-galactose-configured head groups and varying anomeric configuration were synthesized and evaluated for glass transition behaviour, membrane permeability, and ice recrystallization inhibition (IRI) activity. Of these, *n*-octyl β -D-glucopyranoside (**2** β) exhibited a high glass transition temperatures (T_g), both as a neat sample and 20 wt-% aqueous solution. Membrane permeability studies of this compound revealed cellular uptake to concentrations relevant to the inhibition of intracellular ice formation, thus presenting a promising lead candidate for further biophysical and cryopreservation studies. Compounds were also evaluated as ice recrystallization inhibitors; however, no detectable activity was observed for the newly tested compounds.

Manuscript received: 10 April 2019.

Manuscript accepted: 25 July 2019.

Published online: 14 August 2019.

Cryopreservation is a technique that utilizes ultralow temperatures for the long-term preservation and subsequent re-use of structurally intact and biochemically viable cells.^[1] However, unprotected freezing is almost universally lethal and requires the use of chemical additives, or cryoprotective agents (CPAs), to preserve life at the very low temperatures required—ideally well below -100°C .^[2] Combined with carefully optimized cooling (and warming) rates, CPAs make it possible to achieve these low temperatures without the damaging effects of ice formation and excessive freeze-induced cell dehydration. By increasing the overall solute concentration, CPAs can act intracellularly or extracellularly (or both) by several known mechanisms, including restoration of osmotic balance to avoid freeze-induced dehydration, promotion of a glassy state (vitrification), and the elimination of intracellular ice formation (IIF) – a major cause of cryoinjury.^[3]

Since the first use of glycerol as a CPA in 1949,^[4] cryopreservation technologies utilizing CPAs have evolved to the point where it is now possible to successfully preserve animal and plant cells and tissues, including red and white blood cells, plant seeds and leaf tips, some stem cells, and cancer cells.^[5] However, despite decades of research, serious problems associated with the toxicity of conventional CPAs persist, which

has limited their routine use to all but a few cell and tissue types. Widely used cell-penetrating CPAs such as dimethyl sulfoxide (DMSO) and glycerol are toxic to many cell types and can disrupt lipid membranes at high concentrations.^[2,5] Successful freezing protocols using CPAs are highly cell-dependent and require a careful balance between cooling rates and CPA concentration and exposure time. The toxicity of commonly used CPAs also requires rapid thawing followed by time-consuming and expensive removal before re-use of the sample, which is less than ideal for critical applications including reproductive technologies, stem cell therapies, organ and tissue transplantation, and preservation of endangered plant and animal species. Most conventional CPAs also do not inhibit damaging ice recrystallization (the growth of larger ice crystals at the expense of smaller ones) that often occurs during thawing cycles. New, non-toxic CPAs that can penetrate and access all cellular compartments, promote vitrification, and which are capable of inhibiting ice recrystallization are highly sought after in several research fields and industries including biotechnology, regenerative medicine, food technology, and conservation. However, despite decades of research and the clear benefit of these CPAs to humankind, no such breakthrough has eventuated.

*Brendan L. Wilkinson is the winner of the 2017 RACI Athel Beckwith Award.

Many cold-tolerant and freeze-avoiding organisms residing in the Earth's temperate and polar regions produce natural CPAs and macromolecular antifreezes as key adaptations that enable survival in these harsh climates.^[6] For example, soluble sugars such as sucrose, trehalose, and raffinose play essential roles in reducing cold stress and improving cold tolerance in several plant, fungal, and insect species.^[7] These polyhydric molecules also restore osmotic equilibrium during freezing, thus alleviating freeze-induced dehydration and cell death, and stabilize lipid membranes during freeze-induced dehydration by retaining additional water, and hindering the close approach of membranes.^[8,9] Glycolipids of natural and synthetic origin have been shown to promote thermal hysteresis activity in several cold-tolerant organisms,^[10] as well as stabilize proteins^[11] and artificial vesicles during freeze-drying, presumably through hydration of phospholipid head groups within the lipid bilayer.^[12] Owing to their low toxicity, promising ice growth inhibition activity, and high glass transition temperatures in experimental systems, carbohydrates have emerged as attractive candidates for the development of new CPAs. Unfortunately, owing to their high polarity, soluble sugars alone are poor cryoprotectants as they are generally not membrane permeable, and so are incapable of inhibiting IIF.

An alternative, and extremely promising, approach aimed at improving the membrane permeability of soluble sugars is to enhance lipophilicity by modifying the carbohydrate scaffold with hydrophobic groups.^[13–15] In their previous work, Toner and coworkers reported the synthesis and membrane permeability properties of some modified trehalose derivatives possessing enzyme-cleavable acetate esters.^[15] Increasing the intracellular concentration of soluble sugars has also been shown to enhance the survival and viability of mammalian cells post thaw.^[16] Recent work from our laboratory, along with Ben and colleagues, have also demonstrated the significant ice recrystallization inhibition (IRI) activity of amphiphilic carbohydrate derivatives including surfactants and hydrogelators,^[17] azobenzene analogues,^[18,19] and aryl glycosides.^[20] *N*-octyl (thio)glycosides are non-ionic surfactants that have emerged as viable alternatives to ionic surfactants from petrochemical origin due to their clinical mildness, low toxicity, and performance. As such, they have seen widespread use in pharmaceutical and consumer health care industries, as well as in biochemical research.^[21] Non-ionic, carbohydrate-based surfactants have emerged as promising CPAs given their remarkably high, sub-zero glass transition temperatures and ability to inhibit eutectic formation in NaCl/H₂O mixtures.^[22] Despite this, their viability as a new class of penetrating CPAs is yet to be fully explored. Based on these earlier observations and inspired by the natural antifreeze and cryoprotective activity of glycolipids, we were interested in exploring the potential of *n*-octyl (thio)glycosides as a novel and accessible class of penetrating CPA. We reasoned that, given their low toxicity, promising thermal properties, and hydrophobicity, these molecules could induce glass transitions at relatively high temperatures and display sufficient membrane permeability to access intracellular compartments and eliminate IIF. Herein, we report the glass transition properties, membrane permeability, and IRI activity of eight *n*-octyl (thio)glycosides (**1α**, **β–4α**, **β**). These (thio)glycosides possess a variable monosaccharide head group (glucose or galactose) linked to an *n*-octyl tail group via an oxygen or sulfur atom with either α or β anomeric configuration. We demonstrate the high dependence of the glass transition behaviour on the molecular structure of these surfactants, membrane permeability, and IRI

activity, which are preliminary steps in their overall examination as potential cryoprotectants.

In order to understand the effect of the monosaccharide head group and anomeric linkage on the cryoprotective properties of the surfactants, our studies commenced with the synthesis of eight *n*-octyl (thio)glycosides **1α**, **β–4α**, **β**, each possessing a glucose or galactose head group linked to an *n*-octyl tail group via an oxygen or sulfur atom at the anomeric centre (Fig. 1). Optically pure surfactants **1α**, **β–4α**, **β** were synthesized using known and adapted literature procedures employing Lewis acid (BF₃·Et₂O)-promoted glycosylation of 1-octanol or 1-octanethiol with commercial β -D-galactose pentaacetate or β -D-glucose pentaacetate as donors (see Supplementary Material for details).^[23,24] Protected (thio)glycosides were afforded in good yields as anomeric mixtures (2:1 to 2:3 α/β selectivity), which were resolved using flash silica gel chromatography. Optically pure per-*O*-acetylated *n*-octyl (thio)glycosides were then smoothly deprotected under standard Zemplén conditions to give target compounds in quantitative yields.

We next investigated the vitrification behaviour of these *n*-octyl (thio)glycosides using differential scanning calorimetry (DSC), both as neat samples and as 20 wt-% aqueous solutions (0.68 M for **1α**, **β** and **2α**, **β**; 0.65 M for **3α**, **β** and **4α**, **β**) relevant to cryopreservation. The glass transition behaviour (T_g) of octyl β -D-glucopyranoside (**2β**) and octyl β -D-thioglucopyranoside (**4β**) has been previously investigated by Ogawa and coworkers, with relatively high T_g values observed on heating and no ice formation observed at concentrations above ~80 wt-% in water.^[22] We were thus interested in observing the glass transition temperatures of surfactants **1–4** possessing alternative head groups and anomeric configuration at concentrations and temperatures most relevant to cryopreservation. For DSC thermograms of neat surfactants, samples (5–10 mg) were hermetically sealed in aluminium sample pans and cycled between +150°C and –50°C at a rate of 10°C min^{–1}, with 1-min equilibration times at the endpoints (Fig. 2a). The thermal values for neat surfactants are summarized in Table 1. Of the eight samples studied, only thioglycosides **4α** and **4β** did not show any glass transition behaviour as anhydrous solids on warming from –100°C to 25°C (see Fig. S1, Supplementary Material). The remaining soluble samples showed T_g values between 0°C and –15°C, which are clearly visible as step-like inflections in the thermograms, as previously reported for some *n*-octyl glycosides.^[25,26] However, the T_g values for the neat samples are slightly lower than that previously reported, which may be attributable to the adsorption of trace water and the possibility of hemihydrate crystal formation.^[27]

Galactoside **1α**, thiogalactoside **3β**, and thioglycosides **4α**, **β** unfortunately were only partially soluble and so could not be assessed as a 20 wt-% binary system with water. DSC thermograms of the four soluble surfactants (**1β**, **2α**, **2β**, and **3α**) were recorded by warming samples from –120°C to 25°C at a rate of 5°C min^{–1}, with 1-min equilibration time, and the results are shown in Fig. 2b. On cooling, large exothermic peaks could be seen between –15°C and –25°C, thus indicating ice crystallization (see Fig. S2, Supplementary Material). Following glass melting in the warming run, the supercooled solution then underwent freezing, as shown by a positive peak. The ice subsequently melted as it reached the freezing point, as indicated by the large endothermic peaks. The melting temperature, T_m , can thus be defined at the end of ice melting for most of the solutions studied. Encouragingly, all soluble *n*-octyl (thio)glycosides displayed T_g values above –60°C, which are

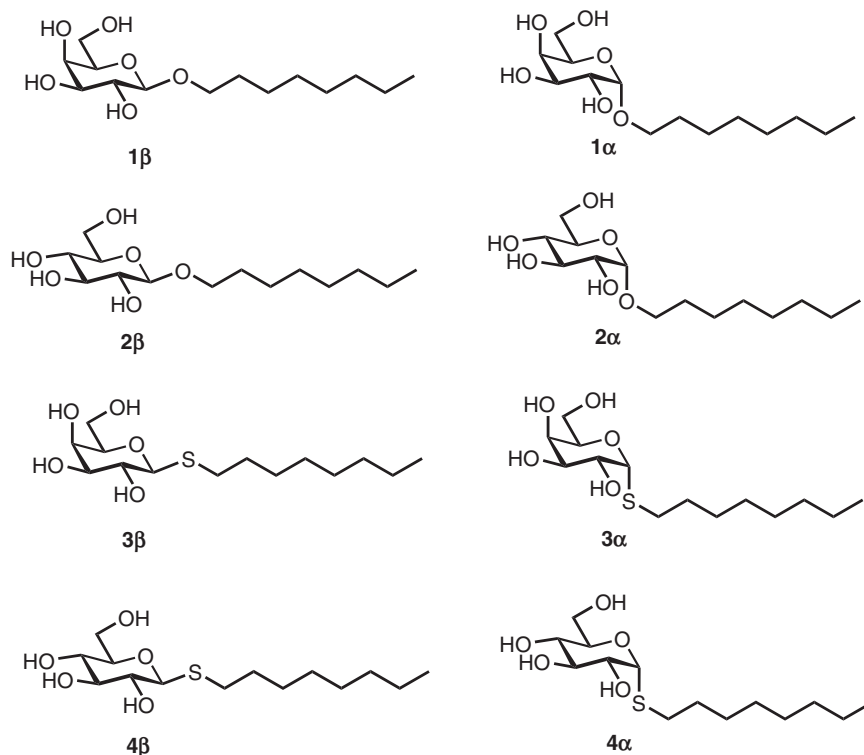


Fig. 1. Chemical structures of *n*-octyl (thio)glycosides 1–4 used in this study.

higher than the commonly used CPA, DMSO (T_g approximately -130°C ; see Fig. 2). Of these, *n*-octyl β -D-glucoside **2 β** showed particular promise, with high T_g values, both as a neat sample ($T_g -4.97^\circ\text{C}$) and in solution ($T_g -48^\circ\text{C}$), which is in good agreement with previous thermal studies on this compound.^[28]

For **2 α** and **3 α** , there were small changes in the baseline that may correspond to T_g , but could also represent liquid crystalline transitions that could not be confirmed based on current data. They are indicated by the small arrows (Fig. 2b) and values with superscript letter ‘A’ in Table 1. In the case of **2 α** , the fact that there is a clear devitrification peak indicates that glass melting must have occurred; however, the value of T_g is unclear. The positive peaks at temperatures just below ice melting could be due to ice recrystallization, but may also be attributed to crystallization of synthesized glycosides, as recently shown by Ogawa and coworkers.^[29] For the purpose of the present study, we are only interested in the glass transition properties, and so this was not pursued further.

Clear devitrification peaks are observed for **1 β** , **2 α** , and **2 β** , which must be preceded by glass melting. The glass transitions are clear for **1 β** and **2 β** , but indistinct for **2 α** , where two possible weak transitions were identified (marked by superscript letter ‘A’). **3 α** shows no devitrification peak, with a weak possible glass transition just before melting (marked by superscript letter ‘A’). The thermal values for aqueous surfactants are summarized in Table 1.

Having established the thermal properties of the *n*-octyl (thio)glycosides, the next stage of our study focussed on the cell permeability of the four molecules possessing promising T_g values and high solubility in water and RPMI cell media (**1 β** , **2 β** , **2 α** , **3 α**). For the most commonly used CPA, DMSO, the cryobiologically relevant concentrations are 5 and 10% by volume, which is equivalent to 0.65 and 1.3 M

respectively. A cell perfusion permeability study was conducted using 0.65 M solutions of each compound using the THP-1 human leukemia monocytic cell line. Although this method can provide detailed concentration-dependent cell permeability data with high temporal sensitivity, it does have intrinsic limitations based on compatible cell types (spherical only), as well as difficulties associated with maintaining the concentration of the CPA used and the position of the settled cell(s) during perfusion within the conventional well plate. As a result, all experiments were repeated several times to obtain consistent results. At this concentration, α -glucoside **2 α** and α -thiogalactoside **3 α** were not permeable and displayed some cytotoxicity (cells started bulging towards the sides with lysis occurring within 1 min). In contrast, β -D-octyl galactoside **1 β** and glucoside **2 β** showed good shrink–swell behaviour, which indicates membrane permeability (Fig. 3). Unfortunately, these compounds also resulted in some cell damage at the end of the incubation period (~ 1 min) as shown from visible cell lysis in the micrographs (Fig. 3a). However, it is not at all surprising to see some cell membrane damage after prolonged exposure given the strong surfactant properties of these molecules, particularly at concentrations well above their reported critical micelle concentration (CMC) values.^[30] To test the concentration dependence of this cytotoxicity, the cell perfusion assay was then repeated at 0.33 M. Encouragingly, at this lower concentration, good shrink–swell behaviour was observed for both *n*-octyl β -D-glycosides **1 β** and **2 β** , similar to that observed at 0.65 M concentration but with little observed membrane damage, particularly for the glucoside **2 β** . Perfusion of glucoside **2 β** resulted in total cell lysis only after ~ 230 s of incubation, with evidence of membrane damage occurring from ~ 160 s of contact time, as shown from the blurring of the cell image in Fig. 3c. Interestingly, in

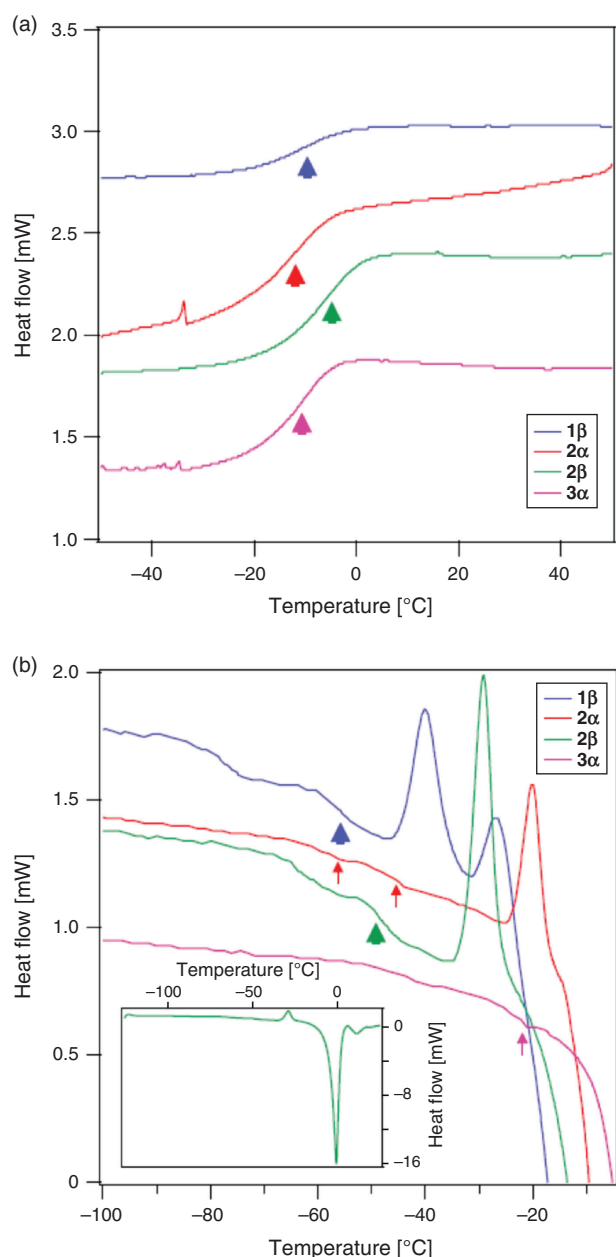


Fig. 2. DSC warming thermograms for (a) neat, and (b) 20 wt-% aqueous samples for the samples indicated in the captions. Only the regions of interest are shown. The inset in (b) shows a complete representative scan for one of the samples, **2β**, showing the large ice melting (negative) peak. Scans have been vertically offset for clarity. Glass transitions (T_g) are indicated by bold arrowheads. Small arrows indicate regions with small changes, which may be glass transitions.

Table 1. T_g values of water-soluble *n*-octyl (thio)glycosides **1β**, **2α**, **2β**, and **3α**

Sample name	Samples, neat, T_g [°C]	Samples, 20 wt-%, T_g [°C]
1β	-9.99	-55.6, devitrification peak
2α	-11.93	-46.0 ^A , -58.9 ^A , devitrification peak
2β	-4.97	-48.0, devitrification peak
3α	-9.73	-22.1 ^A

^AValues may indicate a T_g or liquid crystalline transitions.

contrast to the glucoside, β -D-galactoside **1β** showed evidence of cell damage within 1 min of incubation, with total cell lysis observed within ~ 166 s (Fig. 3b). Unlike the β -D-glycosides **1β** and **2β**, the corresponding α -glucoside **2α** and thiogalactoside **3α** were not membrane-permeable and displayed significant cytotoxicity at both 0.65 and 0.33 M concentrations.

Fig. 4 shows the normalized cell volume as a function of time for **1β** and **2β** (at 0.33 M). For both samples, the normalized volume decreases to $\sim 80\%$ of the initial volume (V_0) after ~ 45 s. For comparison, in the presence of 0.65 M DMSO, the cells shrink to $\sim 65\%$ V_0 in ~ 25 s. Overall, provided that long-term contact with cells is avoided, β -D-glycosides **1β** and **2β** show promising membrane permeability at concentrations relevant to cryopreservation.

Ice recrystallization is a thermodynamic phenomenon whereby larger ice crystals grow at the expense of smaller ones and is a significant cause of cell damage during cryopreservation.^[31] The IRI activity of carbohydrate-based surfactants has been previously determined at concentrations up to 44 mM, with the glucoside **2β** displaying weak to moderate IRI activity, whereas the galactoside **1β** exhibited potent IRI activity.^[17] The IRI activity of amphiphilic carbohydrates is highly sensitive to molecular structure, with the polarity, hydration, and absolute configuration of the carbohydrate head group, as well as tail group hydrophobicity and substitution all regarded as important determinants for inducing potent IRI activity.^[17,19,32] Previous studies have also demonstrated the importance of tail-group hydrophobicity of amino acid derivatives^[33] and amphiphilic block copolymers^[34] for tuning potent IRI activity. Interestingly, although earlier work has evaluated the effect of changing the structure of the head and tail groups of carbohydrate surfactants on IRI activity, an investigation into the effect of the anomeric configuration and linkage type (e.g. *O*- and *S*-glycoside) for carbohydrate-based surfactants has yet to be conducted.

In order to evaluate the effect of substituting the oxygen atom at the anomeric centre with a more hydrophobic sulfur atom, the IRI activity of thioglycosides **3α**, **β** and **4α**, **β** was determined using an established splat-cooling assay up to 5.5 mM concentration, which represents the upper solubility limit for these compounds in PBS buffer (see Fig. S3, Supplementary Material).^[35] Unfortunately, unlike the *n*-octyl glycosides previously reported, the analogous thioglycosides used in the present study did not display any significant IRI activity. Curiously, although the *O*-glycoside **1β** displayed weak to moderate IRI activity at 1 mM concentration ($\sim 80\%$ mean grain size relative to PBS),^[17] replacement with a sulfur atom to give thioglycoside **3β** resulted in complete loss of activity (100% mean grain size relative to PBS), albeit at a lower concentration (0.5 mM). This loss in IRI activity compared with previously described *O*-glycosides is perplexing; however, it may be due to freeze-induced crystallization or precipitation of compounds within the assay. Alternatively, substitution of oxygen for sulfur may have resulted in a decrease in head group polarity, with a concomitant decrease in its hydration index, thus lowering IRI activity.^[36] Regardless of mechanism, these compounds were not IRI-active and this mode of action cannot account for their potential cryoprotective effect.

In conclusion, we have reported the glass transition behaviour, membrane permeability, and IRI activity of a series of *n*-octyl (thio)glycosides (**1α**, **β**-**4α**, **β**). Of all soluble samples studied, *n*-octyl β -D-glucopyranoside **2β** exhibited high

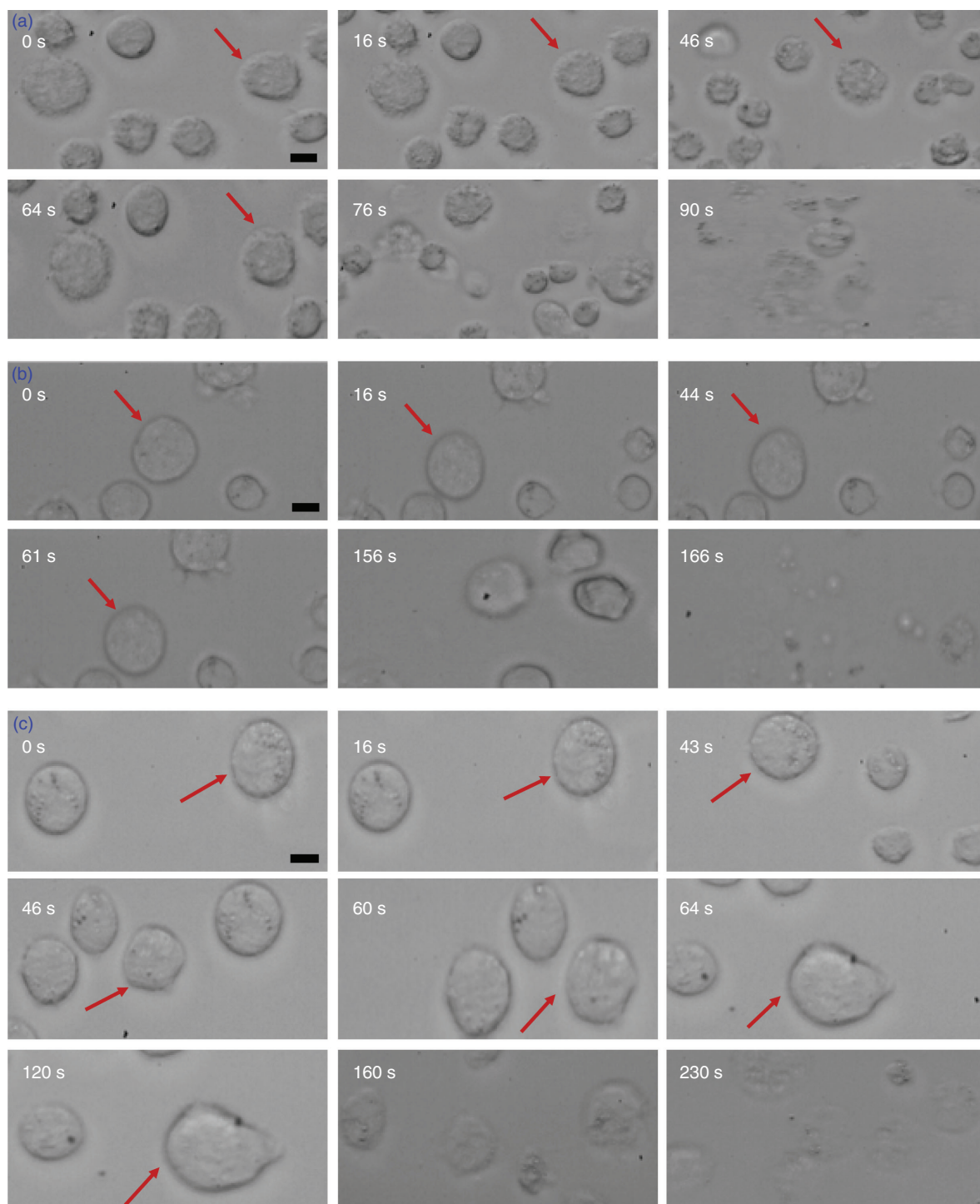


Fig. 3. Micrographs of changes in cell volume as a function of time for THP-1 cells in the presence of: (a) 0.65 M *n*-octyl β -D-galactoside **1 β** ; (b) 0.33 M *n*-octyl β -D-galactoside **1 β** ; and (c) 0.33 M *n*-octyl β -D-glucoside **2 β** . Note that there is some movement of cells between frames, so arrows indicate a cell whose volume is measured in each frame. Where no arrow appears, the cell can no longer be identified. Scale bars = 10 μ m.

sub-zero T_g values from the DSC thermograms, both as a neat sample and as a 20 wt-% aqueous solution. Using a cell perfusion permeability assay against human THP-1 cells, glucoside **2 β** (0.33 M) also exhibited favourable shrink–swell behaviour similar to DMSO. Encouragingly, we observed promising cell permeability with little cytotoxicity, provided the exposure time is kept within \sim 160s, a reasonable timeframe for exposure before cryopreservation. The IRI activity of thioglycosides **3 α** , **β** and **4 α** ,

β was also evaluated and compared with previously published *O*-glycosides **1 β** and **2 β** . Substitution of the anomeric oxygen with a sulfur atom resulted in significantly lower IRI activity, which may be a result of the increased hydrophobicity and decreased hydration of the carbohydrate head group in thioglycosides. In addition to the vitrification and permeability data presented herein, glucoside **2 β** has also previously been shown to display moderate IRI activity and therefore represents a promising lead

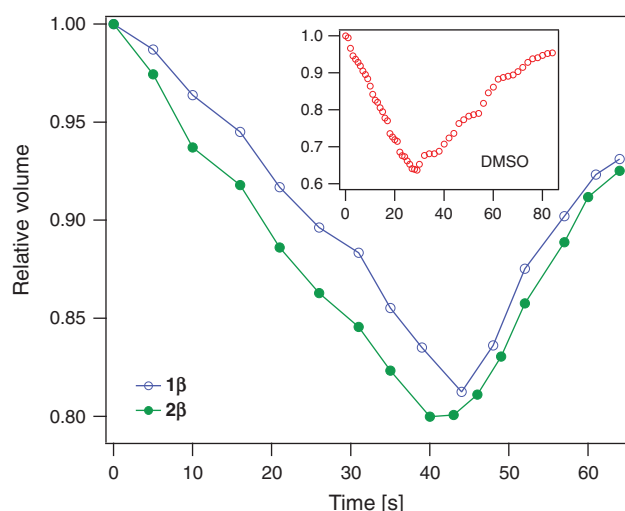


Fig. 4. Cell volume excursion during perfusion of *n*-octyl β -D-glycosides **1 β** and **2 β** at 0.33 M concentration. The timescale and magnitude of the shrink–swell behaviour are similar for the two molecules, but much slower than for DMSO (shown inset), which reaches the minimum after \sim 30 s (versus 45 s) and also reaches a smaller minimum volume.

compound for further biophysical and cryopreservation studies. In future work, we will investigate the mechanisms of cellular uptake for these surfactants, as well as the rational development of new, hydrophobic carbohydrate analogues as potential CPAs capable of promoting vitrification, eliminating IIF, and inhibiting ice recrystallization.

Supplementary Material

General experimental information, supplementary DSC and IRI data, and NMR data are available on the Journal's website.

Conflicts of Interest

The authors declare no conflicts of interest.

Acknowledgements

B.W. and G.B. acknowledge funding from the Australian Research Council (ARC) grant DP190101010. G. B. acknowledges funding by the ARC grants LP140100993 and LP160101496. R.R. acknowledges the support of an Australian Government Research Training Program Scholarship. M. K. A. acknowledges the Natural Sciences and Engineering Research Council of Canada (NSERC) for a Canada Graduate Scholarship (CGS D).

References

- [1] J. G. Baust, D. Gao, J. M. Baust, *Organogenesis* **2009**, *5*, 90. doi:10.4161/ORG.5.3.10021
- [2] G. D. Elliott, S. Wang, B. J. Fuller, *Cryobiology* **2017**, *76*, 74. doi:10.1016/J.CRYOBIOL.2017.04.004
- [3] K. R. Diller, E. G. Cravalho, *Cryobiology* **1971**, *7*, 191. doi:10.1016/0011-2240(70)90021-0
- [4] C. Polge, A. U. Smith, A. S. Parkes, *Nature* **1949**, *164*, 666. doi:10.1038/164666A0
- [5] (a) B. J. Fuller, *Cryo Lett.* **2004**, *25*, 375.
(b) R. Streczynski, H. Clark, L. M. Whelehan, S.-T. Ang, L. K. Hardstaff, B. Funnekotter, E. Bunn, C. A. Offord, K. D. Sommerville, R. L. Mancera, *Aust. J. Bot.* **2019**, *67*, 1. doi:10.1071/BT18147
- [6] K. B. Storey, J. M. Storey, *Annu. Rev. Ecol. Syst.* **1996**, *27*, 365. doi:10.1146/ANNUREV.ECOLSYS.27.1.365

- [7] L. P. Tarkowski, W. Van den Ende, *Front. Plant Sci.* **2015**, *6*, 203. doi:10.3389/FPLS.2015.00203
- [8] B. Kent, T. Hauß, B. Demé, V. Cristiglio, T. Darwish, T. Hunt, G. Bryant, C. J. Garvey, *Langmuir* **2015**, *31*, 9134. doi:10.1021/ACS.LANGMUIR.5B02127
- [9] T. Lenné, G. Bryant, R. Holcomb, K. L. Koster, *Biochim. Biophys. Acta Biomembr.* **2007**, *1768*, 1019. doi:10.1016/J.BBAMEM.2007.01.008
- [10] K. R. Walters, Jr, A. S. Serianni, Y. Voituren, T. Sformo, B. M. Barnes, J. G. Duman, *J. Comp. Physiol. B* **2011**, *181*, 631. doi:10.1007/S00360-011-0552-8
- [11] K. Imamura, K. Murrai, T. Korehisa, N. Shimizu, R. Yamahira, T. Matsuura, H. Tada, H. Imanaka, N. Ishida, K. Nakashini, *J. Pharm. Sci.* **2014**, *103*, 1628. doi:10.1002/JPS.23988
- [12] G. Bendas, F. Wilhelm, W. Ritcher, P. Nuhn, *Eur. J. Pharm. Sci.* **1996**, *4*, 211. doi:10.1016/0928-0987(95)00054-2
- [13] M. F. Ross, T. Da Ros, F. H. Blaikie, T. A. Prime, C. M. Porteous, I. I. Serevina, V. P. Skulachev, H. G. Kjaergaard, R. A. J. Smith, M. P. Murphy, *Biochem. J.* **2006**, *400*, 199. doi:10.1042/BJ20060919
- [14] M. P. Murphy, R. J. Murphy, R. J. Smith, *Annu. Rev. Pharmacol. Toxicol.* **2007**, *47*, 629. doi:10.1146/ANNUREV.PHARMTOX.47.120505.105110
- [15] A. Abazari, L. G. Meimetis, G. Budin, S. S. Bale, R. Weissleder, M. Toner, *PLoS One* **2015**, *10*, e0130323. doi:10.1371/JOURNAL.PONE.0130323
- [16] A. Eroglu, M. J. Russo, R. Bieganski, A. Fowler, S. Cheley, H. Bayley, M. Toner, *Nat. Biotechnol.* **2000**, *18*, 163. doi:10.1038/72608
- [17] C. J. Capicciotti, M. Leclère, F. A. Perras, D. L. Bryce, H. Paulin, J. Harden, Y. Liuc, R. N. Ben, *Chem. Sci.* **2012**, *3*, 1408. doi:10.1039/C2SC00885H
- [18] M. K. Adam, Y. Hu, J. S. Poisson, M. J. Pottage, R. N. Ben, B. L. Wilkinson, *Carbohydr. Res.* **2017**, *439*, 1. doi:10.1016/J.CARRES.2016.12.004
- [19] M. K. Adam, J. S. Poisson, Y. Hu, G. Prasannakumar, M. J. Pottage, R. N. Ben, B. L. Wilkinson, *RSC Adv.* **2016**, *6*, 39240. doi:10.1039/C6RA07030B
- [20] C. J. Capicciotti, J. D. R. Kurach, T. R. Turner, R. S. Mancini, J. P. Acker, R. N. Ben, *Sci. Rep.* **2015**, *5*, 9692. doi:10.1038/SREP09692
- [21] C. J. Drummond, C. Fong, I. Krodkiewska, B. J. Boyd, I. J. A. Baker, in *Novel Surfactants* (Ed. K. Holmberg) **2003**, Ch. 3, pp. 95–128 (Marcel Dekker: New York, NY).
- [22] (a) S. Ogawa, K. Asakura, S. Osanai, *Carbohydr. Res.* **2010**, *345*, 2534. doi:10.1016/J.CARRES.2010.08.004
(b) S. Ogawa, S. Osanai, *Cryobiology* **2007**, *54*, 173. doi:10.1016/J.CRYOBIOL.2007.01.005
- [23] J. Schmidt-Lassen, T. K. Lindhorst, *MedChemComm* **2014**, *5*, 1218. doi:10.1039/C4MD00122B
- [24] H. A. van Doren, R. van der Geest, R. M. Kellogg, H. Wynberg, *Carbohydr. Res.* **1989**, *194*, 71. doi:10.1016/0008-6215(89)85007-4
- [25] B. Hoffmann, W. Milius, G. Voss, M. Wunschel, S. van Smaalen, S. Diele, G. Platz, *Carbohydr. Res.* **1999**, *323*, 192. doi:10.1016/S0008-6215(99)00264-5
- [26] S. Ogawa, S. Osanai, in *Supercooling* (Ed. P. Wilson) **2012**, pp. 29–54 (IntechOpen: Rijeka, Croatia).
- [27] S. Ogawa, Y. Ozaki, I. Takahashi, *ChemPhysChem* **2016**, *17*, 2808. doi:10.1002/CPHC.201600400
- [28] S. Ogawa, K. Asakura, S. Osanai, *Phys. Chem. Chem. Phys.* **2012**, *14*, 16312. doi:10.1039/C2CP41439B
- [29] S. Ogawa, I. Takahashi, M. Koga, K. Asakura, S. Osanai, *J. Oleo Sci.* **2018**, *67*, 627. doi:10.5650/JOS.ESS17232
- [30] R. M. Garavito, S. Ferguson-Miller, *J. Biol. Chem.* **2001**, *276*, 32403. doi:10.1074/JBC.R100031200
- [31] (a) P. Mazur, *Am. J. Physiol. Cell Physiol.* **1984**, *247*, C125. doi:10.1152/AJPCELL.1984.247.3.C125
(b) J.-H. Wang, *Cryobiology* **2000**, *41*, 1. doi:10.1006/CRYO.2000.2265

- [32] C. J. Capicciotti, R. S. Mancini, T. R. Turner, T. Koyama, M. G. Alteen, M. Doshi, T. Inada, J. P. Acker, R. N. Ben, *ACS Omega* **2016**, *1*, 14656.
- [33] A. K. Balcerzak, M. Febraro, R. N. Ben, *RSC Adv.* **2013**, *3*, 3232. doi:10.1039/C3RA23220D
- [34] C. Stubbs, J. Lipceki, M. Gibson, *Biomacromolecules* **2017**, *18*, 295. doi:10.1021/ACS.BIOMAC.6B01691
- [35] M. K. Adam, C. Jarrett-Wilkins, M. Beards, E. Staykov, L. R. MacFarlane, T. D. M. Bell, J. M. Matthews, I. Manners, C. F. J. Faul, P. D. J. Moens, R. N. Ben, B. L. Wilkinson, *Chem. – Eur. J.* **2018**, *24*, 7834. doi:10.1002/CHEM.201800857
- [36] R. Y. Tam, S. S. Ferreira, P. Czechura, J. L. Chaytor, R. N. Ben, *J. Am. Chem. Soc.* **2008**, *130*, 17494. doi:10.1021/JA806284X

Chapter 5

Glass transition, permeability and cryopreservation studies with novel potential cryoprotectants - trehalose derivatives

5.1 Introduction

As discussed in *chapter 1*, there is a need for new non-toxic CPAs that can penetrate cell membranes, access all cellular compartments, promote vitrification, and inhibit ice recrystallization. Applications include biotechnology, regenerative medicine, food technology, and conservation. Owing to their low toxicity, promising ice growth inhibition activity, and high glass transition temperatures, carbohydrates have emerged as attractive candidates for the development of new CPAs. Unfortunately, owing to their high polarity, soluble sugars alone are poor cryoprotectants as they are generally not membrane permeable, and so are incapable of inhibiting IIF^{1,2}. For example, trehalose acts as a CPA in nature, where it is accumulated within cells. However, as an artificial CPA it cannot be used by itself as it can't penetrate the cell membrane, and so the cells may suffer damage due to osmotic shock²⁻⁴. An alternative approach aimed at improving the membrane permeability of soluble sugars is to enhance lipophilicity by modifying the carbohydrate scaffold with hydrophobic groups⁵⁻⁷. If the trehalose derivatives can penetrate into the cell this can potentially lead to better cryoprotection. Toner and co-workers previously reported the synthesis and membrane permeability properties of some modified trehalose derivatives possessing enzyme-cleavable acetate esters⁶. Inspired by these earlier observations and the natural antifreeze and cryoprotective ability of soluble sugars such as trehalose¹, this study aims to explore the potential of trehalose derivatives as a novel and accessible class of penetrating CPA. This chapter reports the glass transition behaviour and membrane permeability of various modified trehalose derivatives. Finally, cryopreservation trials were carried out on those compounds which showed high glass transition temperature and relatively good membrane permeability.

5.2 Experimental: Materials and Methods

Four trehalose derivatives were used for the current study, taking trehalose as a control. These compounds were synthesised in the lab of co-supervisor Dr. Brendan Wilkinson at University of New England. The trehalose derivatives were made by modifying the carbohydrate scaffold with hydrophobic groups such as enzyme-cleavable acetate and pivotate esters. The molecular structures of trehalose and the four trehalose derivatives are shown below (*Fig.5.1*) and represented as S-1, S-2, S-3, S-4 and S-5 respectively in this chapter - (S-1) D-trehalose; (S-2) D-trehalose(2*OAC); (S-3) D-trehalose(2*OPiv); (S-4) D-trehalose(4*OAC) and (S-5) D-trehalose(6*OAC).

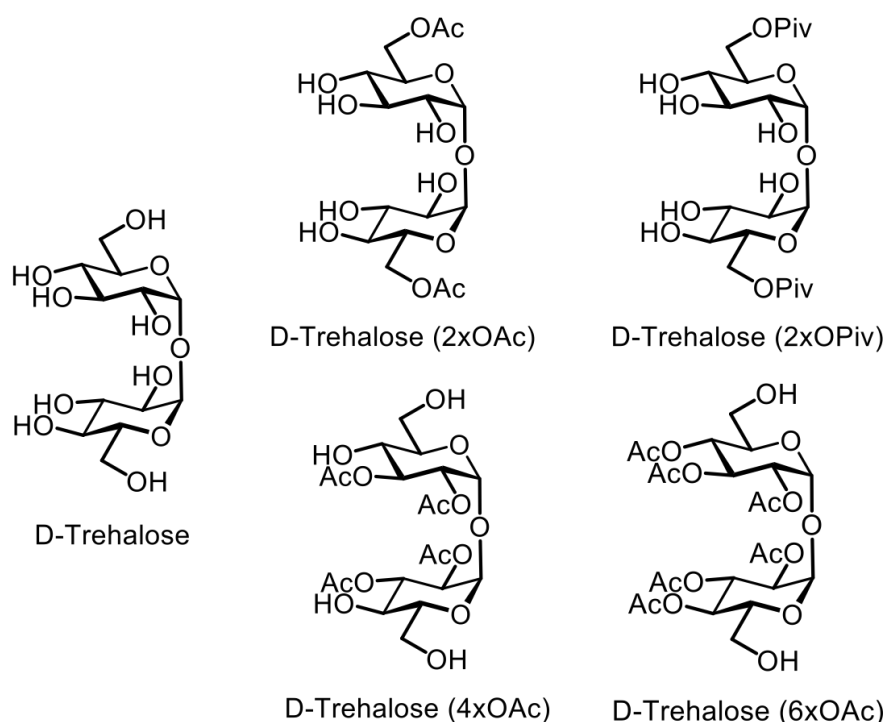


Fig.5.1: Molecular structures of trehalose and its derivatives

Glass transition⁸⁻¹⁴ (vitrification) behaviour of these trehalose derivatives was investigated using DSC, both as neat samples and 20 wt% solutions. For the permeability studies, Poly-L-Lysin coated cover slips were used for cell attachment and immobilization. The cell responses were monitored and recorded via an inverted microscope with a digital camera attached to the microscope. Video was recorded at 20 frames/second until osmotic equilibrium was obtained. In this work, all the perfusion images were captured for at least 5-10 minutes. All experiments were done at room temperature (~22°C). The cell lines used for the permeability and cryopreservation studies are Human monocytes (THP-1 cells). More details about the equipments, method and materials used for the study are explained in the methodology chapter (*section 2.3*).

5.3 Results and Discussion

5.3.1 DSC thermograms – Phases observed on cooling and warming

Of the five samples (trehalose and its four derivatives) studied here, D-trehalose-6*OAc (S-5) was only partially soluble and was not investigated further. *Fig.5.2 (A&B)* represent the warming thermograms of the remaining samples (S-1 to S-4) in neat form and aqueous form respectively. The measured T_g values are given in *Table 5.1*.

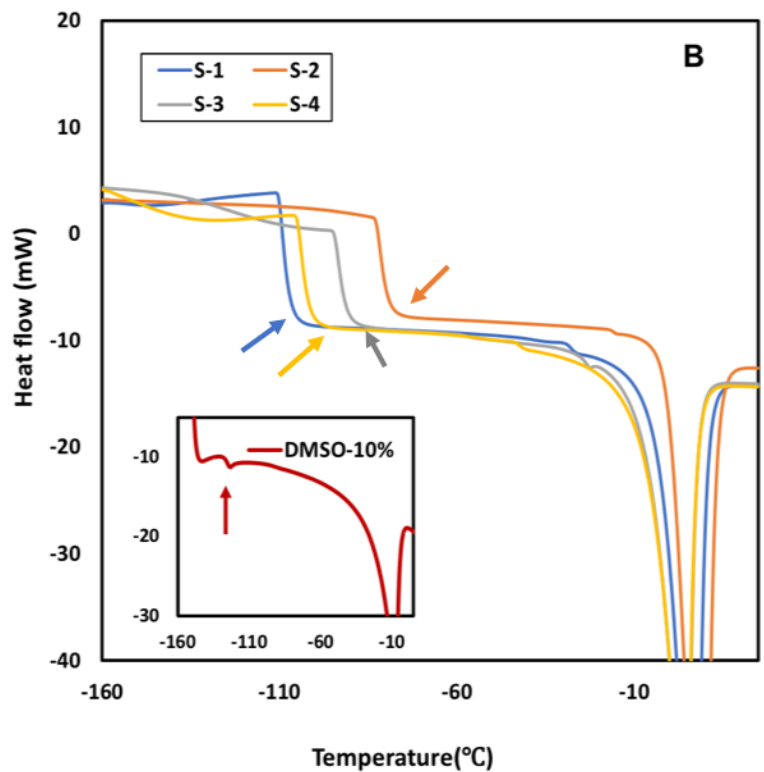
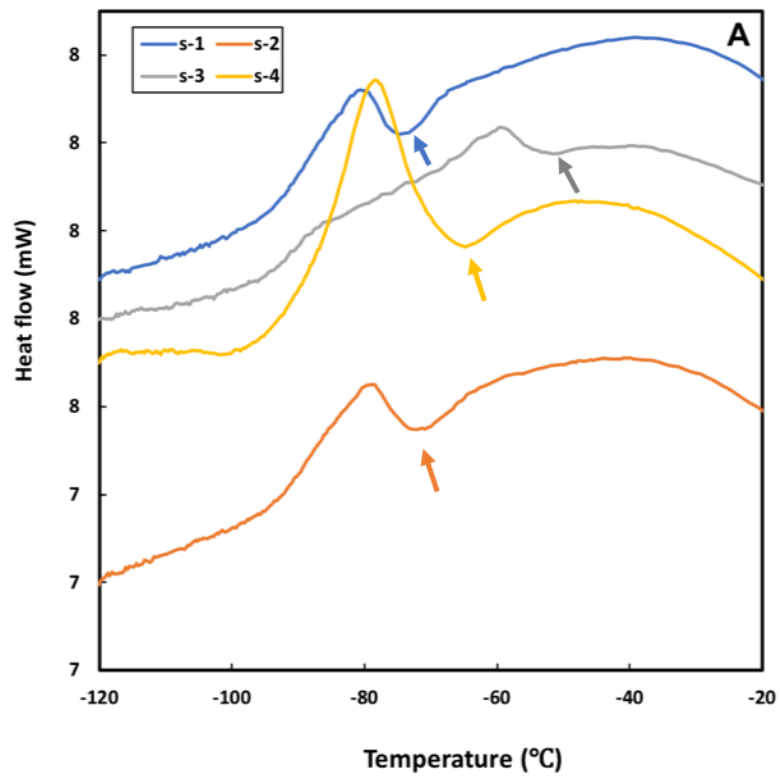


Fig.5.2: DSC warming thermograms showing T_g of Trehalose and its derivatives: (A) Neat samples (B) aqueous samples, inset shows the T_g of 10 vol% DMSO for comparison

Table 5.1: T_g values of trehalose and its derivatives

Sample No:	Sample Name	Neat samples	Aqueous samples (20 wt%)
1	S-1	-74.7	-99.0
2	S-2	-71.8	-75.3
3	S-3	-50.3	-86.5
4	S-4	-64.8	-95.8
5	S-5	--	--

DSC thermograms were recorded by warming the samples from -160 to $+25^\circ\text{C}$ at a rate of $10^\circ\text{C min}^{-1}$ with 1-minute equilibration times at the end points. All four samples showed glass transition between -40°C and -80°C in neat form which are clearly visible as step-like inflections in the thermograms and are indicated with arrows (see *Fig. 5.2 A*). Similarly, for the 20 wt% aqueous samples, the glass transitions were observed in between -70°C and -100°C which are also indicated by arrows (see *Fig. 5.2 B*). The ice subsequently melts as it reaches the freezing point, as indicated by the large endothermic peaks. The melting temperature, T_m , can thus be defined at the end of ice melting for the solutions studied. The small inflections at temperatures just below ice melting could be due to ice recrystallization, but also may be attributed to the crystallization of synthesized trehalose derivatives as has been reported for other carbohydrate based surfactants such as glycosides¹⁵. For the purpose of the present study, we are only interested in the glass transition properties, and so these were not examined further.

Encouragingly, all the soluble trehalose samples showed relatively high T_g between -100°C and -40°C , which are high in comparison with the T_g of the most commonly used CPA, DMSO ($\sim -130^\circ\text{C}$), which is shown in the inset to *Fig. 5.2B* for comparison. The most promising candidates with very high glass transition temperatures were trehalose di pivotate and trehalose tetra acetate (S-3 & S-4).

5.4 Cell permeability- shrink-swell behavior of cells

The next step was to study the cell permeability of the three trehalose derivatives which showed high T_g and solubility in water/RPMI cell media. As (S-1) D-trehalose is well known to be impermeable to cells, the samples analyzed are S-2, S-3 and S-4. Cryobiologically relevant concentrations of DMSO are 5% and 10% by volume which is equivalent to 0.65M and 1.3M respectively, so in this study, cell perfusion experiments were conducted with 0.65M solutions. S-2, trehalose-di acetate didn't show any cell permeability. *Fig. 5.3(A, B)* shows the cell volume excursion of THP-1 cells when perfused with 0.65M concentration of S-3 and S-4, and a graph of the normalised cell volume as a function of time is shown in *Fig. 5.4*. In the inset, DMSO perfusion on THP-1 cells is shown for comparison. The initial volume shrinkage due to the water efflux takes longer ($\sim 80\text{s}$) compared to DMSO ($\sim 22\text{-}29\text{s}$) for both samples S-3 & S-4. The minimum volume attained by the cells in the shrinkage phase in the presence of S-3, trehalose di pivotate was $0.62V_0$ where V_0 is the initial cell volume before CPA perfusion, which is similar to DMSO ($0.67\text{-}0.72V_0$). Interestingly, not only is the volume recovery slower

than for DMSO, the initial shrinkage due to water efflux is also slower. This implies that water permeability is directly affected by the presence of the CPA.

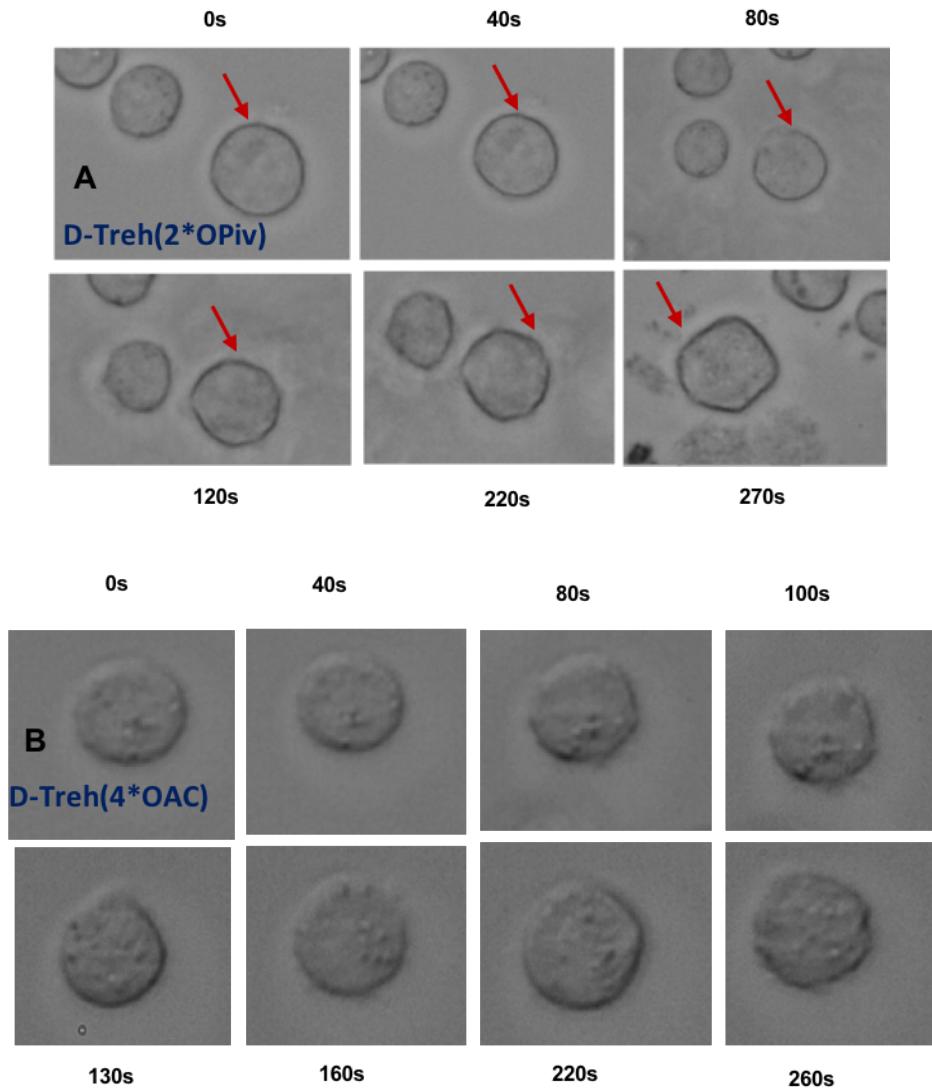


*Fig.5.3: THP-1 cell perfusion with the two trehalose derivatives - (A) Volume response of the cells to 0.65M solution of S-3, trehalose di pivotate (D-treh(2*OPiv)), it has relatively good cell permeability leading to nice shrink-swell behavior (B) Volume response of the cells to 0.65M solution of S-4, trehalose tetra acetate (D-treh(4*OAc)) which also shows some cell permeability but with less swelling back to the initial cell volume.*

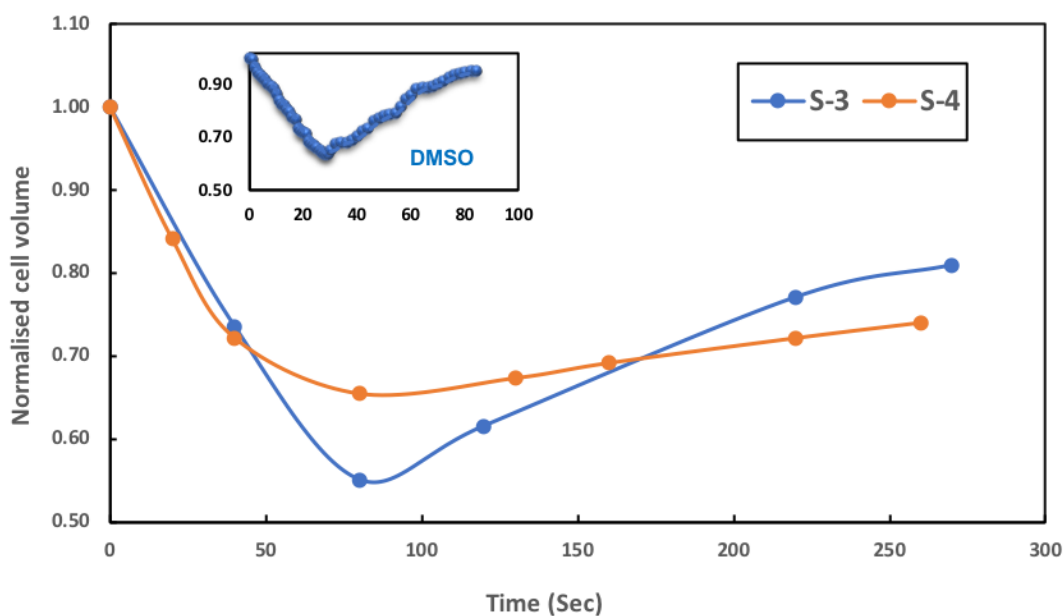


Fig.5.4: Cell volume excursion during perfusion by the two trehalose derivatives. Inset shows the cell shrink-swell response to DMSO perfusion which is considerably faster.

The perfusion method applied here has some limitations. Even though Poly-L-lysine coating favours cell attachment and thereby avoids cell movement while imaging, considerable care is needed at the time of solution addition in order to maintain focus on a single field of view and avoid cell dislodgement. Moreover, as this is a photomicrographic method, its measurement accuracy depends on the quality of captured images and accuracy of image processing. The method also assumes the cells are spherical when converting from a two-dimensional image to three-dimensional volume, which is clearly not always accurate. However, it should be noted that the main purpose of these measurements is a quick diagnostic tool to determine (i) whether or not the compound is permeable; (ii) the approximate permeation time; and (iii) the level of immediate toxicity. Quantitative determination of permeability is therefore not required here.

5.5 Cryopreservation of THP-1 cells using Trehalose derivatives

The two trehalose derivatives (S-3, and S-4) which showed promising cell permeability characteristics were used for cryopreservation studies of THP-1 cells. *Table 5.2* shows the trials including pure DMSO, DMSO/trehalose derivatives and trehalose derivatives alone. All samples were preserved for 1 week in LN. The protocol used for cryopreservation was same for all the samples, which is the optimized protocol for DMSO preservation (*Refer chapter 2.4*). After 1 week in LN, cells were revived, and cell viability measured immediately using Trypan blue exclusion test¹⁶. All samples were then cultured in RPMI cell media and stored in the incubator for regrowing. Sub-culturing was done at 3-4 days intervals, with cell viabilities checked repeatedly. The results are given in *Table 5.2*, with cell images shown in *Fig.5.5*.

Table 5.2: Cell viabilities of the samples cryopreserved using CPAs as DMSO and trehalose derivatives

Vials	Samples	Viability		
		After revival	4 days after sub-culturing	7 days after sub-culturing
1	Cells+ DMSO 1.3M	82%	86%	97%
2	Cells+ DMSO 0.65M	63%	73%	95%
3	Cells+ 0.65M S-3	25%	13%	8%
4	Cells+ 0.65M DMSO + 0.65M S-3	44%	36%	6%
5	Cells+ 0.65M S-4	4%	1%	0%
6	Cells+ 0.65M DMSO + 0.65M S-4	42%	30%	3%

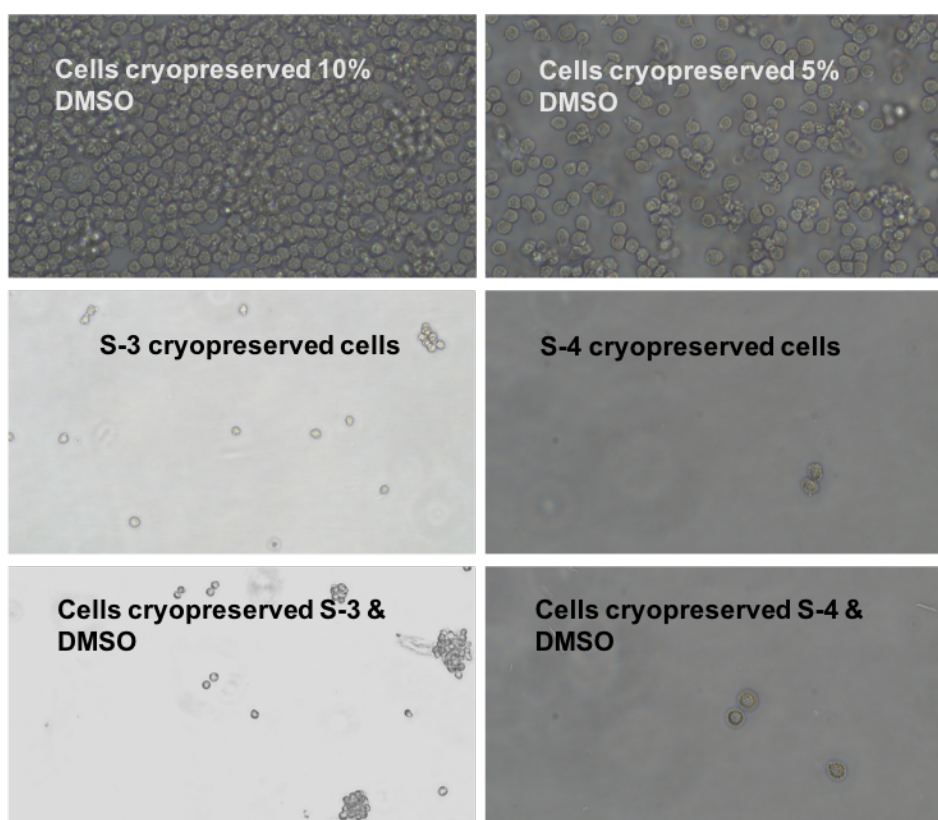


Fig.5.5: Cell images after 1 week of cryopreservation using DMSO and trehalose derivatives

Cells cryopreserved with DMSO showed good viability in the tests as expected. Although the samples cryopreserved with trehalose showed lower viability than the DMSO preserved samples, the viabilities were greater than zero per cent. Samples preserved with the trehalose dipivotate (S-3) showed higher viability (25% after revival) than trehalose tetra acetate (S-4) (4%). The samples with a mixture of DMSO and S-3 or S-4 also showed good viability after revival. For all samples with S-3 and S-4, cell viabilities dropped after each sub culturing stage, though for S-3 some viability was always retained.

While these results are slightly disappointing, the fact that some cells still survived cryopreservation using trehalose derivatives as alternative CPAs shows that this approach is promising and is a steppingstone for further study of similar compounds as future potential CPAs.

5.6 Cryopreservation of THP-1 cells with Trehalose di pivotate using different cryopreservation protocols

The cryopreservation investigations described above used the standard optimised protocol for DMSO cryopreservation. Given that the trehalose derivatives did show some promise, it was decided to determine if the cryopreservation protocol could be adjusted to achieve better results. For these final trials, the most promising candidate molecules was used which is, trehalose di pivotate. Four cryopreservation protocols P1-P4 (*see chapter 2.4*) were trialled and the results are presented in *Tables 5.3-5.6*. Cell images after trehalose dipivotate and DMSO preservations under the four different protocols are shown in *Figures 5.6 & 5.7*.

As expected, cells cryopreserved with both 1.3 M and 0.65M DMSO (samples 1 & 2) showed good viability and were growing nicely after sub-culturing in protocols P-1 and P-2. Viability of these samples were good for protocols P-3 & P-4 but not as good as protocols P-1 & P-2 and the observed growth rates were very slow after sub-culturing. However, the viability results were not much promising for any of the samples cryopreserved with Trehalose dipivotate. Samples cryopreserved with S-3 using protocols P-1 and P-2 showed some viability (less than 15%) but cell growth was not so promising after sub-culturing. For samples cryopreserved with S-3 using protocols P-3 & P-4 the viability and growth rates were very low - almost all the cells were found dead after sub-culturing.

Table 5.3 Cell viabilities of the samples cryopreserved using protocol P-1: Bypassing the first step (transferring to freezing box), otherwise keeping the protocol the same as standard DMSO cryopreservation protocol.

Vials	Samples	Viability		
		After revival	4 days after sub-culturing	7days after sub-culturing
1	Cells+ DMSO 1.3M	76%	88%	97%
2	Cells+ DMSO 0.65M	68%	86%	94%
3	Cells+ 0.65M S-3	12%	5%	2%
4	Cells+ 0.65M DMSO + 0.65M S-3	14%	8%	3%

Table 5.4 Cell viabilities of the samples cryopreserved using protocol P-2: Bypassing the first step (transferring to freezing box), then directly transferring to -80°C freezer and then to LN.

Vials	Samples	Viability		
		After revival	4 days after sub-culturing	7days after sub-culturing
1	Cells+ DMSO 1.3M	76%	89%	96%
2	Cells+ DMSO 0.65M	75%	86%	93%
3	Cells+ 0.65M S-3	11%	3%	0%
4	Cells+ 0.65M DMSO + 0.65M S-3	9%	5%	1%

Table 5.5 Cell viabilities of the samples cryopreserved using protocol P-3: As for P-1 except all procedures were carried out at 4 °C instead of room temperature.

Vials	Samples	Viability		
		After revival	4 days after sub-culturing	7days after sub-culturing
1	Cells+ DMSO 1.3M	46%	58%	63%
2	Cells+ DMSO 0.65M	43%	56%	58%
3	Cells+ 0.65M S-3	3%	0%	-
4	Cells+ 0.65M DMSO + 0.65M S-3	4%	0%	-

Table 5.6 Cell viabilities of the samples cryopreserved using protocol P-4: As for P-2 except all procedures were carried out at 4 °C instead of room temperature.

Vials	Samples	Viability		
		After revival	4 days after sub-culturing	7days after sub-culturing
1	Cells+ DMSO 1.3M	43%	52%	61%
2	Cells+ DMSO 0.65M	39%	42%	54%
3	Cells+ 0.65M S-3	2%	0%	-
4	Cells+ 0.65M DMSO + 0.65M S-3	2%	0%	-

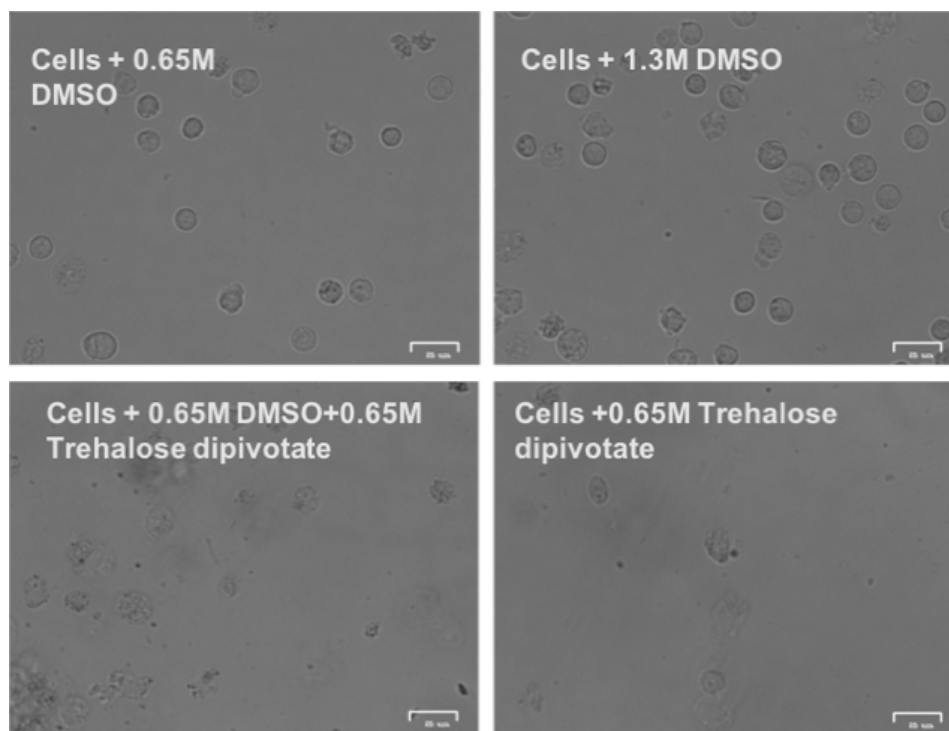


Fig.5.6: Cell images after 1week cryopreservation using DMSO as well as trehalose dipivotate in protocols P-1& P-2

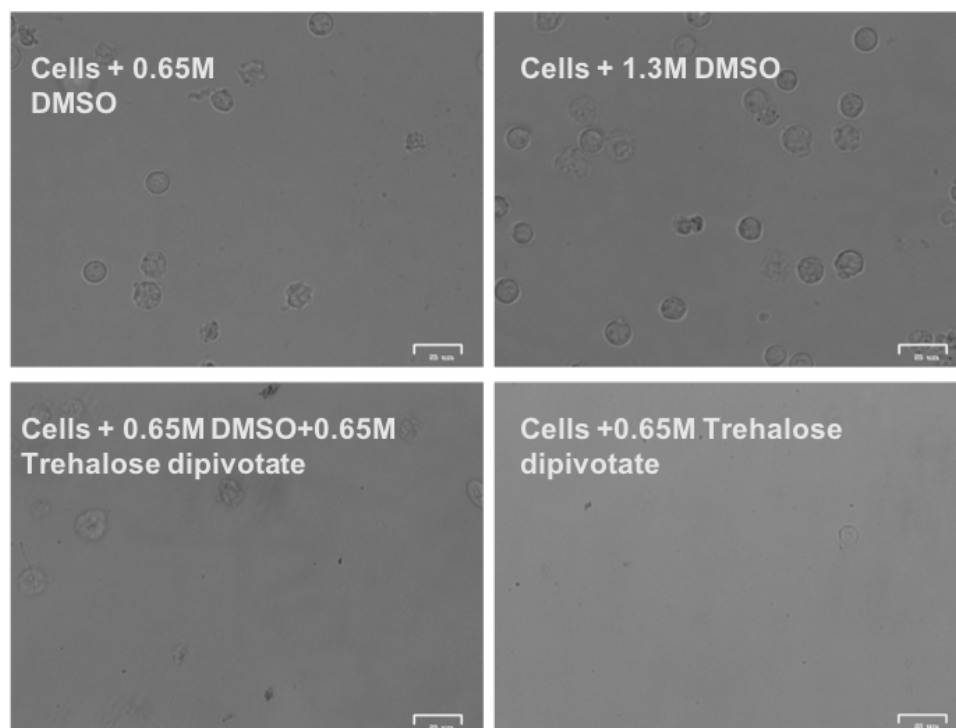


Fig.5.7: Cell images after 1week cryopreservation using DMSO as well as trehalose dipivotate in protocols P-3& P-4

5.7 Conclusions and future work

This chapter presented studies of the glass transition temperature, cell permeability and cryopreservation success of various trehalose derivatives.

Of the four trehalose derivatives studied, only trehalose hexa acetate (S-5) showed no glass transition, while the other samples showed relatively high glass transitions compared to the most commonly used CPA-DMSO.

Cell permeability studies showed that two of the compounds, S-3 and S-4, were cell permeable. In both cases the permeability was slower than for DMSO, with S-3 having a faster permeability than S-4.

Initial cryopreservation trials were carried out with these two promising candidates. THP-1 cells were cryopreserved using various concentrations and combinations of DMSO as well as the two compounds. Even though the cell viabilities using trehalose derivatives as CPAs were relatively low compared to those with DMSO as CPA, the viability was non-zero - ie, some cells survived.

Trehalose dipivotate (S-3) showed the highest viability, so several cryopreservation protocols were trialed to see if viability might be improved. The results were disappointing, with all protocols worse than the standard one.

These results have shown that trehalose derivatives are promising candidates for alternative CPAs and will be the steppingstone for further investigation of the cryoprotective nature of these and related compounds. Based on these results, future work will involve the development of further trehalose derivatives followed by physical testing and cryopreservation studies.

In addition, cell membrane permeability to cryoprotectants and the optimum protocols for cryopreservation varies with cell type - for example, even though glycerol permeability is found to be low compared to that of other cryoprotectants such as DMSO, ethylene glycol and formamides^{17,18}, many successful cryopreservation protocols still utilize glycerol. On the other hand, both methyl formamide and dimethyl formamide are reported as adequate alternative cryoprotectants for stallion sperm preservation yielding better survival than glycerol¹⁹⁻²¹. Similarly, DMSO is found to be a better cryoprotectant than glycerol and other cryoprotectants for some viruses²², methanotrophic bacteria²³, yeasts²⁴ etc. At the same time, DMSO has also been found to be toxic to some biological systems compared to other cryoprotectants^{25,26}. Based on this variability, future studies will also include permeability and cryopreservation studies on other cell types to determine if these trehalose derivatives might be suitable as alternative CPAs for some cells.

5.8 References

- 1 Tarkowski, t. P. & Van den Ende, W. Cold tolerance triggered by soluble sugars: a multifaceted countermeasure. *Frontiers in Plant Science* **6**, 203 (2015).
- 2 Kent, B. *et al.* Direct comparison of disaccharide interaction with lipid membranes at reduced hydrations. *Langmuir* **31**, 9134-9141, doi:10.1021/acs.langmuir.5b02127 (2015).
- 3 Lenné, T., Garvey, C. J., Koster, K. L. & Bryant, G. Effects of sugars on lipid bilayers during dehydration – SAXS/WAXS measurements and quantitative model. *The Journal of Physical Chemistry B* **113**, 2486-2491, doi:10.1021/jp808670t (2009).
- 4 Lenné, T., Bryant, G., Holcomb, R. & Koster, K. L. How much solute is needed to inhibit the fluid to gel membrane phase transition at low hydration? *Biochimica et Biophysica Acta (BBA)-Biomembranes* **1768**, 1019-1022 (2007).
- 5 Ross, M. F. *et al.* Accumulation of lipophilic dications by mitochondria and cells. *Biochemical Journal* **400**, 199-208 (2006).
- 6 Abazari, A. *et al.* Engineered trehalose permeable to mammalian cells. *PLoS One* **10**, e0130323, doi:10.1371/journal.pone.0130323 (2015).
- 7 Murphy, M. P. & Smith, R. A. J. Targeting antioxidants to mitochondria by conjugation to lipophilic cations. *Annual Review of Pharmacology and Toxicology* **47**, 629-656, doi:10.1146/annurev.pharmtox.47.120505.105110 (2007).
- 8 Kitamura, S. & Kuge, T. A differential scanning calorimetric study of the conformational transitions of schizophyllan in mixtures of water and dimethylsulfoxide. *Biopolymers* **28**, 639-654, doi:10.1002/bip.360280208 (1989).
- 9 Chiu, M. H. & Prenner, E. J. Differential scanning calorimetry: An invaluable tool for a detailed thermodynamic characterization of macromolecules and their interactions. *Journal of Pharmacy and Bioallied Sciences* **3**, 39-59, doi:10.4103/0975-7406.76463 (2011).
- 10 Bonora, S., Markarian, S. A., Trincherò, A. & Grigorian, K. R. DSC study on the effect of dimethylsulfoxide (DMSO) and diethylsulfoxide (DESO) on phospholipid liposomes. *Thermochimica Acta* **433**, 19-26, doi:<http://dx.doi.org/10.1016/j.tca.2005.02.011> (2005).
- 11 Wang, H.-Y., Lu, S.-S. & Lun, Z.-R. Glass transition behavior of the vitrification solutions containing propanediol, dimethyl sulfoxide and polyvinyl alcohol. *Cryobiology* **58**, 115-117, doi:<https://doi.org/10.1016/j.cryobiol.2008.10.131> (2009).
- 12 Markarian, S. A., Bonora, S., Bagramyan, K. A. & Arakelyan, V. B. Glass-forming property of the system diethyl sulphoxide/water and its cryoprotective action on Escherichia coli survival. *Cryobiology* **49**, 1-9, doi:<http://dx.doi.org/10.1016/j.cryobiol.2004.04.001> (2004).
- 13 Baudot, A. & Boutron, P. Glass-forming tendency and stability of aqueous solutions of diethylformamide and dimethylformamide. *Cryobiology* **37**, 187-199, doi:<http://dx.doi.org/10.1006/cryo.1998.2112> (1998).
- 14 Baudot, A., Alger, L. & Boutron, P. Glass-forming tendency in the system water–dimethyl sulfoxide. *Cryobiology* **40**, 151-158 (2000).
- 15 Ogawa, S., Takahashi, I., Koga, M., Asakura, K. & Osanai, S. Effect of freeze–thaw treatment on the precipitation of Octyl β -D-Galactoside hemihydrate crystal

- from the aqueous solution. *Journal of Oleo Science* **67**, 627-637, doi:10.5650/jos.ess17232 (2018).
- 16 Strober, W. Trypan blue exclusion test of cell viability. *Current Protocols in Immunology* **21**, A. 3B. 1-A. 3B. 2 (1997).
- 17 Meryman, H. Cryoprotective agents. *Cryobiology* **8**, 173-183 (1971).
- 18 Hubálek, Z. Protectants used in the cryopreservation of microorganisms. *Cryobiology* **46**, 205-229, doi:10.1016/s0011-2240(03)00046-4 (2003).
- 19 Squires, E., Keith, S. & Graham, J. Evaluation of alternative cryoprotectants for preserving stallion spermatozoa. *Theriogenology* **62**, 1056-1065 (2004).
- 20 Alvarenga, M. A., Papa, F. O., Landim-Alvarenga, F. & Medeiros, A. Amides as cryoprotectants for freezing stallion semen: a review. *Animal Reproduction Science* **89**, 105-113 (2005).
- 21 Medeiros, A., Gomes, G., Carmo, M., Papa, F. O. & Alvarenga, M. A. Cryopreservation of stallion sperm using different amides. *Theriogenology*, 273-276 (2002).
- 22 Nagasaki, K. & Yamaguchi, M. Cryopreservation of a virus (HaV) infecting a harmful bloom causing microalga, *Heterosigma akashiwo* (Raphidophyceae). *Fisheries Science* **65**, 319-320 (1999).
- 23 Green, P. & Woodford, S. Preservation studies on some obligately methanotrophic bacteria. *Letters in Applied Microbiology* **14**, 158-162 (1992).
- 24 Mikata, k. Preservation of yeast cultures by freezing at -80 C: I. Viability after 2 yeast storage and the effects of repeated thawing-freezing. *IFO Res. Commun.* **13**, 59-68 (1987).
- 25 Nell, E. E. & Hardy Jr, P. H. The use of freeze-preserved treponemes in the *Treponema pallidum* immobilization test. *Cryobiology* **9**, 404-410 (1972).
- 26 Prentice, M. & Farrant, J. Survival of chlamydiae after cooling to -196 degrees C. *Journal of Clinical Microbiology* **6**, 4-9 (1977).

Chapter 6

Measuring volume kinetics of human monocytes in response to cryoprotectants using microfluidic technologies

This work has been peer reviewed and published as a research article in Applied Physics Letters. Citation of the publication is:

Rekha Raju, Hannes Höhn, Christian Karnutsch, Khashayar Khoshmanesh, and Gary Bryant. "Measuring volume kinetics of human monocytes in response to cryoprotectants using microfluidic technologies." *Applied Physics Letters* 114, no. 22 (2019): 223702; <https://doi.org/10.1063/1.5096199>

Author contributions:

- I performed all cell permeability (volume kinetics) experiments, data analysis and interpretation, and wrote the initial draft of the manuscript.
- I performed the design and fabrication of the microfluidic trapping structures in collaboration with Hannes Höhn under the guidance of Dr. Khashayar Khoshmanesh.
- Prof. Gary Bryant advised on the data interpretation and contributed to the writing of the manuscript.
- Dr. Khashayar Khoshmanesh and Prof. Christian Karnutsch contributed to the writing of the manuscript

See Appendix II for the supplementary materials from this paper.




Candidate's Name:	Ms. Rekha Raju	Date
		11/11/2019

Principal Supervisor's Name:	Prof. Gary Bryant	Date
		11/11/2019

Measuring volume kinetics of human monocytes in response to cryoprotectants using microfluidic technologies

Cite as: Appl. Phys. Lett. **114**, 223702 (2019); <https://doi.org/10.1063/1.5096199>

Submitted: 14 March 2019 . Accepted: 21 May 2019 . Published Online: 07 June 2019

Rekha Raju , Hannes Höhn, Christian Karnutsch, Khashayar Khoshmanesh , and Gary Bryant 



View Online



Export Citation



CrossMark

ARTICLES YOU MAY BE INTERESTED IN

[Iontronic control of GaInAsP photonic crystal nanolaser](#)

Applied Physics Letters **114**, 221105 (2019); <https://doi.org/10.1063/1.5098119>

Lock-in Amplifiers up to 600 MHz

starting at

\$6,210



 Zurich Instruments

Watch the Video 



Measuring volume kinetics of human monocytes in response to cryoprotectants using microfluidic technologies

Cite as: Appl. Phys. Lett. **114**, 223702 (2019); doi: 10.1063/1.5096199

Submitted: 14 March 2019 · Accepted: 21 May 2019 ·

Published Online: 7 June 2019



View Online



Export Citation



CrossMark

Rekha Raju,¹ Hannes Höhn,^{2,3} Christian Karnutsch,² Khashayar Khoshmanesh,^{3,a)} and Gary Bryant¹

AFFILIATIONS

¹Centre for Molecular and Nanoscale Physics, School of Science, RMIT University, Melbourne, Victoria 3001, Australia

²Institute for Sensor- and Information Systems (ISIS), Research Group "Integrated Optofluidics and Nanophotonics (IONAS)," University of Applied Sciences Karlsruhe, Karlsruhe 76133, Germany

³School of Engineering, RMIT University, Melbourne, Victoria 3001, Australia

^{a)}Author to whom correspondence should be addressed: khashayar.khoshmanesh@rmit.edu.au

ABSTRACT

Cryopreservation is a common strategy for the preservation of biological cells and tissues. While conventional platforms such as cell culture well plate systems enable measuring cell responses to various cryoprotectants, the drawbacks associated with capturing and imaging of cells limit the utility of such systems. Microfluidic technologies facilitate the capturing, chemical stimulation, and imaging of cells using low sample volumes. Here, we utilized microfluidic technologies for the hydrodynamic capturing of single human monocytes and studying the cell volume kinetics in response to a cryoprotectant in real time. Our approach facilitates conducting multistep cellular assays, especially for studying individual cell osmotic response and determining cell membrane permeability to cryoprotectants.

Published under license by AIP Publishing. <https://doi.org/10.1063/1.5096199>

Cryopreservation, the storage of samples in liquid nitrogen (-196°C), is generally used for preservation of cells and tissues.^{1–4} Cryopreservation protocols rely on the penetration of cryoprotective agents (CPAs) to the cell to reduce the damage induced by the freezing process. In this regard, studying the biophysical response of cells to CPAs and especially the cell permeability is an important step in the development of “cell specific” cryopreservation protocols.⁵

When cells are exposed to a hypertonic solution of permeable solutes such as CPAs, the osmotic gradient across the cell membrane leads to the efflux of water, resulting in the initial “shrinkage” of the cells. The penetration of CPA into the cell reverses the osmotic gradient causing the influx of water, enabling the cell to “swell” back to approximately its initial volume.^{6,7} Thus, the total cell response to permeable CPAs can be described as a “shrink-swell behavior.” Membrane permeability can be calculated from this volume response using the Kedem-Katchalsky two-parameter transport equations.^{8–11}

Several methods have been used to quantify the permeability of cells based on their volume changes. These include the use of differential scanning calorimetry,¹² electronic particle counters,¹³ stopped-flow light scattering,^{14,15} and micropipette perfusion.^{16,17} However, problems associated with the capture of cells, ambiguity of images,

exchange of solutions, and requirement of a large volume of cell sample might limit the application of these methods.

Microfluidic technologies address these limitations, as they enable the user to: (i) confine cells within a chamber/trap, preventing imaging ambiguity due to overlapping of cells or their movement out of the focus plane, (ii) monitor the changes of cellular conditions following the perfusion of various isotonic and nonisotonic media, (iii) analyze cell kinetics over extended periods without any dislodgement, thus allowing for better image acquisition, and (iv) use low cell numbers and reagent volumes.^{18–25} Due to these unique features, microfluidic systems have been used for investigating cell membrane transport properties such as permeability to water and CPAs.^{6,26–29}

In the present study, we utilized microfluidic technology for hydrodynamic capturing of single human monocytes (THP-1 cells) and analyzing their volumetric response to CPAs in real-time.

We utilized cup-shaped²¹ and serpentine-shaped¹⁹ microfluidic cell traps and compared their suitability for measuring the volumetric response of THP-1 cells to CPAs. These microfluidic structures were fabricated by direct laser writing using two-photon polymerization³⁰ and replicated in poly-dimethylsiloxane (PDMS) using soft lithography³¹ techniques. Direct laser writing facilitated the rapid prototyping

of microfluidic structures with aspect ratios of ~ 9 , which is rather challenging using conventional lithography techniques.³² The fabrication involved design, preparation, laser writing, developing, replicating, and assembly, as described in [supplementary material S1](#), and is schematically shown in [Fig. 1](#).

[Figure 2](#) presents the experimental procedure, which can be divided into five steps, including channel filling, cell loading, cell stabilization, cell shrinking, and cell swelling, as described below.

Channel filling: This involved applying 70% ethanol solution for degassing followed by applying phosphate buffered saline (PBS) and

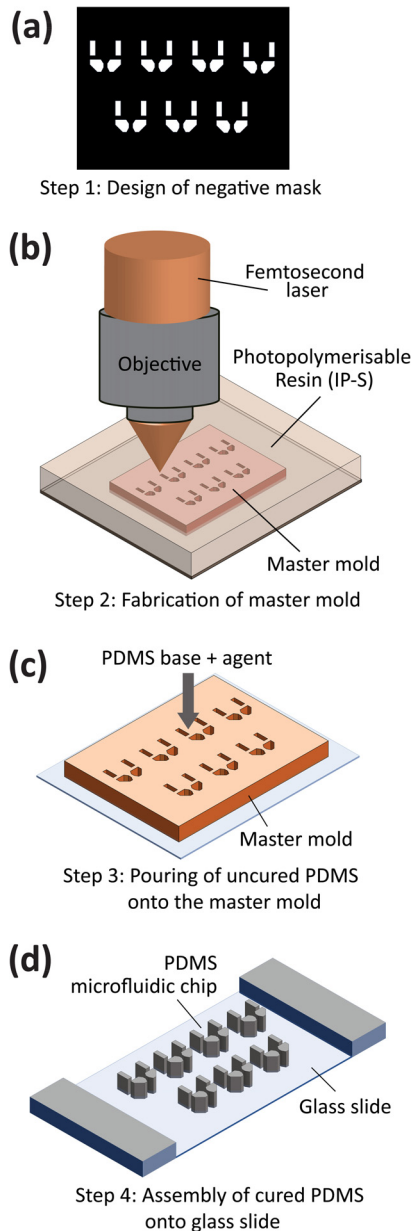


FIG. 1. Fabrication process of the microfluidic traps combining direct laser writing and soft lithography techniques.

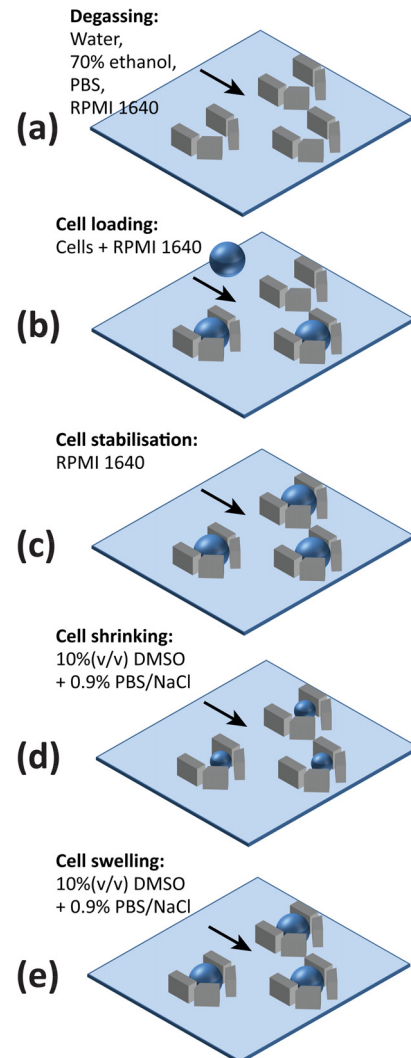


FIG. 2. Studying the shrink-swell behavior of cells in response to permeable CPA (DMSO) perfusion using a cup-shaped trap microfluidic device: (a) degassing and channel filling, (b) cell loading, (c) cell stabilization, (d) cell shrinking following the application of hypertonic DMSO, and (e) cell swelling due to the DMSO penetration and subsequent water influx into the cell.

RPMI1640 cell culture medium to fill the channel [[Fig. 2\(a\)](#)]. These solutions were added into the inlet reservoir and withdrawn through the outlet port using a syringe pump (PHD 2000 Infusion, Harvard Apparatus).

Cell loading: This involved applying an aliquot of cell suspension ($\sim 30\text{--}50\ \mu\text{l}$, $\sim 2.5 \times 10^5$ cells/ml) to the channel to facilitate hydrodynamic capturing of cells [[Fig. 2\(b\)](#)]. Further details on THP-1 cells can be found in [supplementary material S2](#).

Cell stabilization: This involved the withdrawal of RPMI1640 for at least 30 s to enable cell equilibrium [[Fig. 2\(c\)](#)].

Cell shrinking: This involved applying a hypertonic solution of a permeable CPA [dimethyl sulfoxide (DMSO)]. The higher extracellular osmolality of CPA led to the efflux of intracellular water, resulting in the shrinkage of the cells [[Fig. 2\(d\)](#)].

Cell swelling: The constant water loss along with the constant influx of CPA due to the concentration gradient across the cell membrane reversed the osmotic gradient across the cell membrane just after the cells experienced the maximum shrinkage. The reversed osmotic gradient led to an influx of water into the cells, causing the swelling of cells [Fig. 2(e)].

Figure 3 presents the cryoprotectant permeability measurement of human monocyte cells using cup-shaped traps. This design incorporated an array of 17 independent traps [Fig. 3(a)]. Each trap had a width of $25\ \mu\text{m}$ and a height of $35\ \mu\text{m}$ in order to capture and retain individual THP-1 cells. Each trap consisted of four elements isolated with a gap of $4\ \mu\text{m}$ to minimize the pressure drop and maximize the chance of hydrodynamic trapping of cells. This gap was set to $4\ \mu\text{m}$ to ensure that the cells would not squeeze through them and escape from the traps.

This allowed us to capture single THP-1 cells and monitor their dynamic volume changes in response to 10% (v/v) DMSO in real-time [Fig. 3(b)], based on which we obtained the average volume kinetics of multiple captured cells [Fig. 3(c)]. Numerical simulations revealed that the concentration of CPA solution in the first few seconds of perfusion and the hydrodynamic pressure are higher at the front side of the trapped cells due to the direction of flow (supplementary material S3), with both parameters affecting the osmotic gradient across the cell membrane.

Images were captured using an inverted microscope (Olympus IX71 inverted optical microscope) equipped with a CCD camera at a

resolution of 1024×1024 and a CMOS sensor (Mikrotron MC1362). For this camera ($14\ \mu\text{m}/\text{pixel}$ on CCD, $10\times$ magnification, 1×1 binning), the pixel size was obtained as image pixel size = camera pixel size \times binning/magnification = $1.4\ \mu\text{m}$, which was sufficient for monitoring the THP-1 cells with a diameter range of $15 \pm 3\ \mu\text{m}$ (average \pm standard deviation). Images were processed using ImageJ (<https://imagej.nih.gov/ij/>). Given the nonuniformity of the osmotic gradient across the cell membrane, the area of trapped cells was measured using the “freehand selections/measure” tabs of ImageJ, based on which the equivalent radius and volume of the cells were calculated.

Our results indicated the instantaneous shrinkage of captured cells due to water efflux in response to the osmotic gradient across the cell membrane. The minimum cell volume was obtained as $73.3\% \pm 0.99\%$ of the isotonic initial volume, which occurred at $23 \pm 1\ \text{s}$. Next, the cells began to swell as DMSO diffused into the cells. During this “swelling” phase, water also reenters the cells driven by the osmotic pressure gradient generated by DMSO.

Figure 4 presents the results obtained by the serpentine-shaped cell traps. Each trap had a width of $25\ \mu\text{m}$ and a height of $30\ \mu\text{m}$ with a gap of $4\ \mu\text{m}$ at the downstream of each trap [Fig. 4(a)]. Similar shrink-swell behavior was obtained [Fig. 4(b)]. The minimum cell volume was obtained as $68.4\% \pm 2.8\%$ of the isotonic initial volume, which occurred at $28 \pm 1\ \text{s}$ [Fig. 4(c)]. Compared to the cup-shaped traps, the minimum cell volume increased by $\sim 5\%$ and delayed by $\sim 5\ \text{s}$. This is attributed to the localized deformation of the cells at their backside facing the $4\ \mu\text{m}$ gap that significantly reduced the sphericity

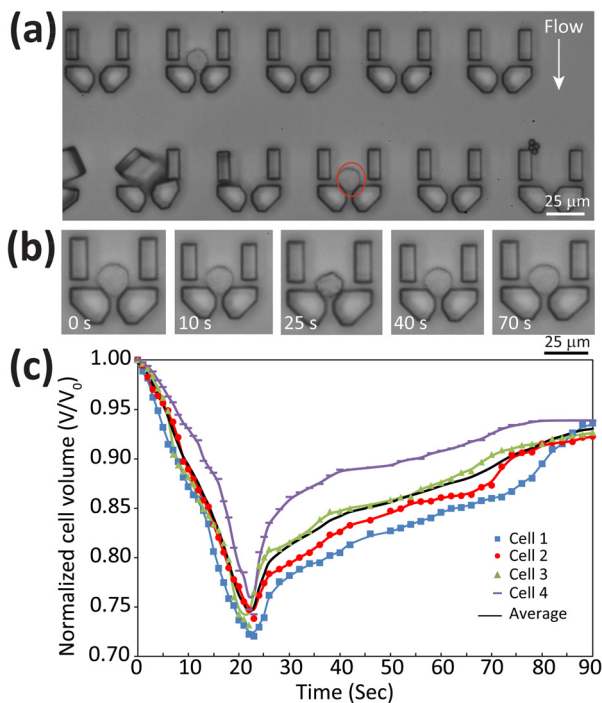


FIG. 3. THP-1 cell volume kinetics using the cup-shaped cell trap in response to hypertonic CPA solution 10% (v/v) DMSO in 0.9% PBS/NaCl: (a) cup-shaped cell traps, (b) time-lapse images showing the volume changes of a representative THP-1 cell, and (c) volume kinetics of four THP-1 cells captured with the average shown as a black curve.

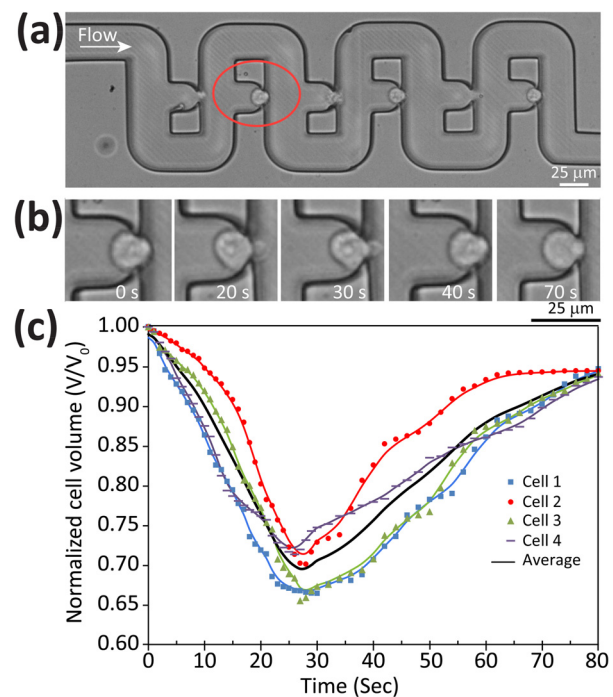


FIG. 4. THP-1 cell volume kinetics using the serpentine-shaped cell trap in response to 10% (v/v) DMSO in 0.9% PBS/NaCl: (a) serpentine-shaped cell traps, (b) time-lapse images showing the volume changes of a representative THP-1 cell, and (c) volume kinetics of four THP-1 cells captured with the average shown as a black curve.

of the cell. Our experiments showed the superiority of cup-shaped traps for (i) studying the shrink-swell behavior of cells due to a higher number of captured cells per each channel (8_{cup} vs $4_{\text{serpentine}}$) and (ii) maintaining the cell sphericity (0.913_{cup} vs $0.822_{\text{serpentine}}$) during the cell shrinkage.

In summary, we investigated the volume kinetics (shrink-swell behavior) of THP-1 cells in response to a CPA (DMSO) using microfluidic technologies. Compared to existing technologies, our method facilitated (i) rapid capturing of single cells without secondary mechanisms such as surface functionalization, (ii) providing desired osmotic gradients across the cell membrane by perfusing cryoprotective agents, and (iii) real-time imaging of cells during the shrinkage and swelling phases due to their stability. Future work includes developing microfluidic systems with multiple trapping arrays to enable parallel studying of cell volume kinetics to various CPAs and developing more sophisticated microfluidic platforms capable of conducting multistep cellular assays, paving the way for discovering CPAs.

See the [supplementary material](#) for S1: Fabrication details, S2: Cell preparation process, and S3: Numerical simulations.

The authors wish to acknowledge RMIT's MicroNano Research Facility (MNRF) for fabrication of microfluidic devices. R.R. acknowledges the Australian Government Research Training Program Scholarship. H.H. acknowledges funding from The Australian-German Study Centre for Optofluidics and Nanophotonics (SCON) for visiting RMIT University.

K.K. acknowledges the Australian Research Council for the Discovery Grant (No. DP180102049). G.B. acknowledges funding from the Australian Research Council under Linkage Grant (Nos. LP140100993 and LP160101496).

REFERENCES

- B. M. Reed, *Plant Cryopreservation: A Practical Guide* (Springer, New York, 2008).
- A. Kaczmarczyk, V.-M. Rokka, and E. J. Keller, *Potato Res.* **54**(1), 45–79 (2011).
- A. Kaczmarczyk, B. Funnekotter, S. R. Turner, E. Bunn, G. Bryant, T. E. Hunt, and R. L. Mancera, *Cryoletters* **34**(5), 508–519 (2013).
- J. R. Youn and Y. S. Song, *Appl. Phys. Lett.* **101**(13), 133701 (2012).
- Y. Zheng, G. Zhao, Y. Zhang, and R. Gao, *Sens. Actuators, B: Chem.* **255**, 647–656 (2018).
- L. Weng, F. Ellett, J. Edd, K. H. Wong, K. Uygun, D. Irimia, S. L. Stott, and M. Toner, *Lab Chip* **17**(23), 4077–4088 (2017).
- O. M. Karlsson and M. Toner, in *Principles of Tissue Engineering*, 2nd ed., edited by R. Langer and J. Vacanti (Academic Press, San Diego, 2000), pp. 293–307.
- P. Mazur, *J. Gen. Physiol.* **47**(2), 347–369 (1963).
- P. Mazur, *Am. J. Physiol.-Cell Physiol.* **247**(3), C125–C142 (1984).
- P. Mazur, *Science* **168**(3934), 939–949 (1970).
- O. Kedem and A. Katchalsky, *Biochim. Biophys. Acta* **27**, 229–246 (1958).
- R. V. Devireddy, D. Raha, and J. C. Bischof, *Cryobiology* **36**(2), 124–155 (1998).
- J. Gilmore, L. McGann, J. Liu, D. Gao, A. Peter, F. Kleinhans, and J. Critser, *Biol. Reprod.* **53**(5), 985–995 (1995).
- A. Verkman and H. E. Ives, *Am. J. Physiol. -Renal Physiol.* **250**(4), F633–F643 (1986).
- H. J. Worman, T. A. Brasitus, P. K. Dudeja, H. A. Fozzard, and M. Field, *Biochemistry* **25**(7), 1549–1555 (1986).
- D. Gao, J. McGrath, J. Tao, C. Benson, E. Critser, and J. Critser, *J. Reprod. Fertil.* **102**(2), 385–392 (1994).
- L. De Santis, G. Coticchio, S. Paynter, D. Albertini, K. Hutt, I. Cino, M. Iaccarino, A. Gambardella, C. Flamigni, and A. Borini, *Hum. Reprod.* **22**(10), 2776–2783 (2007).
- D. Di Carlo, N. Aghdam, and L. P. Lee, *Anal. Chem.* **78**(14), 4925–4930 (2006).
- W.-H. Tan and S. Takeuchi, *Proc. Natl. Acad. Sci. U. S. A.* **104**(4), 1146–1151 (2007).
- A. M. Skelley, O. Kirak, H. Suh, R. Jaenisch, and J. Voldman, *Nat. Methods* **6**(2), 147–152 (2009).
- D. Wlodkowic, S. Faley, M. Zagnoni, J. P. Wikswa, and J. M. Cooper, *Anal. Chem.* **81**(13), 5517–5523 (2009).
- T. D. Nguyen, V. T. Tran, Y. Q. Fu, and H. Du, *Appl. Phys. Lett.* **112**(21), 213507 (2018).
- C. B. Zhang, W. Gao, Y. J. Zhao, and Y. P. Chen, *Appl. Phys. Lett.* **113**(20), 203702 (2018).
- D. Wlodkowic, K. Khoshmanesh, J. C. Sharpe, Z. Darzynkiewicz, and J. M. Cooper, *Anal. Chem.* **83**(17), 6439–6446 (2011).
- S. Baratchi, F. J. Tovar-Lopez, K. Khoshmanesh, M. S. Grace, W. Darby, J. Almazi, A. Mitchell, and P. McIntyre, *Biomicrofluidics* **8**(4), 044117 (2014).
- H. H. Chen, J. J. Purttman, S. Heimfeld, A. Folch, and D. Gao, *Cryobiology* **55**(3), 200–209 (2007).
- C. Fang, F. Ji, Z. Shu, and D. Gao, *Lab Chip* **17**(5), 951–960 (2017).
- G. Zhao, Z. Zhang, Y. Zhang, Z. Chen, D. Niu, Y. Cao, and X. He, *Lab Chip* **17**(7), 1297–1305 (2017).
- G. Zhao and J. Fu, *Biotechnol. Adv.* **35**(2), 323–336 (2017).
- A. Selimis, V. Mironov, and M. Farsari, *Microelectron. Eng.* **132**, 83–89 (2015).
- D. Qin, Y. Xia, and G. M. Whitesides, *Nat. Protocols* **5**(3), 491–502 (2010).
- A. del Campo and E. Arzt, *Chem. Rev.* **108**(3), 911–945 (2008).

Chapter 7

General discussions, Conclusions and Future directions

7.1 General discussions and conclusions

The aim of this thesis was to examine the critical molecular properties that lead to good cryoprotective performance and use this knowledge to test novel non-toxic compounds which can be optimized to use as cryoprotectants. In order to achieve this aim, biophysical investigations of both traditional CPAs and novel potential candidate molecules were performed. This has been done by analyzing their cryobiologically important properties such as glass transition temperature, cell permeability and interaction with membrane lipids.

The toxicity of currently employed CPAs imposes limitations on many biological and medical technologies. Two areas of critical medical importance are highlighted here as examples:

- Stem cells which are pluripotent (i.e. can form stable cell culture lines which can differentiate) are difficult to cryopreserve¹; such cells are vital for a wide range of stem cell therapies, and the ability to easily cryopreserve and culture these cell lines would be a major breakthrough in medical science.
- Hepatocytes (liver cells) can be used as an alternative to liver transplants to treat liver disease or failure. Although they can be cryopreserved using DMSO, survival rates are low, making them impractical for transplants, and concerns have been raised about the DMSO toxicity². Successful cryopreservation using less toxic CPAs would be of worldwide significance.

To date the search for new CPAs has been reliant on educated guesswork and trial and error. This project, for the first time developed a systematic, quantitative understanding of the molecular properties vital to cryopreservation. This knowledge is essential to design new synthetic CPAs based on non-toxic carbohydrate derivatives. Focusing attention on carbohydrate derivatives will lead to promising new compounds which may be significantly less toxic than DMSO and glycerol. Tuning the molecular characteristics of these compounds, will help to systematically control their vitrification and cell permeation characteristics.

Thus, the current study opens new avenues for the development of novel non-toxic carbohydrate-based CPAs vital to the field of cryopreservation. Interaction between the traditional penetrating CPAs and cell membrane lipids have been investigated using Langmuir monolayer technique. Carbohydrate derivatives (sugar surfactants) which have shown effective ice recrystallization inhibition (IRI) nature in the literature³⁻⁶ were selected for analysis as potential candidates with cryoprotective capability for achieving the goals of this research. Glass transition temperatures (T_g) of carbohydrate derivatives such as Octyl (thio) glycosides and trehalose derivatives were studied using Differential Scanning calorimetry (DSC). The

compounds which showed high T_g were used for further permeability studies. Cell permeability investigations were started with identifying the suitable cells. Literature review revealed that human monocyte leukemia (THP-1) cells are ideal for the purpose of this project. These cells are large (12-18 μm) and spherical which are the two main criteria required for single cell permeability studies. Single cells were separated from cell solutions by traditional surface coating methods as well as by using microfluidic trapping technologies. The cryopreservation trials were conducted using standard cell lines (THP-1 cells) with standard freezing protocols, replacing the traditional CPA (eg. DMSO) with the promising candidate molecules.

A chapter by chapter summary of the key results is presented below.

Chapter 3 investigated the effects of four common cryoprotective agents (dimethyl sulfoxide, ethylene glycol, glycerol and dimethyl formamide) on phospholipid monolayers. Four different phospholipids (DOPC, DPPC, POPC & POPE) were studied to determine if the headgroup and level of chain saturation influence the interactions. DMSO showed interesting lipid specific effects – causing expansion of DPPC monolayers but compression for POPC monolayers, while having little effect for DOPC and POPE. These results demonstrate that the effects are subtle and conducting studies with a single model lipid is not sufficient to come to a complete understanding.

For glycerol and EG, the results were largely consistent – each caused a small expansion of the monolayer at fixed pressure, regardless of lipid species, consistent with their ability to penetrate membranes. DMF showed the most interesting behavior. First, the presence of DMF caused a compression for all four lipid species – perhaps related to the small inherent surface activity of DMF, which reduced the surface tension by 5.6 $\text{mN}\cdot\text{m}^{-1}$ compared to pure water. This surface activity may also be responsible for the fact that DMF had the highest maximum insertion pressure (ie showed the strongest affinity to stay in the monolayer). DMF has been used as a cryoprotectant, but there have been very few studies of its lipid interactions and so more studies need to be done.

The results highlight the need to study concentrations relevant to cryopreservation, as there is evidence of significant concentration dependence. Some of the conflicting results found in the literature appear to be due to concentration dependent differences.

Finally, the insertion studies showed that the phospholipid species has a notable impact on the interactions with the CPAs. DPPC was the most difficult lipid to penetrate (as expected, as it is in the liquid condensed phase) while DOPC was the most facile. This study provided new insights into the interactions between lipids and traditional CPAs.

Chapter 4 explored the cryobiologically important properties of eight n-octyl (thio)glycosides (1 α , β – 4 α , β) to determine if they have cryobiological relevance. Of the compounds studied, n-octyl β -D-glucopyranoside 2 β exhibited high sub-zero T_g values, both as a neat sample and as a 20 wt-% aqueous solution. Cell perfusion permeability assays exhibited favourable shrink–

swell behaviour similar to DMSO. Promising cell permeability was observed for this compound, with low cytotoxicity provided the exposure time is kept within 160s, a reasonable time frame for exposure before cryopreservation. Glucoside 2 β also displayed moderate IRI activity and therefore represents a promising compound for further biophysical and cryopreservation studies.

Chapter 5 investigated the cryoprotective potential of four trehalose derivatives to assess their cryobiological promise. Three of the samples showed relatively high T_g between -100°C and -40°C, which were very high in comparison with the T_g of DMSO (~-130°C). Permeability trials on these molecules showed that S-2, trehalose-di acetate has no cell permeability, whereas both S-3 trehalose di pivotate and S-4 Trehalose tetra acetate have moderate permeability. The most promising candidate with high glass transition temperature and relatively good permeability was trehalose di pivotate (S-3), so this compound was further used for cryopreservation studies on THP-1 cells using various protocols. Unfortunately, the viability and the cell growth results were not promising compared to those of DMSO cryopreserved cells. Despite this, it is evident that this approach of making structural modification to naturally occurring cryoprotectants shows promise for the development of novel CPAs.

Chapter 6 presented the design and implementation of new microfluidic cell trapping devices for studies of cryoprotectant permeability. Cup-shaped⁷ and serpentine-shaped⁸ microfluidic cell traps were fabricated by combining direct laser writing and soft lithography techniques and were tested by studying the volumetric response of THP-1 cells to DMSO. The experiments showed the superiority of cup-shaped traps for (i) studying the shrink-swell behavior of cells due to a higher number of captured cells per channel (8_{cup} vs $4_{\text{serpentine}}$) and (ii) maintaining cell sphericity (0.913_{cup} vs $0.822_{\text{serpentine}}$) during shrinkage. Using the two newly fabricated microfluidic devices, individual human monocyte cells could be successfully trapped, and their cell permeability was studied. The cells showed good shrink-swell behavior revealing the cryoprotectant permeability. Compared to existing technologies, the current method allowed: (i) rapid capture of single cells without surface functionalization; (ii) the rapid exchange of solvent to generate osmotic gradients across the cell membrane; and (iii) real-time imaging of cells during the shrinkage and swelling phases due to imaging stability provided by the traps.

To the best of the author's knowledge, this is the first time that the permeability of the human monocyte (THP-1) cells to DMSO has been measured using microfluidic technologies (Appendix III). Thus, this study also provided a platform to use this cell line as a tool for understanding the permeability of other potential cryoprotectants.

The research presented here is significant as it is the first study to investigate two vital aspects of cryopreservation, namely cell permeability and vitrification, for new candidate CPAs. The study has shown the potential of new carbohydrate-based surfactants to be used as alternative CPAs with potential applications in biological science, medicine and food science. This thesis has resulted in two peer-reviewed journal articles, with a third currently undergoing peer-review. The results of chapter 5 are currently being prepared for publication, and a literature

review based on chapter 1 will also be submitted for publication.

7.2 Recommendations for the future work

1. The Langmuir monolayer study highlighted the importance of different lipid species when measuring the interactions with potential CPAs. Thus, more studies are needed with membrane models other than the standard molecules (eg. DPPC), and with models which more closely mimic biological membranes. In particular, almost all previous studies have been conducted with zwitterionic (neutral) lipids. However, one might expect charged lipids (such as phosphatidylinositol) to play a significant role in interactions with polarizable molecules such as CPAs. Further studies of such systems are clearly needed. In addition to that, Langmuir monolayer studies of potential new CPAs will be an important part of understanding their interactions. Finally, this research highlighted the importance of concentration dependent effects - future studies should use concentrations relevant to cryopreservation.
2. This work showed that modified carbohydrate-based surfactants such as octyl thioglycosides have the potential to be novel cryoprotective candidates, as they only showed toxicity on long-time contact with cells. Future research should include investigating the mechanisms of cellular uptake, as well as further biophysical and cryopreservation studies.
3. This work has shown the potential of trehalose derivatives, which exhibit high glass transition temperatures, good cell permeability and relatively low toxicity. Cell viability after cryopreservation may be improved by further modifying the structure of these compounds, as well as optimisation of the cryopreservation protocols. Based on these, future work will involve the development of further trehalose derivatives followed by physical testing and cryopreservation studies.
4. In addition, cell membrane permeability to cryoprotectants and the optimum protocols for cryopreservation varies with cell type - for example, even though glycerol permeability is found to be low compared to that of other cryoprotectants such as DMSO, ethylene glycol and formamides^{9,10}, many successful cryopreservation protocols still utilize glycerol. On the other hand, both methyl formamide and dimethyl formamide are reported as adequate alternative cryoprotectants for stallion sperm preservation yielding better survival than glycerol¹¹⁻¹³. Similarly, DMSO is found to be a better cryoprotectant than glycerol and other cryoprotectants for some viruses¹⁴, methanotrophic bacteria¹⁵, yeasts¹⁶ etc. At the same time, DMSO has also been found to be toxic to some biological systems compared to other cryoprotectants^{17,18}. Based on this variability, future studies will also include permeability and cryopreservation studies on other cell types to determine if these trehalose derivatives might be suitable as alternative CPAs for some cells.
5. Developing microfluidic systems with multiple trapping arrays will enable parallel study of cell volume kinetics to various CPAs. Therefore, future work will also include developing more sophisticated microfluidic platforms capable of conducting multistep cellular assays and thereby paving the way for discovering novel CPAs.

7.3 References

- 1 Hunt, C. J. Cryopreservation of human stem cells for clinical application: A review. *Transfusion Medicine and Hemotherapy* **38**, 107-123 (2011).
- 2 Cardoso, L. M. d. F., Pinto, M. A., Henriques Pons, A. & Alves, L. A. Cryopreservation of rat hepatocytes with disaccharides for cell therapy. *Cryobiology* **78**, 15-21, doi:<https://doi.org/10.1016/j.cryobiol.2017.07.010> (2017).
- 3 Adam, M. K. *et al.* Carbohydrate-based surfactants as photocontrollable inhibitors of ice recrystallization. *RSC Advances* **6**, 39240-39244 (2016).
- 4 Adam, M. K. *et al.* Photoswitchable carbohydrate-based fluorosurfactants as tuneable ice recrystallization inhibitors. *Carbohydrate research* **439**, 1-8 (2017).
- 5 Capicciotti, C. J. *et al.* O-aryl-glycoside ice recrystallization inhibitors as novel cryoprotectants: A structure–function study. *ACS Omega* **1**, 656-662 (2016).
- 6 Capicciotti, C. J. *et al.* Potent inhibition of ice recrystallization by low molecular weight carbohydrate-based surfactants and hydrogelators. *Chemical Science* **3**, 1408-1416 (2012).
- 7 Wlodkowic, D., Faley, S., Zagnoni, M., Wikswo, J. P. & Cooper, J. M. Microfluidic single-cell array cytometry for the analysis of tumor apoptosis. *Analytical Chemistry* **81**, 5517-5523 (2009).
- 8 Tan, W.-H. & Takeuchi, S. A trap-and-release integrated microfluidic system for dynamic microarray applications. *Proceedings of the National Academy of Sciences* **104**, 1146-1151 (2007).
- 9 Meryman, H. Cryoprotective agents. *Cryobiology* **8**, 173-183 (1971).
- 10 Hubálek, Z. Protectants used in the cryopreservation of microorganisms. *Cryobiology* **46**, 205-229, doi:10.1016/s0011-2240(03)00046-4 (2003).
- 11 Squires, E., Keith, S. & Graham, J. Evaluation of alternative cryoprotectants for preserving stallion spermatozoa. *Theriogenology* **62**, 1056-1065 (2004).
- 12 Alvarenga, M. A., Papa, F. O., Landim-Alvarenga, F. & Medeiros, A. Amides as cryoprotectants for freezing stallion semen: a review. *Animal Reproduction Science* **89**, 105-113 (2005).
- 13 Medeiros, A., Gomes, G., Carmo, M., Papa, F. O. & Alvarenga, M. A. Cryopreservation of stallion sperm using different amides. *Theriogenology*, 273-276 (2002).
- 14 Nagasaki, K. & Yamaguchi, M. Cryopreservation of a virus (HaV) infecting a harmful bloom causing microalga, *Heterosigma akashiwo* (Raphidophyceae). *Fisheries Science* **65**, 319-320 (1999).
- 15 Green, P. & Woodford, S. Preservation studies on some obligately methanotrophic bacteria. *Letters in Applied Microbiology* **14**, 158-162 (1992).
- 16 Mikata, k. Preservation of yeast cultures by freezing at -80 C: I. Viability after 2 yeast storage and the effects of repeated thawing-freezing. *IFO Res. Commun.* **13**, 59-68 (1987).
- 17 Nell, E. E. & Hardy Jr, P. H. The use of freeze-preserved treponemes in the *Treponema pallidum* immobilization test. *Cryobiology* **9**, 404-410 (1972).
- 18 Prentice, M. & Farrant, J. Survival of chlamydiae after cooling to -196 degrees C. *Journal of Clinical Microbiology* **6**, 4-9 (1977).

Appendix I: Supplementary material- Chapter 4

Supplementary Material

***n*-Octyl (thio)glycosides as Potential Cryoprotectants: Glass Transition Behaviour, Membrane Permeability, and Ice Recrystallization Inhibition Studies**

Rekha Raju,^A Theresa Merl,^B Madeleine K. Adam,^C Emiliyan Staykov,^C Robert
N. Ben,^C Gary Bryant,^{A,D} and Brendan L. Wilkinson^{B,D}

^ACentre for Molecular and Nanoscale Physics, School of Science, RMIT University,
Melbourne, Vic. 3000, Australia.

^BSchool of Science and Technology, University of New England, Armidale, NSW 2351,
Australia.

^CDepartment of Chemistry and Biomolecular Sciences, University of Ottawa, Ottawa,
Canada K1N 6N5.

^DCorresponding authors. Email: Gary.bryant@rmit.edu.au; brendan.wilkinson@une.edu.au

Contents

1.0	Materials and Methods	3
	General.....	3
	Differential scanning calorimetry	3
	Cell permeability studies.....	4
	Ice recrystallization inhibition (IRI) analysis	6
2.0	Synthesis	8
	General method 1 – synthesis of <i>O</i> -glycosides. ¹	8
	General method 2 – synthesis of <i>S</i> -glycosides. ²	8
	General method 3 – deprotection of glycosides under Zemplén conditions. ³	9
	<i>n</i> -Octyl (2,3,4,6-tetra- <i>O</i> -acetyl) α/β -D-galactopyranoside (1α-Ac and 1β-Ac)	9
	<i>n</i> -Octyl (2,3,4,6-tetra- <i>O</i> -acetyl) α/β -D-glucopyranoside (2α-Ac and 2β-Ac)	10
	<i>n</i> -Octyl (2,3,4,6-tetra- <i>O</i> -acetyl) α/β -D-thiogalactopyranoside (3α-Ac and 3β-Ac) ...	11
	<i>n</i> -Octyl (2,3,4,6-tetra- <i>O</i> -acetyl) α/β -D-thioglucopyranoside (4α-Ac and 4β-Ac).....	12
	<i>n</i> -Octyl α -D-galactopyranoside (1α).....	13
	<i>n</i> -Octyl β -D-galactopyranoside (1β).....	14
	<i>n</i> -Octyl α -D-glucopyranoside (2α).....	14
	<i>n</i> -Octyl β -D-glucopyranoside (2β)	15
	<i>n</i> -Octyl α -D-thiogalactopyranoside (3α).....	15
	<i>n</i> -Octyl β -D-thiogalactopyranoside (3β)	16
	<i>n</i> -Octyl α -D-thioglucopyranoside (4α)	16
	<i>n</i> -Octyl β -D-thioglucopyranoside (4β)	17
	NMR spectra (1β , 2α , 2β , and 3α).....	18
3.0	References	21

1.0 Materials and Methods

General

Analytical thin layer chromatography (TLC) was performed on commercially prepared silica plates (ChemSupply Silica Gel 60 0.20 mm F254). Flash column chromatography was performed using 230–400 mesh Kieselgel 60 silica eluting with distilled solvents as described. Solvents and reagents were purchased from Sigma-Aldrich and ChemSupply and used without further purification. Solvents for anhydrous reactions were distilled and dried accordingly. ^1H NMR and ^{13}C NMR spectra were recorded on a Bruker Ascend 500 NMR spectrometer at frequencies of 500 MHz and 125 MHz, respectively. Chemical shifts are reported as parts per million (ppm) downfield shift relative to the tetramethylsilane (TMS) internal standard (CDCl_3 only). The data are reported as chemical shift (δ), multiplicity, relative integral, coupling constant ($J = \text{Hz}$) and assignment where possible. IR spectra were recorded on a Perkin Elmer FT-IR (ATR) spectrometer. Optical rotation was measured on a Rudolph Research Analytical Autopol 1 automatic polarimeter (589 nm) using a 10 mL cell. ESI mass spectra were recorded on an Agilent 6120 single quadrupole mass spectrometer operating in positive mode unless otherwise stated.

Differential scanning calorimetry

DSC thermograms on warming were obtained with TA Instruments DSC 2920 Modulated differential scanning calorimeter using 5–10 mg of sample in hermetically sealed aluminum pans. Octyl (thio)glycosides were studied as neat samples and as 20% (w/v) aqueous solutions. For solutions, the samples were warmed from -120°C to 25°C at $5^\circ\text{C}/\text{min}$ with one-minute equilibration times at the end points. Neat surfactants samples (5–10 mg) were hermetically sealed in aluminum sample pans and cycled between 25°C and -160°C at a rate of $10^\circ\text{C}/\text{min}$, with one-minute equilibration times at the endpoints. For all samples, measurements were made on several (at least 2) successive runs to confirm the consistency in thermal behaviour. T_g values were interpreted as the extrapolated mid-point from the inflection of the curve.

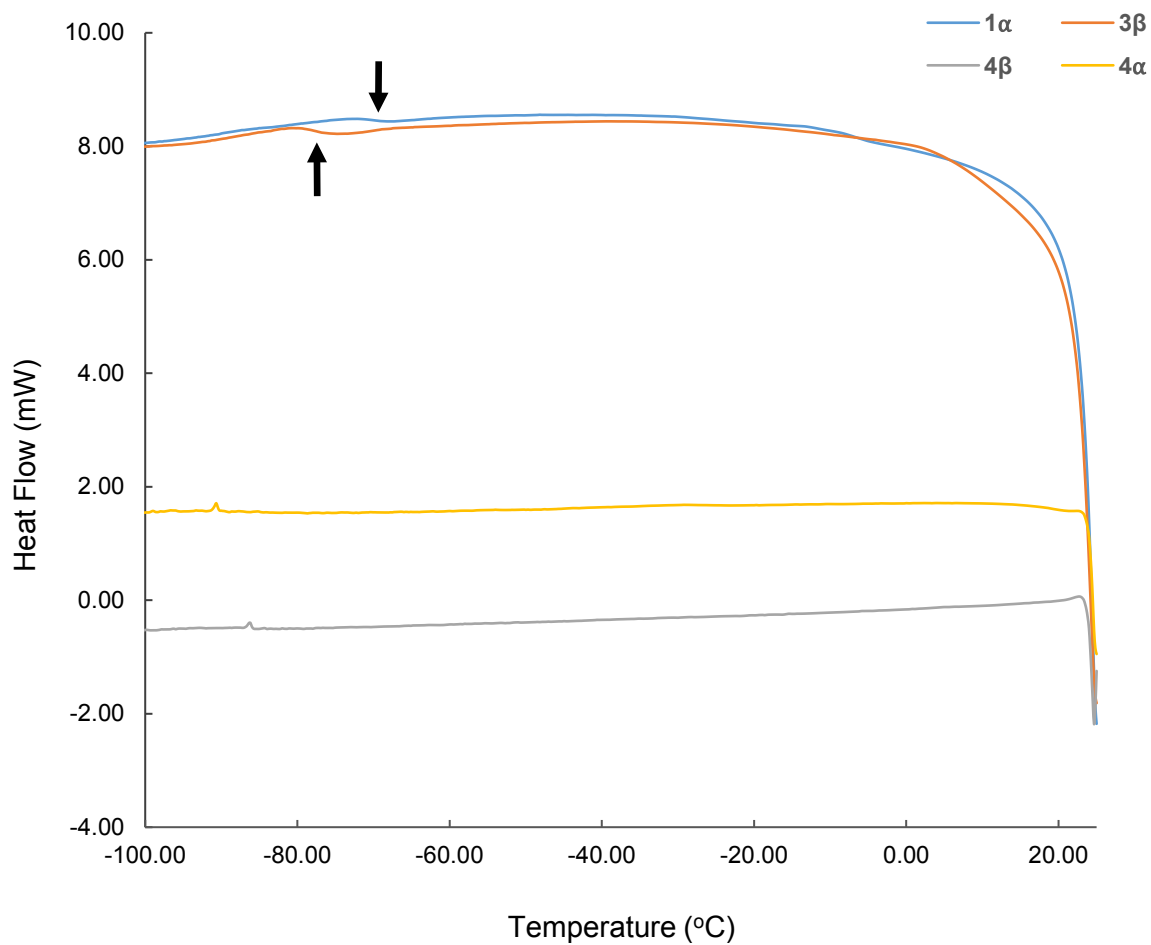


Figure S1. DSC warming thermograms for compounds neat surfactants **1α**, **3β**, **4α**, and **4β**. Only the regions of interest are shown. Scans have been vertically offset for clarity. Possible glass transitions are indicated by bold arrowheads.

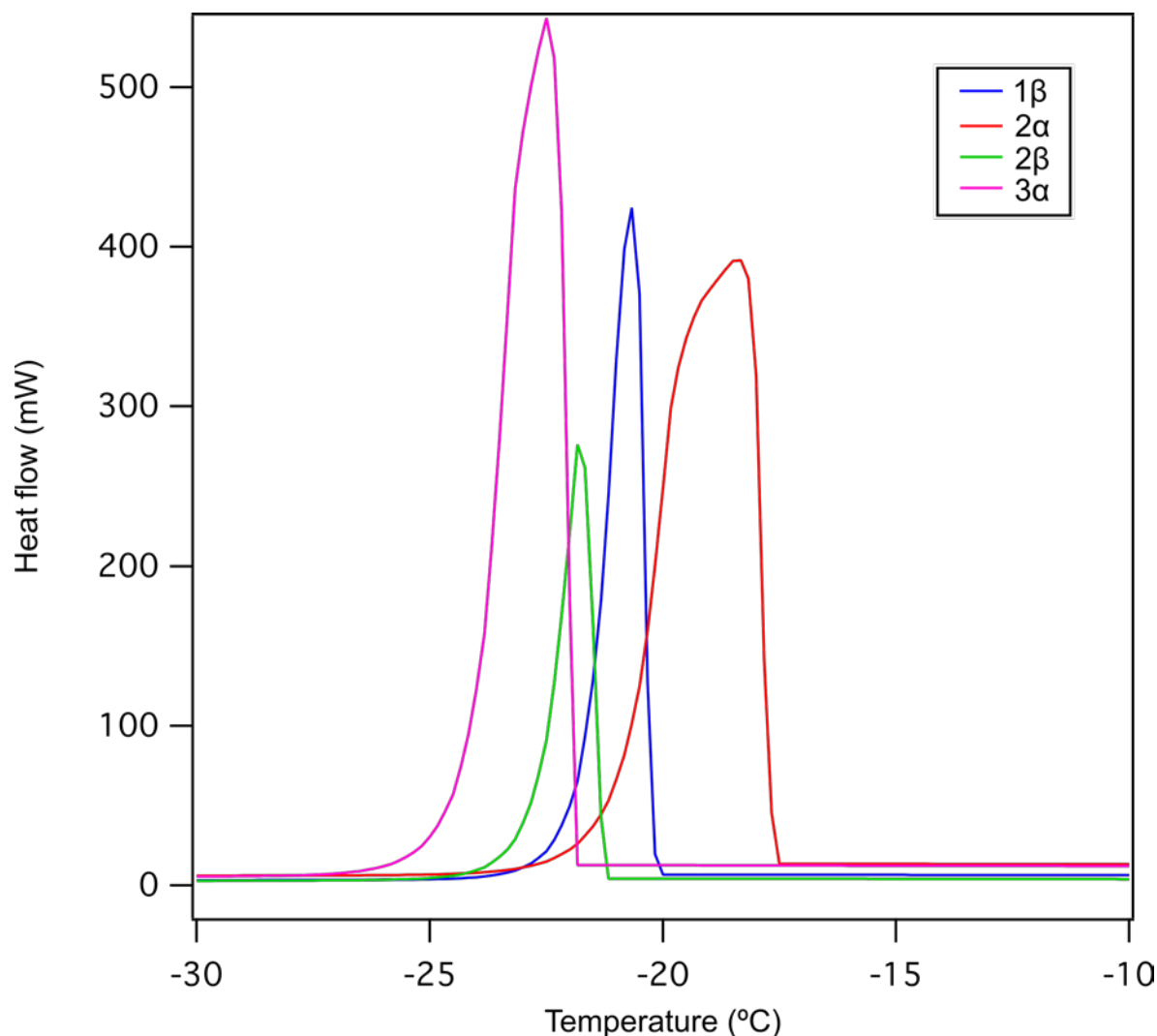


Figure S2. DSC cooling thermograms for soluble compounds (**1 β** , **2 α** , **2 β** , and **3 α**), as 20% wt. aqueous solutions. Only the relevant temperature range is shown. The large endothermic peaks represent ice crystallisation.

Cell permeability studies

An aliquot of cell suspension (50–100 μL) was added to each well of a micro well plate. After the cells settled, the thioglycoside samples were added as small droplets slowly through the side walls of the wells avoiding any violent perturbation to the cell solution to ensure elimination of imaging ambiguities. Samples were prepared in RPMI1640 cell medium and used for cell perfusion with final concentrations 0.65M and 0.33M. For each sample and perfusion experiment, fresh cell suspensions were loaded to the micro wells from the incubator. The cell volume excursion history was recorded with live cell imaging using video microscopy. Video was recorded at 20 frames / second until osmotic equilibrium was obtained. All perfusion

images were captured for at least 5–10 minutes at room temperature (~22°C). An inverted microscope (Olympus IX71 inverted optical microscope) equipped with a CCD camera at 1024×1024 resolution and a CMOS sensor (Mikrotron MC1362) was utilized for visualization. Automated time-lapse image acquisition was used for periods of up to 15 min under the control of StreamPix software (NorPix, Montreal) to capture the cell volume excursion history.

The captured video was converted into image frames by exporting the full sequence at 1 frame/sec. Cells were cropped from each frame of the image. Images were extracted and processed using ImageJ (<https://imagej.nih.gov/ij/>). Several images were analyzed at regular time intervals to understand the volume response (shrinking and swelling) of the cells. The areas of the selected cells were manually measured using oval/free hand selections. Radii and normalized volumes were calculated assuming the cells to be spheres.

Ice recrystallization inhibition (IRI) analysis

The ice recrystallization inhibition (IRI) activities of the thioglycosides were measured using the splat cooling assay.¹ A 10 µL aliquot of the compound dissolved in phosphate-buffered saline (PBS) was dropped from a height of 2 metres onto a polished aluminium block cooled to approximately -80 °C using dry ice. The resulting circular ice wafer (approximately 1 cm in diameter and 20 µm thick) was transferred to a cryostage which was maintained at -6.4 °C using a programmable Peltier unit (S3 Series 800 temperature controller, Alpha Omega Instruments). The ice wafer was annealed for 30 minutes at -6.4 °C. Using a digital camera (Nikon CoolPix 5000) fitted to a microscope, images of the ice wafer were captured between crossed polarizing filters. A novel domain recognition software was then used to measure the cross-sectional areas of randomly-selected ice crystals in each of the three images analyzed per sample. The resulting mean grain size (MGS) of ice crystals was then calculated. IRI activities of the compounds are reported as percent mean grain size (% MGS) and compared to the % MGS of the positive control, PBS. The error bars in Figure 5 represent the percent standard error of the mean (% SEM). Testing for each compound was performed in triplicate.

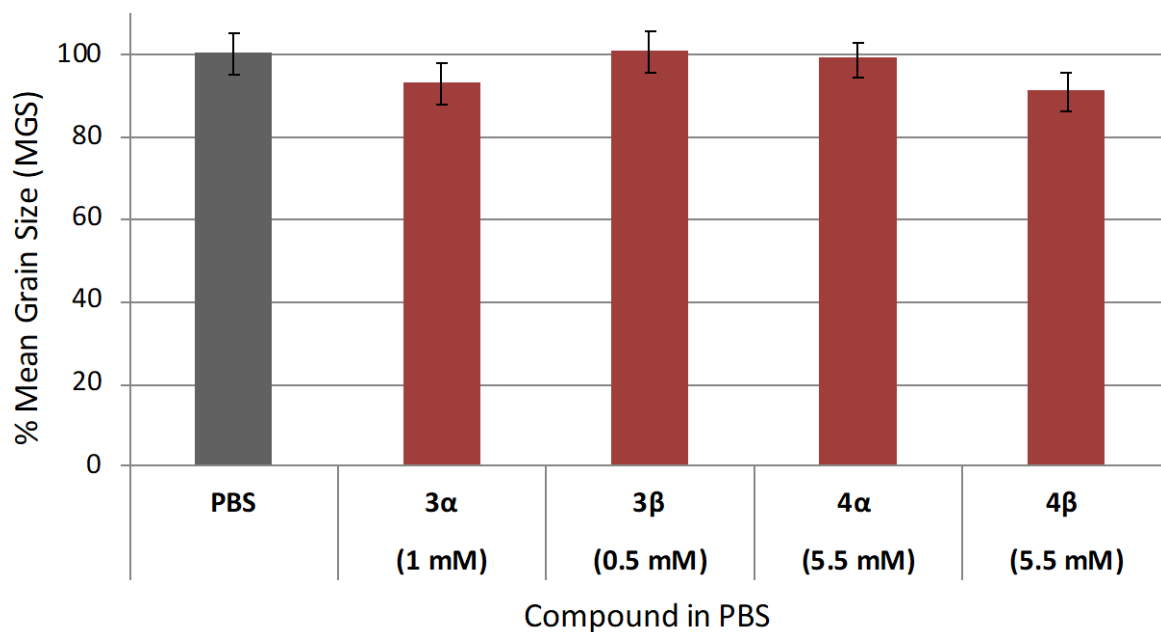
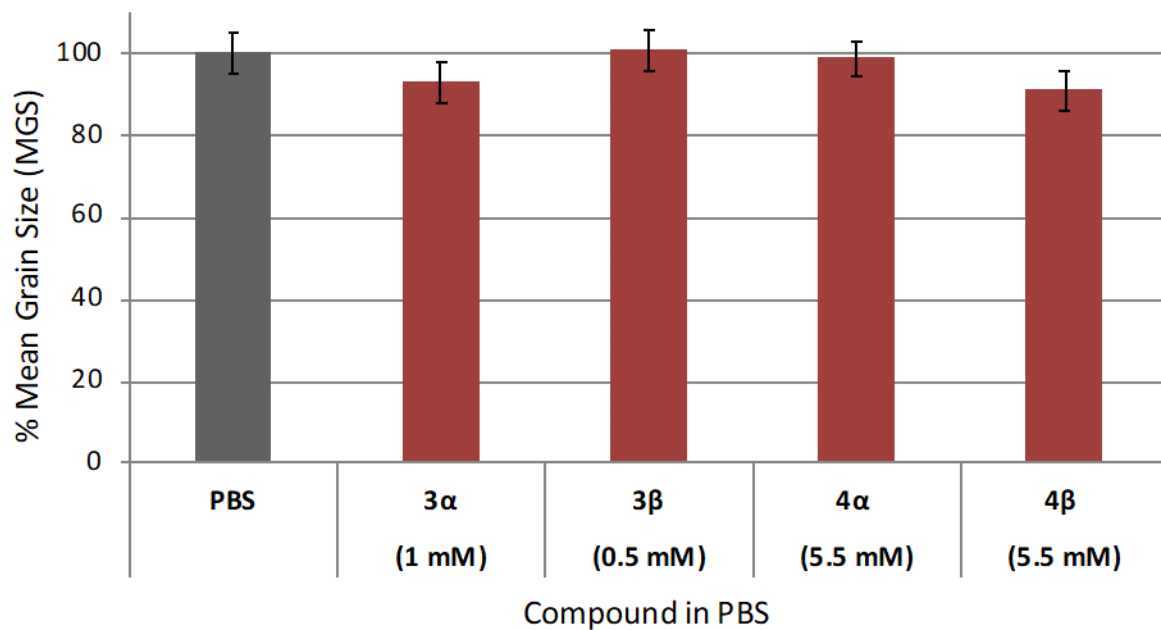
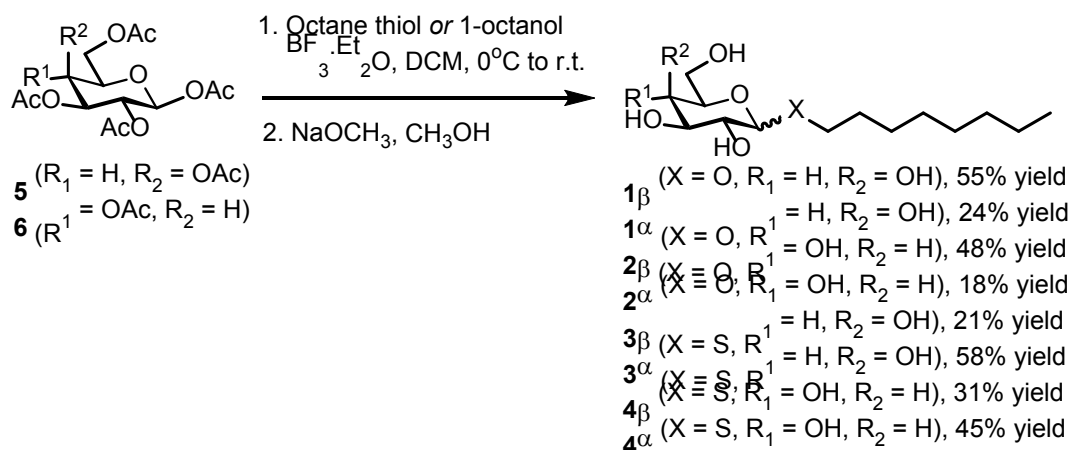


Figure S3. IRI activities of thioglycosides 3 α / β and 4 α / β at their upper solubility limits in PBS. Inhibitory activity is depicted as percent mean grain size (% MGS) with error bars representing percent standard error of the mean (% SEM).

2.0 Synthesis



Scheme S1. Synthesis of *n*-octyl (thio)glycosides **1–4**.

General method 1 – synthesis of *O*-glycosides.²

The synthesis was adapted from a procedure by Lindhorst and co-workers.² To a stirred solution of the sugar pentaacetate (2.0 g, 5.1 mmol) in dry CH_2Cl_2 (10 mL) under N_2 atmosphere was successively added 1-octanol (1.35 mL, 10.2 mmol, 2.1 equiv) and $\text{BF}_3 \cdot \text{Et}_2\text{O}$ (1.6 mL, 12.8 mmol, 2.5 equiv) drop-wise. The solution was then stirred at room temperature for 4 h, at which time TLC analysis (1:1 ethyl acetate/petroleum spirit) indicated consumption of starting material and formation of product. The reaction was carefully neutralized by the drop-wise addition of saturated aqueous NaHCO_3 solution (*ca.* 20 mL). CH_2Cl_2 (20 mL) was then added and the organic layer was separated and washed successively with saturated aqueous NaHCO_3 solution (2 x 20 mL) and brine (1 x 20 mL). The organic layer was dried with anhydrous Na_2SO_4 , filtered, and evaporated. The residue was purified by flash silica chromatography (1:5 v/v ethyl acetate-petroleum spirit) to give the optically pure α - and β -D-glycosides (**1 α /1 β -OAc** and **2 α /2 β -OAc**).

General method 2 – synthesis of *S*-glycosides.³

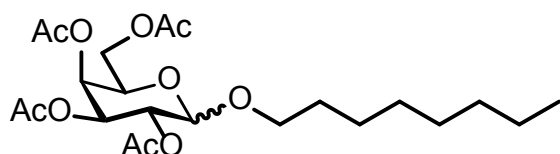
The synthesis was adapted from a procedure by Wynberg and co-workers.³ To a stirred solution of the sugar pentaacetate (2.0 g, 5.1 mmol) in dry CHCl_3 (10 mL) under N_2 atmosphere was added 1-octanethiol (890 μL , 5.12 mmol, 1.0 equiv) followed by $\text{BF}_3 \cdot \text{Et}_2\text{O}$ (3.2 mL, 25.6 mmol, 5.0 equiv) drop-wise. The deep red solution was then stirred at room temperature for 2 h, at which time TLC analysis (1:1 ethyl acetate/petroleum spirit) indicated consumption of starting

material and formation of product. The reaction was carefully neutralized by the drop-wise addition of saturated aqueous NaHCO₃ solution (*ca.* 20 mL). CHCl₃ (20 mL) was then added and the organic layer was separated and washed successively with saturated aqueous NaHCO₃ solution (2 x 20 mL) and brine (1 x 20 mL). The organic layer was dried with anhydrous Na₂SO₄, filtered, and evaporated. The residue was purified by flash silica chromatography (petroleum spirit / ethyl acetate, 4:1) to give the optically pure α - and β -D-thioglycosides (**3 α /3 β -OAc** and **4 α /4 β -OAc**).

General method 3 – deprotection of glycosides under Zemplén conditions.⁴

Purified per-*O*-acetylated glycosides were deprotected using conditions adapted from Zemplén and Pascau.⁴ The per-*O*-acetylated glycoside was dissolved in anhydrous methanol and a freshly prepared solution of sodium methoxide (1 M in methanol) was added. The mixture was stirred until TLC indicated consumption of starting material and formation of a single product (ethyl acetate / methanol, 19:1). The mixture was neutralized by the addition of Amberlite IR120 (H⁺) resin, filtered, and evaporated to dryness to give pure *n*-octyl (thio)glycoside.

n-Octyl (2,3,4,6-tetra-*O*-acetyl) α/β -D-galactopyranoside (**1 α -Ac** and **1 β -Ac**)



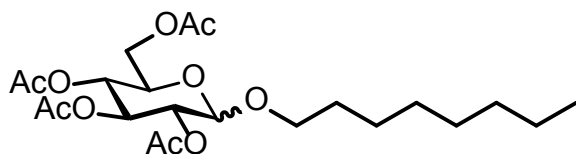
Compounds **1 α -Ac** and **1 β -Ac** were synthesised according to general method 1. The anomeric mixture (2:3 α/β) was purified by flash chromatography as described to yield the pure α -anomer (**1 α -Ac**, 0.54 g, 1.17 mmol, 23%) and pure β -anomer (**1 β -Ac**, 0.85 g, 1.83 mmol, 36%) as a colourless syrup.

β -anomer (1 β -Ac): $R_f = 0.24$ (petroleum ether/ethyl acetate, 4:1); $[\alpha]_D^{20} = +16.7$ ($c = 0.36$, CHCl₃); ¹H NMR (500 MHz, CDCl₃): $\delta = 5.38$ (dd, 1H, $J_{3,4} = 3.5$ Hz, $J_{4,5} = 1.0$ Hz, H-4), 5.20 (dd, 1H, $J_{2,3} = 10.57$, $J_{1,2} = 8.08$ Hz, H-2), 5.01 (dd, 1H, $J_{2,3} = 10.5$ Hz, $J_{3,4} = 3.6$ Hz, H-3), 4.45 (d, 1H, $J_{1,2} = 8.01$ Hz, H-1), 4.18 (dd, 1H, $J_{6a-6b} = 11.25$ Hz, $J_{5-6a} = 6.4$ Hz, H-6a), 4.12 (dd, 1H, $J_{6a-6b} = 11.25$ Hz, $J_{5-6b} = 7.05$ Hz, H-6b), 3.91–3.86 (m, 2H, H-5, Gal-OCHH), 3.46 (dt, 1H, $J_{CH-CH} = 9.60$ Hz, $J_{CH-CH_2} = 6.61$ Hz, Gal-OCHH), 2.14 (s, 3H, OAc CH₃), 2.05 (s, 3H, OAc CH₃), 2.04 (s, 3H, OAc CH₃), 1.98 (s, 3H, OAc CH₃), 1.62–1.51 (m, 2H, Gal-OCH₂-CH₂), 1.32–1.23 (m, 10H, 5 x CH₂), 0.88 (t, 3H, $J = 6.85$ Hz, CH₃) ppm; ¹³C NMR (125 MHz, CDCl₃): $\delta =$

170.56, 170.45, 170.36, 169.51 (4 x COCH₃), 101.48 (C-1), 71.11 (C-3), 70.68 (C-5), 70.44 (Gal-OCH₂), 69.07 (C-2), 67.21 (C-4), 61.42 (C-6), 31.92 (CH₂), 29.53 (Gal-OCH₂CH₂), 29.40, 29.37, 25.92, 22.77 (4 x CH₂), 20.87, 20.81 (2), 20.73 (4 x COCH₃), 14.21 (CH₃) ppm. MS (ESI+): calcd. for C₂₂H₃₆O₁₀ : m/z = 483.22 [M+Na]⁺; found: m/z = 483.2.

α -anomer (1 α -Ac): R_f = 0.31 (petroleum ether/ethyl acetate, 4:1); $[\alpha]_D^{20}$ = +95.8 (c = 0.72, CHCl₃); ¹H NMR (500 MHz, CDCl₃): δ = 5.46 (dd, 1H, $J_{3,4}$ = 3.46 Hz, $J_{4,5}$ = 1.32 Hz, H-4), 5.37–5.34 (m, 1H, H-3), 5.12–5.09 (m, 2H, H-1, H-2), 4.24–4.21 (m, 1H, H-5), 4.13–4.06 (m, 2H, H-6a, H-6b), 3.68 (dt, 1H, J_{CH-CH} = 9.81 Hz, J_{CH-CH_2} = 6.60 Hz, Gal-OCHH), 3.42 (dt, 1H, J_{CH-CH_2} = 9.89 Hz, J_{CH-CH_2} = 6.61 Hz, Gal-OCHCH), 2.14 (s, 3H, OAc CH₃), 2.07 (s, 3H, OAc CH₃), 2.05 (s, 3H, OAc CH₃), 1.99 (s, 3H, OAc CH₃), 1.61–1.55 (m, 2H, Gal-OCH₂CH₂), 1.36–1.26 (m, 10H, 5 x CH₂), 0.89 (t, 3H, J = 6.94 Hz, CH₃) ppm; ¹³C NMR (125 MHz, CDCl₃): δ = 170.33, 170.32, 170.20, 169.97 (4 x COCH₃), 96.11 (C-1), 68.71 (Gal-OCH₂), 68.33 (C-2), 68.19 (C-4), 67.74 (C-3), 66.19 (C-5), 61.85 (C-6), 31.85 (CH₂), 29.33 (Gal-OCH₂CH₂), 29.32, 29.30, 26.11, 22.68 (4 x CH₂), 20.79, 20.71 (2), 20.67 (4 x COCH₃), 14.11 (CH₃) ppm. MS (ESI+): calcd. for C₂₂H₃₆O₁₀ : m/z = 483.22 [M+Na]⁺; found: m/z = 483.2.

***n*-Octyl (2,3,4,6-tetra-*O*-acetyl) α/β -D-glucopyranoside (2 α -Ac and 2 β -Ac)**



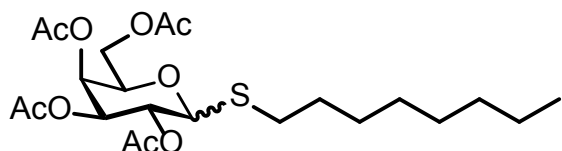
Compounds **2 α -Ac** and **2 β -Ac** were synthesised according to general method 1. The anomeric mixture (2:3 α/β) was purified by flash chromatography as described to yield the pure α -anomer (**2 α -Ac**, 0.61 g, 1.32 mmol, 26%) and pure β -anomer (**2 β -Ac**, 0.90 g, 1.93 mmol, 38%) as a colourless syrup.

β -anomer (2 β -Ac): R_f = 0.22 (petroleum ether/ethyl acetate, 4:1); $[\alpha]_D^{20}$ = +14.6 (c = 0.48, CHCl₃); ¹H NMR (500 MHz, CDCl₃): δ = 5.20 (dd~t, 1H, $J_{2,3}$ = $J_{3,4}$ = 9.57 Hz, H-3), 5.09 (dd~t, 1H, $J_{3,4}$ = $J_{4,5}$ = 9.61 Hz, H-4), 4.98 (dd, 1H, $J_{2,3}$ = 9.62, $J_{1,2}$ = 7.97, H-2), 4.49 (d, 1H, $J_{1,2}$ = 7.99 Hz, H-1), 4.26 (dd, 1H, $J_{6a,6b}$ = 12.23 Hz, $J_{5,6a}$ = 4.72 Hz, H-6a), 4.13 (dd, 1H, $J_{6a,6b}$ = 12.31 Hz, $J_{5,6b}$ = 2.45 Hz, H-6b), 3.87 (dt, 1H, J_{CH-CH} = 9.70 Hz, J_{CH-CH_2} = 6.33 Hz, Glc-OCHH), 3.69 (ddd, 1H, $J_{4,5}$ = 9.90 Hz, $J_{5,6a}$ = 4.73 Hz, $J_{5,6b}$ = 2.43 Hz, H-5), 3.47 (dt, 1H, J_{CH-CH} = 9.57 Hz, J_{CH-CH_2} = 6.63 Hz, Glc-OCHH), 2.08 (s, 3H, OAc CH₃), 2.04 (s, 3H, OAc, CH₃), 2.03 (s, 3H, OAc CH₃), 2.01 (s, 3H, OAc CH₃), 1.60–1.51 (m, 2H, Glc-OCH₂-CH₂), 1.34–1.23 (m, 10H, 5 x CH₂), 0.88

(t, 3H, $J = 6.81$ Hz, CH₃) ppm; ¹³C NMR (125 MHz, CDCl₃): $\delta = 170.77, 170.39, 169.49, 169.35$ (4 x COCH₃), 100.90 (C-1), 72.95 (C-3), 71.80 (C-5), 71.43 (C-2), 70.31 (Glc-OCH₂), 68.56 (C-4), 62.08 (C-6), 31.87 (CH₂), 29.45 (Glc-OCH₂CH₂), 29.32 (2), 25.87, 22.71 (4 x CH₂), 20.81, 20.71, 20.70, 20.61 (4 x COCH₃), 13.16 (CH₃) ppm. MS (ESI⁺): calcd. for C₂₂H₃₆O₁₀ : $m/z = 483.22$ [M+Na]⁺; found: $m/z = 483.2$.

α -anomer (2 α -Ac): $R_f = 0.28$ (petroleum ether/ethyl acetate, 4:1); $[\alpha]_D^{20} = +91.0$ ($c = 0.56$, CHCl₃); ¹H NMR (500 MHz, CDCl₃): $\delta = 5.49$ (dd~t, 1H, $J_{2,3} = J_{3,4} = 9.80$ Hz, H-3), 5.07–5.03 (m, 2H, H-2, H-4), 4.85 (dd, 1H, $J_{2,3} = 10.25$ Hz, $J_{1,2} = 3.81$ Hz, H-2), 4.26 (dd, 1H, $J_{6a,6b} = 12.21$ Hz, $J_{5,6a} = 4.51$ Hz, H-6a), 4.09 (dd, 1H, $J_{6a,6b} = 12.24$ Hz, $J_{5,6b} = 2.41$ Hz, H-6b), 4.02 (ddd, 1H, $J_{4,5} = 10.25$ Hz, $J_{5,6a} = 4.51$ Hz, $J_{5,6b} = 2.41$ Hz, H-5), 3.68 (dt, 1H, $J_{CH,CH} = 9.96$ Hz, $J_{CH,CH_2} = 6.58$ Hz, Glc-OCHH), 3.42 (dt, 1H, $J_{CH,CH} = 9.82$ Hz, $J_{CH,CH_2} = 6.58$ Hz, Glc-OCHH), 2.09 (s, 3H, OAc CH₃), 2.06 (s, 3H, OAc CH₃), 2.03 (s, 3H, OAc CH₃), 2.01 (s, 3H, OAc CH₃), 1.62–1.55 (m, 2H, Glc-OCH₂CH₂), 1.35–1.23 (m, 10H, 5 x CH₂), 0.89 (t, 3H, $J = 6.85$ Hz, CH₃) ppm; ¹³C NMR (125 MHz, CDCl₃): $\delta = 170.76$ (COCH₃), 170.28 (COCH₃), 170.25 (COCH₃), 169.74 (COCH₃), 95.27 (C-1), 71.05 (C-2), 70.37 (C-3), 68.83 (Glc-OCH₂), 68.74 (C-4), 67.22 (C-5), 62.05 (C-6), 31.91 (CH₂), 29.37 (Glc-OCH₂CH₂), 29.34 (2), 26.12, 22.74 (4 x CH₂), 20.81 (2), 20.76, 20.73 (4 x COCH₃), 14.18 (CH₃) ppm. MS (ESI⁺): calcd. for C₂₂H₃₆O₁₀ : $m/z = 483.22$ [M+Na]⁺; found: $m/z = 483.2$.

n-Octyl (2,3,4,6-tetra-*O*-acetyl) α/β -D-thiogalactopyranoside (3 α -Ac and 3 β -Ac)



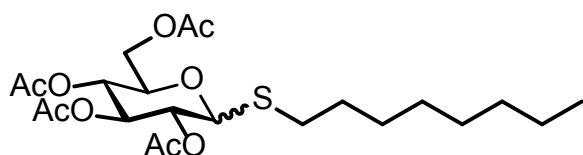
Compounds **3 α -Ac** and **3 β -Ac** were synthesised according to general method 2. The anomeric mixture (~2:1 α/β) was purified by flash chromatography as described to yield the pure α -anomer (**3 α -Ac**, 1.31 g, 2.75 mmol, 54%) and pure β -anomer (**3 β -Ac**, 0.78 g, 1.63 mmol, 32%) as a pale yellow syrup.

β -anomer (3 β -Ac): $R_f = 0.30$ (petroleum ether/ethyl acetate, 4:1); $[\alpha]_D^{20} = -5.2$ ($c = 0.6$, CHCl₃); ¹H NMR (500 MHz, CDCl₃): $\delta = 5.44$ (dd, 1H, $J_{3,4} = 3.44$ Hz, $J_{4,5} = 1.04$ Hz, H-4), 5.23 (dd~t, 1H, $J_{2,3} = J_{1,2} = 9.95$ Hz, H-2), 5.05 (dd, 1H, $J_{2,3} = 9.95$ Hz, $J_{3,4} = 3.42$ Hz, H-3), 4.84 (d, 1H, $J_{1,2} = 10.04$ Hz, H-1), 4.17 (dd, 1H, $J_{6a,6b} = 11.28$ Hz, $J_{5,6a} = 6.73$ Hz, H-6a), 4.11 (dd, 1H, $H_{6a,6b} =$

11.28 Hz, $J_{5,6b} = 6.73$ Hz, H-6b), 3.95–3.91 (m, 1H, H-5), 2.75–2.63 (m, 2H, Gal-SCH₂), 2.16 (s, 3H, OAc CH₃), 2.07 (s, 3H, OAc CH₃), 2.05 (s, 3H, OAc CH₃), 1.99 (s, 3H, OAc CH₃), 1.66–1.56 (m, 2H, Gal-SCH₂CH₂), 2.41–2.34 (m, 2H, CH₂), 1.30–1.25 (m, 8H, 4 x CH₂), 0.88 (t, 1H, $J = 7.02$ Hz, CH₃); ¹³C NMR (125 MHz, CDCl₃): $\delta = 170.53, 170.38, 170.23, 169.71$ (4 x COCH₃), 84.40 (C-1), 74.53, 72.53, 67.45 (2), 61.59 (C-2, C-3, C-4, C-5, and C-6), 31.96, 30.42, 29.85, 29.33, 29.29, 28.97, 22.89 (7 x CH₂), 20.99, 20.85 (2) 20.77 (COCH₃), 14.25 (CH₃) ppm. MS (ESI⁺): calcd. for C₂₂H₃₆O₉S : $m/z = 499.2$ [M+Na]⁺; found: $m/z = 499.2$

α -anomer (3 α -Ac): $R_f = 0.37$ (petroleum ether/ethyl acetate, 4:1); $[\alpha]_D^{20} = +154.7$ ($c = 1.4$, CHCl₃); ¹H NMR (500 MHz, CDCl₃): $\delta = 5.72$ (d, 1H, $J_{1,2} = 5.18$ Hz, H-1), 5.45 (dd, 1H, $J_{3,4} = 3.31$ Hz, $J_{4,5} = 1.15$ Hz, H-4), 5.27 (dd, 1H, $J_{2,3} = 11.01$ Hz, $J_{1,2} = 5.20$ Hz, H-2), 5.22 (dd, 1H, $J_{2,3} = 11.02$ Hz, $J_{3,4} = 3.27$ Hz, H-3), 4.61–4.57 (m, 1H, H-5), 4.12 (dd, 1H, $J_{6a,6b} = 11.41$ Hz, $J_{5,6a} = 6.15$ Hz, H-6a), 4.09 (dd, 1H, $J_{6a,6b} = 11.41$ Hz, $J_{5,6b} = 6.93$ Hz, H-6b), 2.59–2.46 (m, 2H, Gal-SCH₂), 2.15 (s, 3H, OAc CH₃), 2.08 (s, 3H, OAc CH₃), 2.05 (s, 3H, OAc CH₃), 1.99 (s, 3H, OAc CH₃), 1.62–1.54 (m, 2H, CH₂), 1.39–1.22 (m, 10H, 5 x CH₂), 0.88 (t, $J = 6.81$ Hz, 3H, CH₃) ppm; ¹³C NMR (125 MHz, CDCl₃): $\delta = 170.29, 170.13$ (2), 169.82 (4 x COCH₃), 82.27 (C-1), 68.31, 68.14, 68.11, 61.95, 66.58 (C-2, C-3, C-4, C-5, and C-6), 31.89, 29.95, 29.45, 29.29, 29.21, 29.02, 22.75 (7 x CH₂), 20.94, 20.79, 20.74 (2) (COCH₃), 14.20 (CH₃) ppm. MS (ESI⁺): calcd. for C₂₂H₃₆O₉S : $m/z = 499.2$ [M+Na]⁺; found: $m/z = 499.2$

***n*-Octyl (2,3,4,6-tetra-*O*-acetyl) α/β -D-thioglucopyranoside (4 α -Ac and 4 β -Ac)**



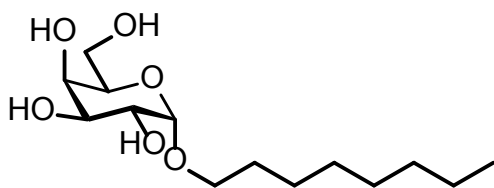
Compounds **4 α -Ac** and **4 β -Ac** were synthesised according to general method 2. The anomeric mixture (~2:1 α/β) was purified by flash chromatography as described to yield the pure α -anomer (**4 α -Ac**, 1.24 g, 2.60 mmol, 51%) and pure β -anomer (**4 β -Ac**, 0.85 g, 1.78 mmol, 35%) as a colourless syrup which slowly crystallized on standing in the refrigerator.

β -anomer (4 β -Ac): $R_f = 0.27$ (petroleum ether/ethyl acetate, 4:1); $[\alpha]_D^{20} = -18.5$ ($c = 0.65$, CHCl₃); ¹H NMR (500 MHz, CDCl₃): $\delta 5.22$ (dd~t, 1H, $J_{2,3} = J_{3,4} = 9.36$ Hz, H-3), 5.09 (dd~t, 1H, $J_{2,3} = J_{1,2} = 9.70$ Hz, H-2), 5.03 (dd, 1H, $J_{4,5} = 9.56$ Hz, $J_{3,4} = 9.42$ Hz, H-4), 4.48 (d, 1H, $J_{1,2} = 10.05$ Hz, H-1), 4.25 (dd, 1H, $J_{6a,6b} = 12.41$ Hz, $J_{5,6a} = 4.92$ Hz, H-6a), 4.14 (dd, 1H, $J_{6a,6b} = 12.41$ Hz, $J_{5,6b} = 2.42$ Hz, H-6b), 3.71 (ddd, 1H, $J_{4,5} = 9.62$ Hz, $J_{5,6a} = 4.91$ Hz, $J_{5,6b} = 2.44$ Hz,

H-5), 2.72–2.61 (m, 2H, Glc-SCH₂), 2.08 (s, 3H, OAc, CH₃), 2.06 (s, 3H, OAc, CH₃), 2.03 (s, 3H, OAc, CH₃), 2.01 (s, 3H, OAc, CH₃), 1.65–1.53 (m, 2H, Glc-SCH₂-CH₂), 1.40–1.22 (m, 10H, 5 x CH₂), 0.88 (t, 1H, *J* = 6.88 Hz, CH₃); ¹³C NMR (125 MHz, CDCl₃): δ 170.81, 170.37, 169.58, 169.55 (4 x COCH₃), 83.79 (C-1), 76.01 (C-2), 74.08 (C-3), 70.05 (C-4), 68.49 (C-5), 62.35 (C-6), 31.95, 30.17, 29.78, 29.33, 29.27, 28.95, 22.79 (7 x CH₂), 20.89 (2), 20.79, 20.76 (4 x COCH₃), 14.25 (CH₃) ppm. MS (ESI⁺): calcd. for C₂₂H₃₆O₉S : *m/z* = 499.2 [M+Na]⁺; found: *m/z* = 499.2.

α-anomer (4α-Ac): *R*_f = 0.37 (petroleum ether/ethyl acetate, 4:1); [α]_D²⁰ = +135.4 (*c* = 1.3, CHCl₃); ¹H NMR (500 MHz, CDCl₃): δ 5.65 (d, 1H, *J*_{1,2} = 5.85 Hz, H-1), 5.37 (dd~t, 1H, *J*_{2,3} = *J*_{3,4} = 9.64 Hz, H-3), 5.04 (dd, 1H, *J*_{4,5} = 10.21 Hz, *J*_{3,4} = 9.50 Hz, H-4) 5.02 (dd, 1H, *J*_{2,3} = 10.23 Hz, *J*_{1,2} = 5.85 Hz, H-2), 4.43 (ddd, 1H, *J*_{4,5} = 10.21 Hz, *J*_{5,6a} = 4.71 Hz, *J*_{5-6b} = 2.27 Hz, H-5), 4.30 (dd, 1H, *J*_{6a,6b} = 12.23 Hz, *J*_{5,6a} = 4.69 Hz, H-6a), 4.07 (dd, 1H, *J*_{6a,6b} = 12.31 Hz, *J*_{5,6b} = 2.31 Hz, H-6b), 2.58–2.46 (m, 2H, Gal-SCH₂), 2.09 (s, 3H, OAc CH₃), 2.06 (s, 3H, OAc CH₃), 2.03 (s, 3H, OAc CH₃), 2.01 (s, 3H, OAc CH₃), 1.39–1.21 (m, 10H, CH₂), 0.88 (t, 3H, *J* = 6.93 Hz, CH₃); ¹³C NMR (125 MHz, CDCl₃): δ = 170.73, 170.08, 170.04, 169.78 (4 x COCH₃), 82.13 (C-1), 70.90 (C-2), 70.67 (C-3), 68.72 (C-4), 67.63 (C-5), 62.09 (C-6), 31.91, 30.29, 29.51, 29.30, 29.22, 28.99, 22.76 (7 x CH₂), 20.89, 20.86, 20.81, 20.76 (4 x COCH₃), 14.22 (CH₃) ppm. MS (ESI⁺): calcd. for C₂₂H₃₆O₉S : *m/z* = 499.2 [M+Na]⁺; found: *m/z* = 499.2

n-Octyl α-D-galactopyranoside (1α)

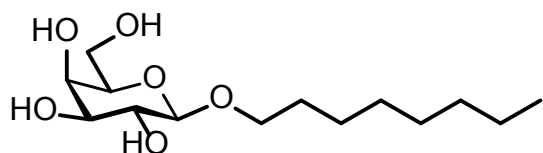


Compound **1α** were synthesised according to general method 3 and isolated as a waxy solid (352 mg, 1.12 mmol, 96%).

1α: *R*_f = 0.44 (ethyl acetate/methanol, 6:1); [α]_D²⁰ = +95.3 (*c* = 0.53, CH₃OH); ¹H NMR (500 MHz, CD₃OD): δ 4.79 (d, 1H, *J*_{1,2} = 3.43 Hz, H-1), 3.89 (dd, 1H, *J*_{3,4} = 3.03 Hz, *J*_{4,5} = 1.13 Hz, H-4), 3.80 (td, *J*_{5,6} = 9.21 Hz, *J*_{3,4} = 1.13 Hz, H-5), 3.76 (dd, *J*_{2,3} = 10.10 Hz, *J*_{1,2} = 3.43 Hz, H-2), 3.74–3.73 (m, 1H, H-3), 3.73–3.69 (3H, Gal-OCHH, H-6a, H-6b), 3.44 (dt, 1H, *J*_{CH,CH} = 9.69 Hz, *J*_{CH,CH₂} = 6.57 Hz, Gal-OCHH), 1.70–1.57 (m, 2H, Gal-OCH₂CH₂), 1.42–1.27 (m, 10H, 5 x CH₂), 0.90 (t, 3H, *J* = 7.12 Hz, CH₃) ppm; ¹³C NMR (125 MHz, CD₃OD): δ ¹³C NMR (125

MHz, CD₃OD): δ 100.47 (C-1), 72.41 (C-5), 71.69 (C-3), 71.26 (C-4), 70.42 (C-2), 69.35 (Gal-OCH₂), 62.86 (C-6), 33.16 (Gal-OCH₂CH₂), 30.74 (2), 30.56, 27.49, 23.86 (4 x CH₂), 14.58 (CH₃) ppm. MS (ESI⁺): calcd. for C₁₄H₂₈O₆ : m/z = 315.2 [M+Na]⁺; found: m/z = 315.2.

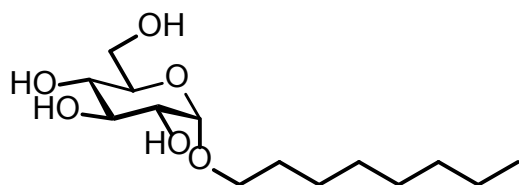
***n*-Octyl β -D-galactopyranoside (1 β)**



Compound **1 β** were synthesised according to general method 3 and isolated as a waxy solid (554 mg, 1.76 mmol, 96%).

1 β : R_f = 0.36 (ethyl acetate/methanol, 6:1); $[\alpha]_D^{20}$ = -21.3 (c = 0.65, CH₃OH); ¹H NMR (500 MHz, CD₃OD): δ 4.20 (d, 1H, $J_{1,2}$ = 7.48 Hz, H-1), 3.89 (dt, 1H, $J_{CH,CH}$ = 9.54 Hz, J_{CH,CH_2} = 6.89 Hz, Gal-OCHCH), 3.83 (dd, 1H, $J_{3,4}$ = 3.32 Hz, $J_{4,5}$ = 1.02 Hz, H-4), 3.75 (dd, 1H, $J_{6a,6b}$ = 11.30 Hz, $J_{5,6a}$ = 6.63 Hz, H-6a), 3.72 (dd, 1H, $J_{6a,6b}$ = 11.30 Hz, $J_{5,6b}$ = 5.60 Hz, H-6b), 3.56–3.47 (m, 3H, Gal-OCHH, H-2, H-5), 3.45 (dd, 1H, $J_{2,3}$ = 9.68 Hz, $J_{3,4}$ = 3.30 Hz, H-3), 1.68–1.59 (m, 2H, Gal-OCH₂CH₂), 1.41–1.27 (m, 10H, 5 x CH₂), 0.90 (t, 3H, J = 7.19 Hz, CH₃) ppm; ¹³C NMR (125 MHz, CD₃OD): δ 105.12 (C-1), 76.67 (C-5), 75.19 (C-3), 72.73 (C-2), 70.99 (Gal-OCH₂), 70.49 (C-4), 62.57 (C-6), 33.15 (CH₂), 30.98 (Gal-OCH₂CH₂), 30.73, 30.57, 27.27, 23.86 (4 x CH₂), 14.58 (CH₃) ppm. MS (ESI⁺): calcd. for C₁₄H₂₈O₆ : m/z = 315.2 [M+Na]⁺; found: m/z = 315.2.

***n*-Octyl α -D-glucopyranoside (2 α)**

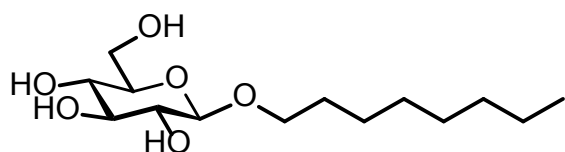


Compound **2 α** were synthesised according to general method 3 and isolated as a waxy solid (416 mg, 1.32 mmol, 100%).

2 α : R_f = 0.47 (ethyl acetate/methanol, 6:1); $[\alpha]_D^{20}$ = +95.6 (c = 0.54, CH₃OH); ¹H NMR (500 MHz, CD₃OD): δ 4.78 (d, 1H, $J_{1,2}$ = 3.78 Hz, H-1), 3.79 (dd, 1H, $J_{6a,6b}$ = 11.82 Hz, $J_{5,6a}$ = 2.40 Hz, H-6a), 3.73 (dt, 1H, $J_{CH,CH}$ = 9.54 Hz, J_{CH,CH_2} = 6.61 Hz, Glc-OCHCH), 3.67 (dd, 1H, $J_{6a,6b}$ = 11.78 Hz, $J_{5,6b}$ = 5.46 Hz, H-6b), 3.63 (dd~t 1H, $J_{2,3}$ = $J_{3,4}$ = 9.22 Hz, H-3), 3.57 (ddd, 1H, $J_{4,5}$ =

9.92 Hz, $J_{5,6b} = 5.52$ Hz, $J_{5,6a} = 2.40$ Hz, H-5), 3.44 (dt, 1H, $J_{CH,CH} = 9.65$ Hz, $J_{CH,CH_2} = 6.38$ Hz, Glc-OCHH), 3.38 (dd, $J_{2,3} = 9.67$ Hz, $J_{1,2} = 3.73$ Hz, 1H, H-2), 3.28 (dd, 1H, $J_{4,5} = 9.91$ Hz, $J_{3,4} = 8.97$ Hz, H-4), 1.70–1.57 (m, 2H, Glc-OCH₂CH₂), 1.43–1.26 (m, 10H, 5 x CH₂), 0.90 (t, 3H, $J = 7.10$ Hz, CH₃) ppm; ¹³C NMR (125 MHz, CD₃OD): δ 100.22 (C-1), 75.28 (C-3), 73.77 (C-5), 73.72 (C-2), 72.02 (C-4), 69.26 (Glc-OCH₂), 62.80 (C-6), 33.16 (CH₂), 30.78, 30.74, 30.57, 27.28, 23.87 (5 x CH₂), 14.59 (CH₃) ppm. MS (ESI+): calcd. for C₁₄H₂₈O₆ : $m/z = 315.2$ [M+Na]⁺; found: $m/z = 315.2$.

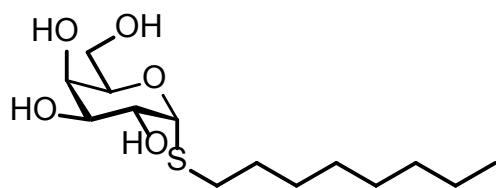
n-Octyl β-D-glucopyranoside (2β)



Compound **2β** were synthesised according to general method 3 and isolated as a waxy solid (608 mg, 1.93 mmol, 100%).

2β: $R_f = 0.65$ (ethyl acetate/methanol, 6:1); $[\alpha]_D^{20} = -21.2$ ($c = 0.65$, CH₃OH); ¹H NMR (500 MHz, CD₃OD): δ 4.24 (d, 1H, $J_{1,2} = 7.82$ Hz, H-1), 3.90 (dt, 1H, $J_{CH,CH} = 9.55$ Hz, $J_{CH,CH_2} = 6.68$ Hz, Gal-OCHCH), 3.86 (dd, 1H, $J_{6a,6b} = 11.98$ Hz, $J_{5,6a} = 2.01$ Hz, H-6a), 3.66 (dd, 1H, $J_{6a,6b} = 11.98$ Hz, $J_{5,6b} = 5.41$ Hz, H-6b), 3.53 (dt, $J_{CH,CH} = 9.33$ Hz, $J_{CH,CH_2} = 6.79$ Hz, Glc-OCHH), 3.34 (dd~t, 1H, $J_{2,3} = J_{3,4} = 9.10$ Hz, H-3), 3.28 (dd~t, 1H, $J_{2,3} = J_{3,4} = 9.10$ Hz, H-4), 3.26–3.23 (m, 1H, H-5), 3.16 (dd, 1H, $J_{2,3} = \text{Hz}$, $J_{1,2} = \text{Hz}$, H-2), 1.64–1.59 (m, 2H, Glc-OCH₂CH₂), 1.40–1.27 (m, 10H, 5 x CH₂), 0.90 (t, 3H, $J = 7.12$ Hz, CH₃) ppm; ¹³C NMR (125 MHz, CD₃OD): δ 104.43 (C-1), 78.20 (C-3), 77.96 (C-5), 75.19 (C-2), 71.75 (C-4), 71.01 (Glc-OCH₂), 62.86 (C-6), 33.12 (CH₂), 30.90 (Glc-OCH₂CH₂), 30.71, 30.53, 27.22, 23.83 (4 x CH₂), 14.58 (CH₃) ppm. MS (ESI+): calcd. for C₁₄H₂₈O₆ : $m/z = 315.2$ [M+Na]⁺; found: $m/z = 315.2$.

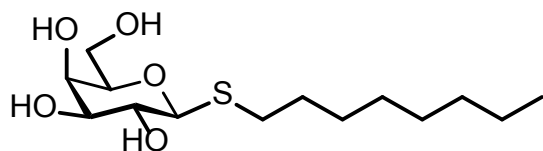
n-Octyl α-D-thiogalactopyranoside (3α)



Compound **3α** were synthesised according to general method 3 and isolated as a colourless gym (910 mg, 2.75 mmol, 100%).

3 α : $R_f = 0.53$ (ethyl acetate/methanol, 6:1); $[\alpha]_D^{20} = +200$ ($c = 0.8$, CH₃OH); ¹H NMR (500 MHz, CD₃OD): δ 5.37 (d, 1H, $J_{1,2} = 5.65$ Hz, H-1), 4.21–4.18 (m, 1H, H-5), 4.07 (dd, 1H, $J_{2,3} = 10.16$ Hz, $J_{1,2} = 5.64$ Hz, H-2), 3.90 (dd, 1H, $J_{3,4} = 3.39$ Hz, $J_{4,5} = 1.22$ Hz, H-4), 3.74–3.72 (m, 2H, H-6a, H-6b), 3.62 (dd, 1H, $J_{2,3} = 10.13$ Hz, $J_{3,4} = 3.36$ Hz, H-3), 2.67–2.54 (m, 2H, Gal-SCH₂), 1.73–1.60 (m, 2H, Gal-SCH₂-CH₂), 1.46–1.29 (m, 10H, 5 x CH₂), 0.92 (t, 3H, CH₃) ppm; ¹³C NMR (125 MHz, CD₃OD): δ 87.45 (C-1), 72.70 (C-5), 72.30 (C-3), 70.96 (C-4), 69.86 (C-2), 62.66 (C-6), 33.12, 30.88 (2), 30.49, 30.46, 30.20, 23.83 (7 x CH₂), 14.58 (CH₃) ppm. MS (ESI+): calcd. for C₁₄H₂₈O₆ : $m/z = 315.2$ [M+Na]⁺; found: $m/z = 315.2$.

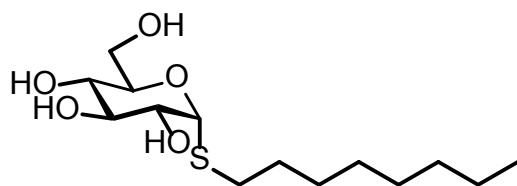
***n*-Octyl β -D-thiogalactopyranoside (3 β)**



Compound **3 β** were synthesised according to general method 3 and isolated as an amorphous solid (538 mg, 1.63 mmol, 100%).

3 β : $R_f = 0.56$ (ethyl acetate/methanol, 6:1); $[\alpha]_D^{20} = -19.2$ ($c = 0.8$, CH₃OH); ¹H NMR (500 MHz, CD₃OD): δ 4.29 (d, 1H, $J_{1,2} = 9.54$ Hz, H-1), 3.88 (dd, 1H, $J_{3,4} = 3.36$ Hz, $J_{4,5} = 0.95$ Hz, H-4), 3.53 (dd~t, 1H, $J_{1,2} = J_{2,3} = 9.48$ Hz, H-2), 3.73 (dd, 1H, $J_{6a,6b} = 11.37$ Hz, $J_{5,6a} = 6.81$ Hz, H-6a), 3.68 (dd, 1H, $J_{6a,6b} = 11.37$ Hz, $J_{5,6b} = 5.43$ Hz, H-6b), 3.53–3.49 (m, 1H, H-5), 3.45 (dd, 1H, $J_{2,3} = 9.27$ Hz, $J_{3,4} = 3.35$ Hz, H-3), 2.78–2.66 (m, 2H, Gal-SCH₂), 1.71–1.59 (m, Gal-SCH₂-CH₂), 1.44–1.26 (m, 10H, 5 x CH₂), 0.90 (t, 3H, $J = 6.92$ Hz, CH₃) ppm; ¹³C NMR (125 MHz, CD₃OD): δ 87.82 (C-1), 80.65 (C-5), 76.36 (C-3), 71.56 (C-2), 70.56 (C-4), 62.66 (C-6), 33.12, 31.21, 31.01, 30.48, 30.44, 30.13, 23.83 (7 x CH₂), 14.58 (CH₃) ppm. MS (ESI+): calcd. for C₁₄H₂₈O₆S : $m/z = 331.2$ [M+Na]⁺; found: $m/z = 331.2$.

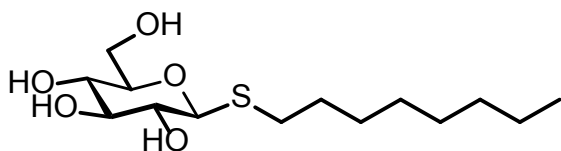
***n*-Octyl α -D-thioglucopyranoside (4 α)**



Compound **4 α** were synthesised according to general method 3 and obtained as an amorphous solid (860 mg, 2.60 mmol, 100%).

4 α : $R_f = 0.56$ (ethyl acetate/methanol, 6:1); $[\alpha]_D^{20} = +218$ ($c = 0.38$); $^1\text{H NMR}$ (500 MHz, CD_3OD): δ 5.30 (d, 1H, $J_{1,2} = 5.51$ Hz, H-1), 3.95 (ddd, 1H, $J_{4,5} = 9.87$ Hz, $J_{5,6b} = 7.73$ Hz, $J_{5,6a} = 2.29$ Hz, H-5), 3.79 (dd, 1H, $J_{5,6a} = 2.45$ Hz, $J_{6a,6b} = 11.48$ Hz, H-6a), 3.71 (dd, 1H, $J_{6a,6b} = 11.89$ Hz, $J_{5,6b} = 5.47$ Hz, H-6b), 3.68 (dd, 1H, $J_{2,3} = 9.72$ Hz, $J_{1,2} = 5.48$ Hz, H-2), 3.52 (dd~t, $J_{3,4} = J_{4,5} = 9.21$ Hz, 1H, H-4), 3.33–3.29 (m, 1H, H-3), 2.64–2.53 (m, 2H, GalS-OCH₂), 1.68–1.59 (m, 2H, GalSOCH₂-CH₂), 1.45–1.26 (m, 10H, 5 x CH₂), 0.90 (t, 1H, $J = 7.14$ Hz, CH₃) ppm; $^{13}\text{C NMR}$ (125 MHz, CD_3OD): δ 87.45 (C-1), 72.70 (C-5), 72.29 (C-2), 70.96 (C-3), 69.85 (C-4), 62.66 (C-6), 33.12, 30.88 (2), 30.49, 30.46, 30.20, 23.83 (7 x CH₂), 14.58 (CH₃) ppm; $^{13}\text{C NMR}$ (100 MHz, CD_3OD): δ 87.30 (C-1), 73.30 (C-4), 74.04 (C-5), 75.80 (C-2), 71.85 (C-3), 62.66 (C-6), 33.14, 31.19, 30.91, 30.51, 30.46, 30.17, 23.84 (7 x CH₂), 14.58 (CH₃) ppm. MS (ESI⁺): calcd. for C₁₄H₂₈O₆S : $m/z = 331.2$ [M+Na]⁺; found: $m/z = 331.2$.

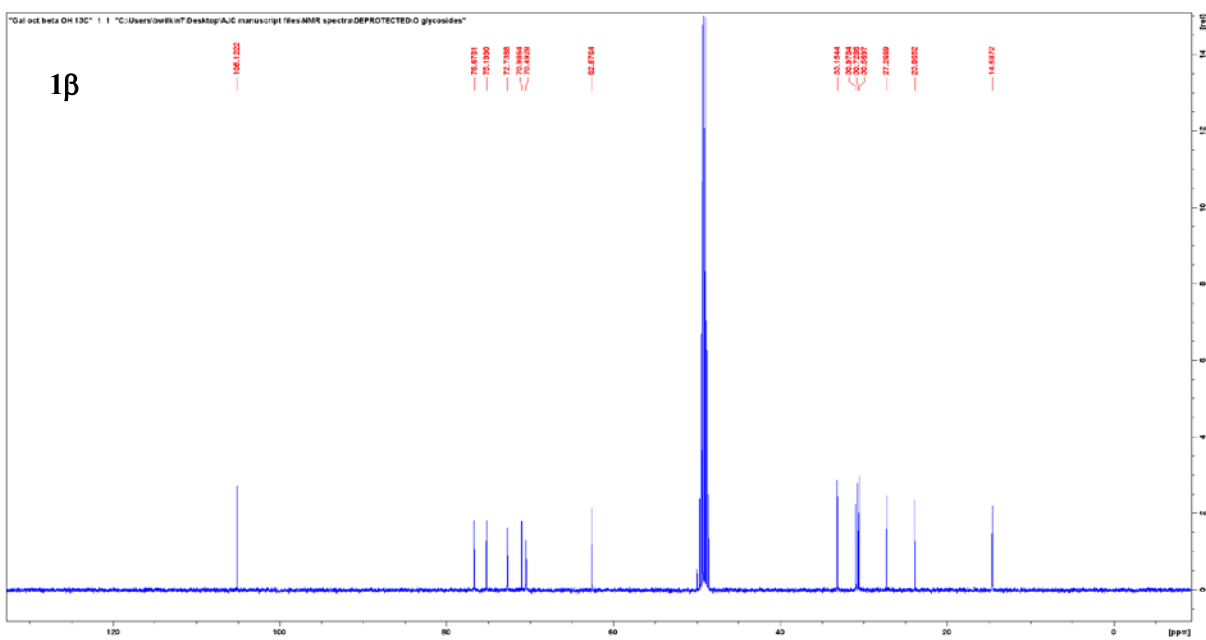
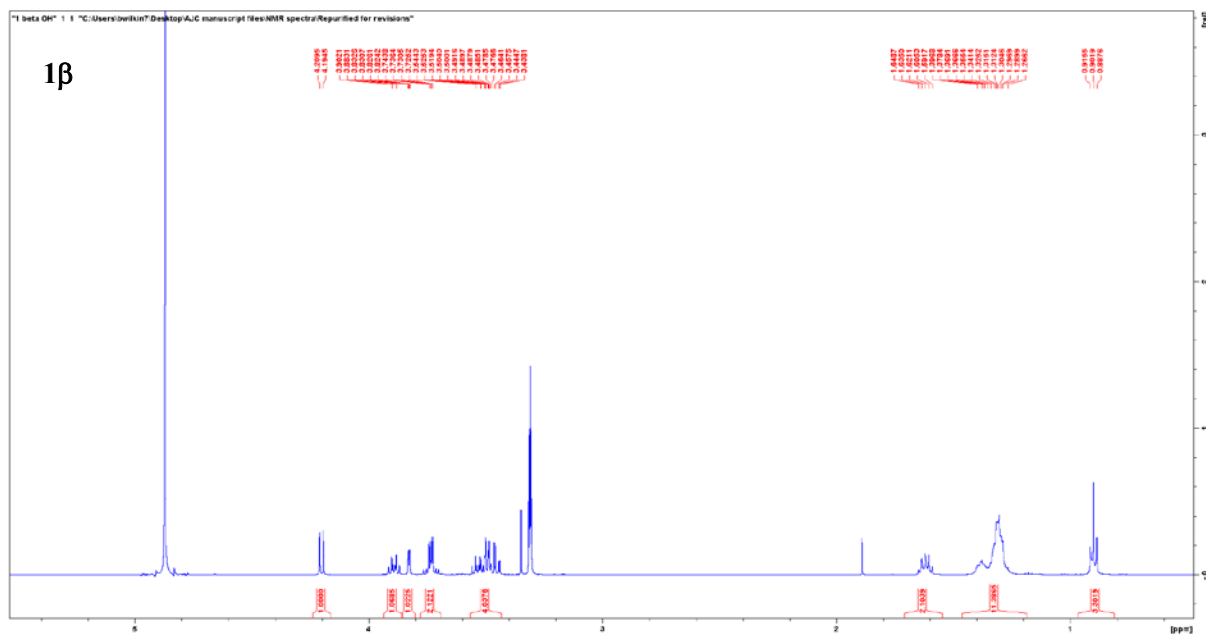
***n*-Octyl β -D-thioglucopyranoside (4 β)**

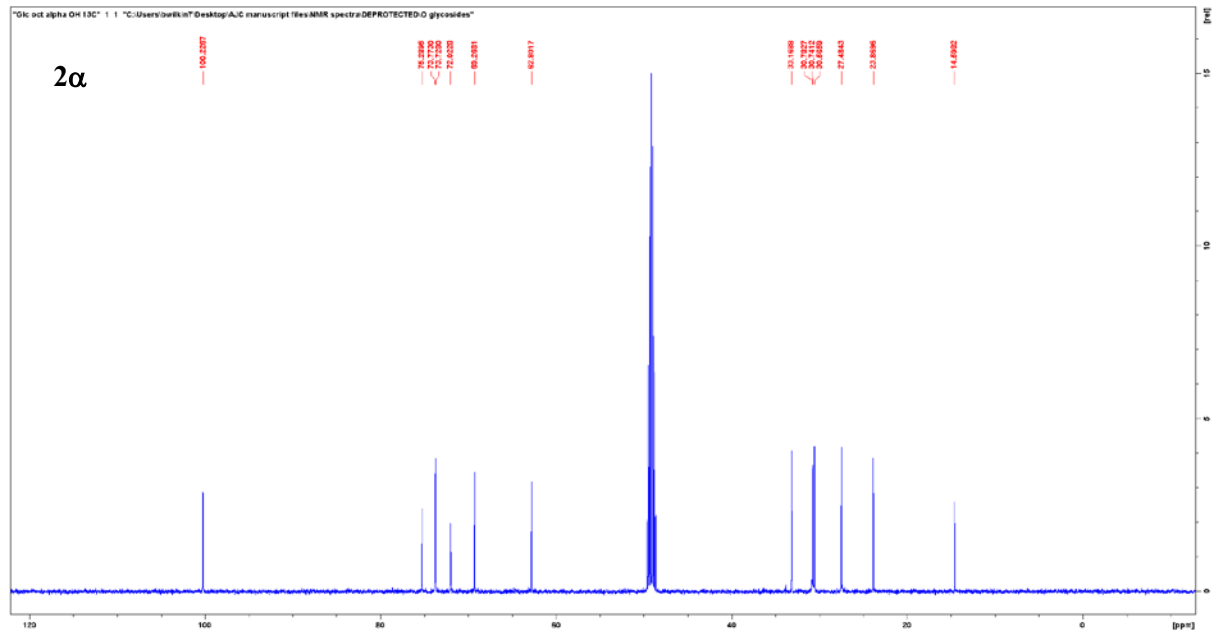
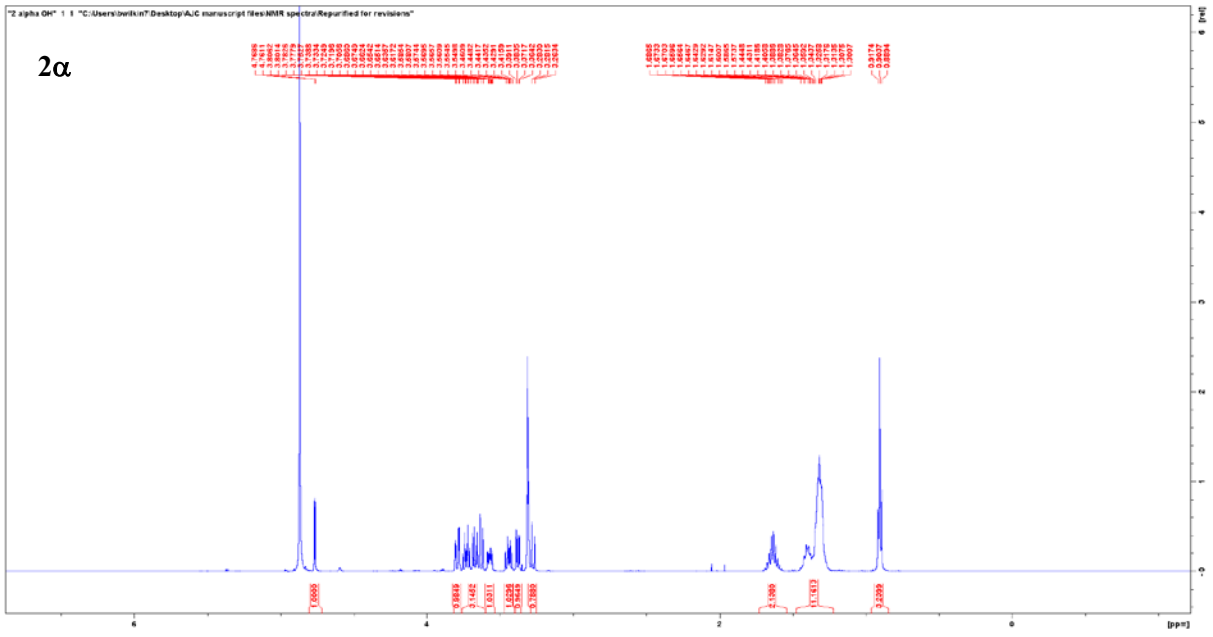


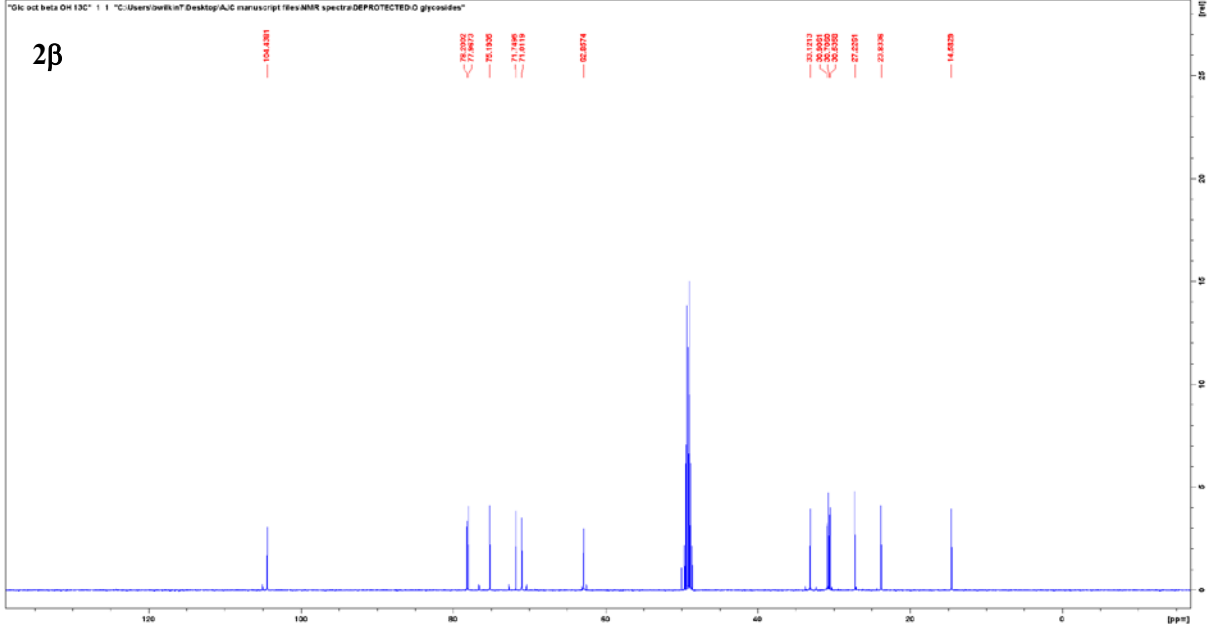
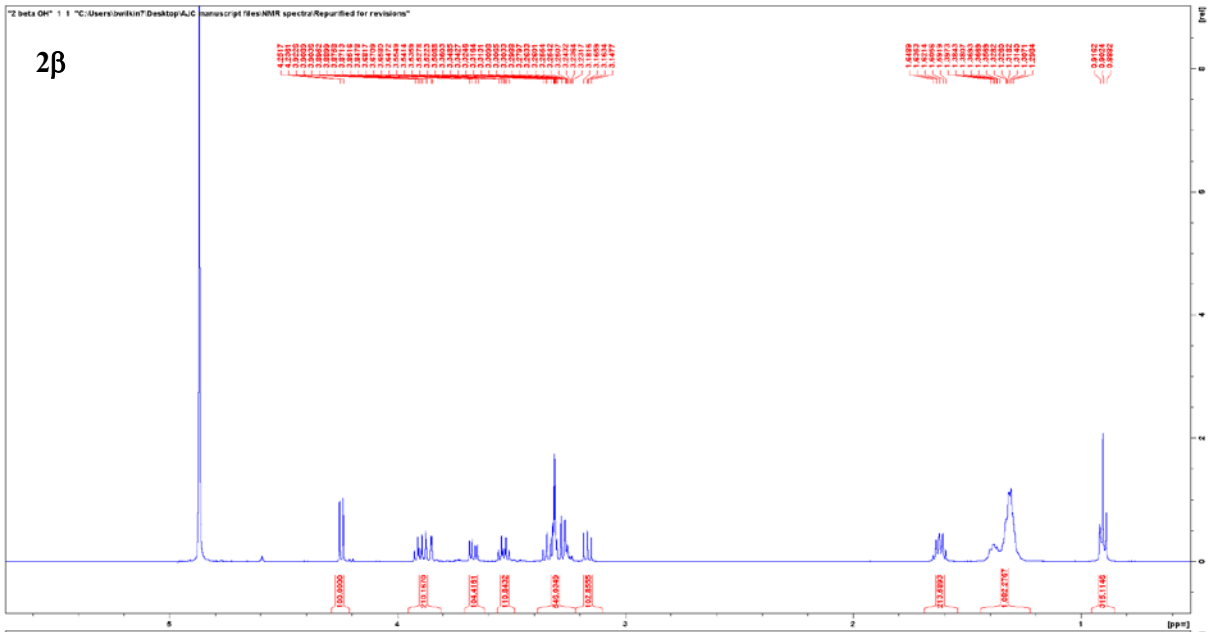
Compound **4 β** were synthesised according to general method 3 and obtained as an amorphous solid (589 mg, 1.78 mmol, 100%).

4 β : $R_f = 0.59$ (ethyl acetate/methanol, 6:1); $[\alpha]_D^{20} = -47.6$ ($c = 0.46$, CH₃OH); $^1\text{H NMR}$ (500 MHz, CD_3OD): δ 4.35 (d, 1H, $J_{1,2} = 9.73$ Hz, H-1), 3.86 (dd, 1H, $J_{6a,6b} = 12.09$ Hz, $J_{6a,5} = 2.19$ Hz, H-6a), 3.66 (dd, 1H, $J_{6a,6b} = 12.04$ Hz, $J_{5,6b} = 5.49$ Hz, H-6b), 3.37–3.25 (m, 3H, H-3, H-4 and H-5), 3.19 (dd, 1H, Hz, $J_{1,2} = 9.78$ Hz, $J_{2,3} = 8.54$ Hz, H-2), 2.79–2.67 (m, 2H, GlcS-OCH₂), 1.67–1.61 (m, 2H, GalS-OCH₂-CH₂), 1.45–1.28 (m, 10H, 5 x CH₂), 0.91 (t, $J = 6.94$ Hz, CH₃) ppm; $^{13}\text{C NMR}$ (125 MHz, CD_3OD): δ 87.23 (C-1), 82.07 (C-5), 79.70 (C-3 or C-4), 74.48 (C-2), 71.57 (C-3 or C-4), 63.01 (C-6), 33.12, 31.16, 30.97, 30.48, 30.44, 30.14, 23.83 (7 x CH₂), 14.58 (CH₃) ppm. MS (ESI⁺): calcd. for C₁₄H₂₈O₆S : $m/z = 331.2$ [M+Na]⁺; found: $m/z = 331.2$.

NMR spectra (compounds 1 β , 2 α , 2 β and 3 α).







Appendix II: Supplementary materials- Chapter 6

Supplementary Information

Measuring volume kinetics of human monocytes in response to cryoprotectants using microfluidic technologies

Rekha Raju ¹, Hannes Höhn ^{2,3}, Christian Karnutsch ²,
Khashayar Khoshmanesh ³, Gary Bryant ¹

¹ Centre for Molecular and Nanoscale Physics, School of Science, RMIT University,
Melbourne, Australia

² Institute for Sensor- and Information Systems (ISIS), Research Group ‘Integrated
Optofluidics and Nanophotonics (IONAS)’, University of Applied Sciences Karlsruhe,
Karlsruhe, Germany

³ School of Engineering, RMIT University, Melbourne, Australia

Supplementary Information S1: Fabrication process

Microfluidic structures were fabricated by direct laser writing technique¹ using the Nanoscribe 3D printer (Nanoscribe GmbH, Germany) available at MicroNano Research Facility (MNRF), RMIT University, Melbourne. The fabrication involved design, preparation, laser writing, developing, replicating, and assembly, as briefly described here.

Design: The microfluidic structures were designed in SolidWorks (Dassault Systèmes, France), and exported to DeScribe, which is the dedicated software of Nanoscribe 3D printer. The designs were based on the (i) Cup-shaped² and (ii) serpentine-shaped³ arrays, both capable of hydrodynamic trapping and perfusion of single cells (**Figure 1(a)**).

Preparation: The substrate (an indium tin oxide coated glass slide) was washed with acetone and isopropanol to remove all residuals, rinsed with distilled water and dried with nitrogen. The glass substrate was fixed to the holder of the Nanoscribe using glue. The photoresist was then poured on the substrate using a pipette. We used IP-S photoresist (Nanoscribe) due to its capability for the fast printing of smooth structures⁴. The substrate was then checked visually to ensure no air bubbles were trapped in the photoresist.

Laser writing: The system operated at a wavelength of 780 nm (near-infrared) in a femtosecond pulse mode at 100 fs and a repetition rate of about 80 MHz (**Figure 1(b)**). The system utilized an inverted microscope, Axio Observer (Carl Zeiss Micro Imaging GmbH, Germany), equipped with a 25× NA 0.8 objective. The microscope took advantage of an on-board autofocus system to produce a focused laser beam at the substrate surface⁴. The scanning speed and laser power were set to 10,000 μm/s and 0.5%, respectively.

Developing: The substrate was inserted in a bath of SU-8 developer for 30 minutes, and then transferred into a bath of isopropanol for 2 minutes. These steps were required to remove the monomeric and other residual material.

Replicating: The microfluidic traps were replicated using standard soft lithography processes⁵⁻⁷. The silicon based PDMS elastomer base and curing agent were mixed at a 10:1 weight ratio, stirred, degassed to remove any residual air bubbles, and poured onto the 3D printed structure to achieve a device thickness of 3-5 mm (**Figure 1(c)**). The PDMS structure was thermally cured at 70°C overnight.

Assembling: The cured PDMS slab with embedded microfluidic structures was peeled off from the substrate and cut into a rectangular shape using a scalpel (**Figure 1(d)**). A 5 mm inlet reservoir and a 0.75 mm outlet port were punched to facilitate the interfacing of the microfluidic system with fluidic tubes. The PDMS slab was sealed onto a glass slide by plasma bonding (Harrick Plasma, Ithaca, NY) to avoid leakage.

Supplementary Information S2: Cell preparation

Human monocytes (THP-1 cell lines) were purchased from ATCC (American Type Culture Collection, MANASSAS, VA). Cells were revived from liquid nitrogen and cultured according to ATCC standard protocol. Briefly, the cell culture consisted of RPMI1640 medium (ATCC, 30-2001) supplemented with 10% FBS (Fetal Bovine Serum) (ATCC, 30-2020) and 1% antibiotic (Penstrip). The cells were cultured in T25 flasks (Corning) inside an incubator at 37°C in a humidified atmosphere containing 5% CO₂.

The cells had a diameter ranging from 12 to 18 μm. The viability of cells was measured using Trypan blue exclusion test⁸ and found to be in the range of 96-98% before experiments. The cells were collected, centrifuged at 200 rcf for 5 min, and then re-suspended in 1× PBS (Phosphate Buffered Saline) (288 mosm/kg) at a cell density of 2.5×10⁵ cells/ml, and used for experiments within 3 hours.

Supplementary Information S3: Characterization of cup-shaped and serpentine-shaped cell traps

Numerical simulations were performed to analyze the distribution of perfused CPA and pressure across the trapped THP-1 cells. Simulations were conducted using the finite volume based ANSYS Fluent (ANSYS Inc.). Differential equations governing the balance of mass, momentum and transport of species were solved in 3D, under laminar conditions, and considering the CPA solution as a Newtonian liquid. Boundary conditions included desired flow rates at the inlet, zero pressure at the outlet, and no-slip at the surface of the microfluidic structures as well as the trapped cells. The trapped cells were assumed as spherical objects with a diameter of 15 μm .

Numerical simulations revealed a slightly higher concentration of CPA solution in the first few seconds of perfusion, and a larger flow-induced pressure at the front side of the trapped cells. Both parameters are governed by the direction of flow and cause the non-uniform distribution of osmotic gradient across the membrane of trapped cells. It should be noted that the concentration of CPA becomes uniform within ~ 5 s.

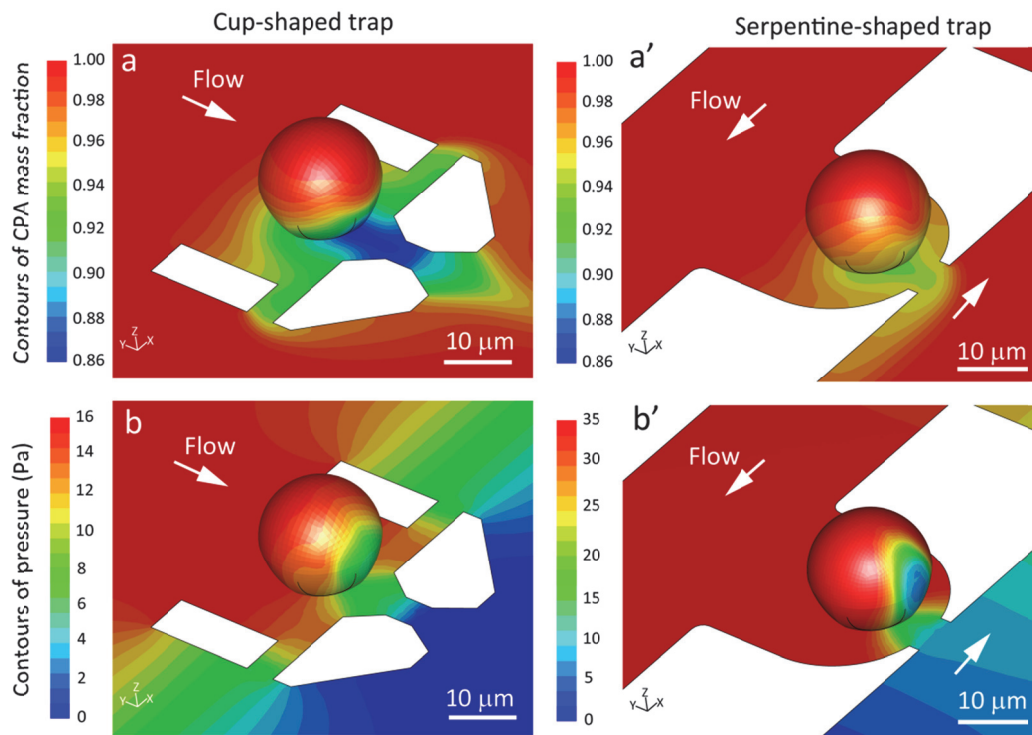


Figure S3. Characterization of cup-shaped and serpentine-shaped cell traps obtained by numerical simulations: (a-a') Contours of CPA mass fraction after 2 s, and (b-b') Contours of pressure (Pa) across the trapped THP-1 cells.

References

1. A. Selimis, V. Mironov and M. Farsari, *Microelectron Eng.* **132**, 83-89 (2015). <http://dx.doi.org/10.1016/j.mee.2014.10.001>
2. D. Wlodkowic, S. Faley, M. Zagnoni, J. P. Wikswo and J. M. Cooper, *Anal. Chem.* **81** (13), 5517-5523 (2009). 10.1021/ac9008463
3. W.-H. Tan and S. Takeuchi, *Proc. Natl. Acad. Sci. USA* **104** (4), 1146-1151 (2007). <https://doi.org/10.1073/pnas.0606625104>
4. Nanoscribe Photonic Professional GT- User manual, Nanoscribe GmbH, Germany, 2015, <https://snf.stanford.edu/SNF/equipment/nSiL/nanoscribe-photonics-professional-gt/nanoscribe-photonics-professional-gt-manual/view>.
5. D. Qin, Y. Xia and G. M. Whitesides, *Nat. Protocols* **5** (3), 491-502 (2010). 10.1038/nprot.2009.234
6. D. C. Duffy, J. C. McDonald, O. J. A. Schueller and G. M. Whitesides, *Anal. Chem.* **70** (23), 4974-4984 (1998). 10.1021/ac980656z
7. S. K. Sia and G. M. Whitesides, *Electrophoresis* **24** (21), 3563-3576 (2003). <https://doi.org/10.1002/elps.200305584>
8. W. Strober, *Curr. Protoc. Immunol.* **21** (1), A. 3B. 1-A. 3B. 2 (1997). 10.1002/0471142735.ima03bs21

Appendix III: Table showing the novelty of current study with THP-1 cells

Permeability studies of some cell types to CPA (mainly DMSO) at room temperature

Cell type	Reference
Rabbit basophilic leukemia cell	[1]
Rabbit oocyte	[2]
Rat hepatocytes and Brx-142 cells	[3]
Rhesus monkey (<i>Macaca mulatta</i>) spermatozoa	[4]
Mouse Ovum	[5]
Mouse Oocyte	[6]
Mouse Oocyte	[7]
Mouse oocytes and embryos	[8]
Mouse dendritic cell	[9]
Mammalian oocytes and embryos (mouse, bovine, pig, human oocytes)	[10]
Bovine chondrocyte	[11]
Golden hamster pancreatic islet	[12, 13]
Umbilical cord blood (UCB) CD34+	[14]
Human prostate cancer cell	[15]
Human mature oocytes	[16]
Human spermatozoa	[17]
Human megakaryocyte cell	[18]
Human granulocyte	[19]
Human Lymphocyte (from blood)	[20]
Human Lymphocyte (from blood)	[21]
Human Placental/Umbilical Cord Blood CD34T+ Cells	[22]
Human vaginal mucosal T cell	[23]
Human vaginal mucosal macrophage	[23]
Human pluripotent stem cells	[24]
Human monocyte leukemia cells (THP-1 cells)	Current study[25, 26]

1. Chen, H.H., et al., *Development of a microfluidic device for determination of cell osmotic behavior and membrane transport properties*. *Cryobiology*, 2007. **55**(3): p. 200-9.
2. Liu, J., et al., *Determination of oocyte membrane permeability coefficients and their application to cryopreservation in a rabbit model*. *Cryobiology*, 2009. **59**(2): p. 127-134.
3. Weng, L., et al., *A highly-occupied, single-cell trapping microarray for determination of cell membrane permeability*. *Lab on a Chip*, 2017. **17**(23): p. 4077-4088.
4. Agca, Y., et al., *Osmotic tolerance and membrane permeability characteristics of rhesus monkey (*Macaca mulatta*) spermatozoa*. *Cryobiology*, 2005. **51**(1): p. 1-14.

5. Leibo, S., *Water permeability and its activation energy of fertilized and unfertilized mouse ova*. The Journal of membrane biology, 1980. **53**(3): p. 179-188.
6. Hunter, J., et al., *Measurements of the membrane water permeability (L_p) and its temperature dependence (activation energy) in human fresh and failed-to-fertilize oocytes and mouse oocyte*. Cryobiology, 1992. **29**(2): p. 240-249.
7. Gao, D., et al., *Membrane transport properties of mammalian oocytes: a micropipette perfusion technique*. Journal of reproduction and fertility, 1994. **102**(2): p. 385-392.
8. PEDRO, P.B., et al., *Permeability of mouse oocytes and embryos at various developmental stages to five cryoprotectants*. Journal of Reproduction and Development, 2005. **51**(2): p. 235-246.
9. Chen, H.-h., et al., *A microfluidic study of mouse dendritic cell membrane transport properties of water and cryoprotectants*. International Journal of Heat and Mass Transfer, 2008. **51**(23-24): p. 5687-5694.
10. Edashige, K., *Permeability of the plasma membrane to water and cryoprotectants in mammalian oocytes and embryos: Its relevance to vitrification*. Reproductive Medicine and Biology, 2017. **16**(1): p. 36-39.
11. Xu, X., Z. Cui, and J.P. Urban, *Measurement of the chondrocyte membrane permeability to Me₂SO, glycerol and 1, 2-propanediol*. Medical engineering & physics, 2003. **25**(7): p. 573-579.
12. Gao, D., et al., *Development of a novel microperfusion chamber for determination of cell membrane transport properties*. Biophysical journal, 1996. **71**(1): p. 443.
13. Benson, C., et al., *Hydraulic Conductivity (L_p) and Its Activation Energy (E_a), Cryoprotectant Agent Permeability (P_s) and Its E_a , and Reflection Coefficients (σ) for Golden Hamster Individual Pancreatic Islet Cell Membranes*. Cryobiology, 1998. **37**(4): p. 290-299.
14. Hunt, C.J., S.E. Armitage, and D.E. Pegg, *Cryopreservation of umbilical cord blood: 1. Osmotically inactive volume, hydraulic conductivity and permeability of CD34+ cells to dimethyl sulphoxide*. Cryobiology, 2003. **46**(1): p. 61-75.
15. Takamatsu, H., et al., *Quantitative examination of a perfusion microscope for the study of osmotic response of cells*. Journal of biomechanical engineering, 2004. **126**(4): p. 402-409.
16. Newton, H., et al., *Osmotically inactive volume, hydraulic conductivity, and permeability to dimethyl sulphoxide of human mature oocytes*. Journal of reproduction and fertility, 1999. **117**(1): p. 27-33.
17. Gilmore, J., et al., *Effect of cryoprotectant solutes on water permeability of human spermatozoa*. Biology of reproduction, 1995. **53**(5): p. 985-995.
18. Tseng, H.-Y., et al., *A microfluidic study of megakaryocytes membrane transport properties to water and dimethyl sulfoxide at suprazero and subzero temperatures*. Biopreservation and biobanking, 2011. **9**(4): p. 355-362.
19. Vian, A.M. and A.Z. Higgins, *Membrane permeability of the human granulocyte to water, dimethyl sulfoxide, glycerol, propylene glycol and ethylene glycol*. Cryobiology, 2014. **68**(1): p. 35-42.
20. Hempling, H., S. Thompson, and A. Dupre, *Osmotic properties of human lymphocyte*. Journal of cellular physiology, 1977. **93**(2): p. 293-302.
21. Porsche, A., et al., *Determination of the permeability of human lymphocytes with a microscope diffusion chamber*. Cryobiology, 1986. **23**(4): p. 302-316.

22. Woods, E.J., et al., *Cutting Edge Communication: Osmometric and Permeability Characteristics of Human Placental/Umbilical Cord Blood CD34T+ Cells and Their Application to Cryopreservation*. Journal of hematotherapy & stem cell research, 2000. **9**(2): p. 161-173.
23. Shu, Z.Q., et al., *A study of the osmotic characteristics, water permeability, and cryoprotectant permeability of human vaginal immune cells*. Cryobiology, 2016. **72**(2): p. 93-99.
24. Xu, Y., et al., *Membrane permeability of the human pluripotent stem cells to Me2SO, glycerol and 1, 2-propanediol*. Archives of biochemistry and biophysics, 2014. **550**: p. 67-76.
25. Raju, R., et al., *Measuring volume kinetics of human monocytes in response to cryoprotectants using microfluidic technologies*. Applied Physics Letters, 2019. **114**(22): p. 223702.
26. Raju, R., et al., *n-Octyl (thio) glycosides as potential cryoprotectants: glass transition behaviour, membrane permeability and ice recrystallization inhibition studies*.